Space Sci Rev (2012) 173:49–102
DOI 10.1007/s11214-012-9874-4

Particle Acceleration in the Magnetotail and Aurora

J. Birn · A.V. Artemyev · D.N. Baker · M. Echim · M. Hoshino · L.M. Zelenyi

Received: 12 December 2011 / Accepted: 1 March 2012 / Published online: 21 April 2012

Abstract This paper deals with acceleration processes in the magnetotail and the processes that enhance particle precipitation from the tail into the ionosphere through electric fields in the auroral acceleration region, generating or intensifying discrete auroral arcs. Particle acceleration in the magnetotail is closely related to substorms and the occurrence, and consequences, of magnetic reconnection. We discuss major advances in the understanding

J. Birn (✉)
Los Alamos National Laboratory, PO Box 1663, MS 466, Los Alamos, NM 87545, USA
e-mail: jbirn@lanl.gov

J. Birn
Space Science Institute, 4750 Walnut Street, Boulder, CO 80301, USA
e-mail: jbirn@spacescience.org

A.V. Artemyev · L.M. Zelenyi
Space Research Institute, Russian Academy of Science, Moscow, Russia

A.V. Artemyev
e-mail: Ante0226@yandex.ru

L.M. Zelenyi
e-mail: iki@cosmos.ru

D.N. Baker
Laboratory for Atmospheric and Space Physics, U. Colorado, Boulder, CO, USA
e-mail: Daniel.baker@lasp.colorado.edu

M. Echim
Belgian Institute for Space Aeronomy, Brussels, Belgium
e-mail: marius.echim@oma.be

M. Echim
Institute for Space Sciences, Bucharest, Romania

M. Hoshino
Space and Planetary Science Group, University of Tokyo, Tokyo, Japan
e-mail: hoshino@eps.s.u-tokyo.ac.jp

of relevant acceleration processes on the basis of simple analytical models, magnetohydrodynamic and test particle simulations, as well as full electromagnetic particle-in-cell simulations. The auroral acceleration mechanisms are not fully understood, although several, sometimes competing, theories and models received experimental support during the last decades. We review recent advances that emphasize the role of parallel electric fields produced by quasi-stationary or Alfvénic processes.

Keywords Magnetotail · Aurora · Reconnection · Substorm injections

1 Introduction

Flux increases of energetic particles and the acceleration of charged particles to high, nonthermal energies are an important consequence of plasma activity, transport, and magnetic reconfiguration in space and astrophysical plasmas. Major sites of particle acceleration in the Earth's magnetosphere include the bow shock, the magnetotail, including its connection to aurora via field-aligned electric fields, and the radiation belts. The general structure of the magnetosphere and its current systems are illustrated in Fig. 1. The importance and uniqueness of studying particle acceleration in the magnetosphere lies in the fact that it is accessible to spacecraft, which provide detailed information of particle fluxes and distribution functions, constraining possible acceleration mechanisms. In this paper we focus primarily on acceleration mechanism that operate in the magnetotail and can be investigated *in situ*. However, magnetotail activity also affects ionospheric and ground current systems and causes auroral displays. The latter are strongly affected by electric fields that enhance particle precipitation from the tail. A separate section therefore is devoted to auroral acceleration.

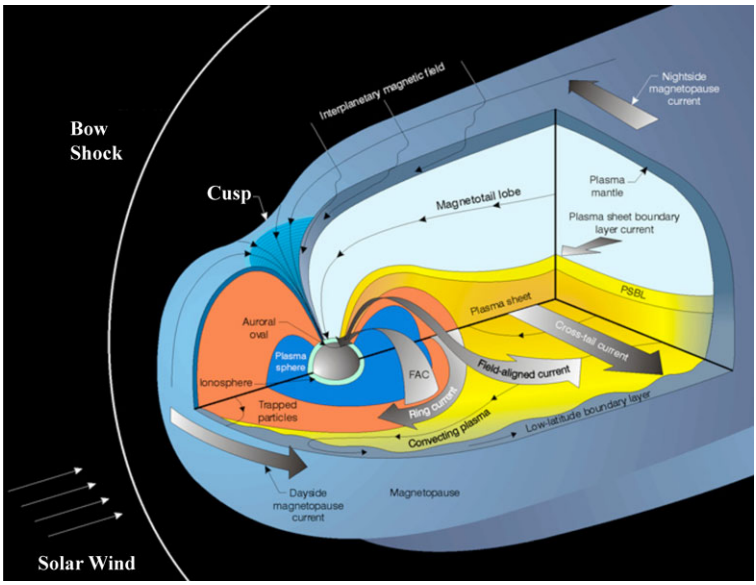

Fig. 1 Schematic of the Earth's magnetosphere. Major acceleration regions include the bow shock, the magnetotail plasma sheet, including its connection to aurora, and the radiation belts located in the inner region of trapped particles

A central role in energetic particle events in the magnetotail is played by magnetospheric substorms (Akasofu 1968) or, more generally, impulsive dissipation events (Sergeev et al. 1996b) that do not necessarily lead to full substorms. Substorms are complex magnetospheric processes driven by energy accumulation, redistribution, magnetic field reconfiguration, non-linear plasma interactions and instabilities leading to acceleration of particles by the fundamental processes described in this review. Part of the energy gained by particles in the magnetotail is carried along magnetic field lines and dissipated in the upper layers of the ionized polar atmosphere. Aurora is perhaps the most spectacular signature of acceleration processes in the tail and in the auroral regions. The coupling between the distant tail and the auroral dynamics is one of the keys to understand the global magnetospheric dynamics and its response to solar wind variability. Despite intensive ground observations and *in situ* measurements performed by rockets and spacecraft, the physical relation between substorm processes and the evolution and morphology of discrete auroral arcs at meso- and microscales remains an outstanding unsolved problem. A new challenge is to relate features and mechanisms of terrestrial charged particle acceleration to those recently discovered on other planets.

Substorms are commonly considered to consist of three phases (McPherron et al. 1973): (a) a "growth phase," during which energy is transferred from the solar wind to the magnetosphere and stored in a compressed and expanded magnetotail; this phase involves reconnection at the front side of the magnetosphere, enabled by a southward interplanetary magnetic field; (b) the substorm "expansion" (or "expansive") phase, during which energy is released and the aurora expands poleward; this phase also involves plasmoid ejection and a magnetic field collapse from a stretched tail-like toward a more dipole-like field ("dipolarization"); and (c) a recovery phase, during which the tail may return to its prior stage. Not all substorms show all stages.

Although details of the expansion phase onset are still under debate, it is clear that magnetic reconnection and its consequences play a central role in the energy release and transfer, not only to the thermal plasma but also to energetic particles. The basic scenario is illustrated in Fig. 2, taken from Baker et al. (1979). Particle acceleration occurs not only at a reconnection site but also in regions of induced electric fields associated with the collapse of magnetic field lines from the reconnection site toward the dipole. *In situ* observations of fields and particles provide stringent conditions for the models, so that the study of particle acceleration in the magnetotail is an excellent test ground for the evaluation of the relative importance of different acceleration mechanisms.

The most common acceleration processes considered within this context include (a) the direct acceleration by the electric field, particularly along a magnetic neutral line or separator, or by a component along the magnetic field, (b) betatron, and (c) Fermi-type acceleration associated with the magnetic field collapse or dipolarization, as well as (d) wave-particle interactions that might be associated with dipolarization events and auroral acceleration. Processes (a)–(c), involving large-scale electric fields, are illustrated for ions in Fig. 3. Each of the processes operates, in different ways, both in the non-adiabatic limit, mostly appropriate for ions, and the adiabatic limit, generally appropriate for electrons.

Direct acceleration (Fig. 3(a)) involves motion parallel (for electrons antiparallel) to the electric field. It is generally considered for non-adiabatic motion in the vicinity of the reconnection site (X-line) and for auroral acceleration by field-aligned electric fields. In the adiabatic limit, cross-tail curvature/gradient drift in the presence of dusk-ward electric field may also result in energy gain. In a general three-dimensional scenario X-line acceleration is replaced by the acceleration from an electric field component along the magnetic field (Giovanelli 1946; Schindler et al. 1988; Hesse and Schindler 1988). In either case the electric field must be sustained locally by non-ideal processes involving, for instance, electron

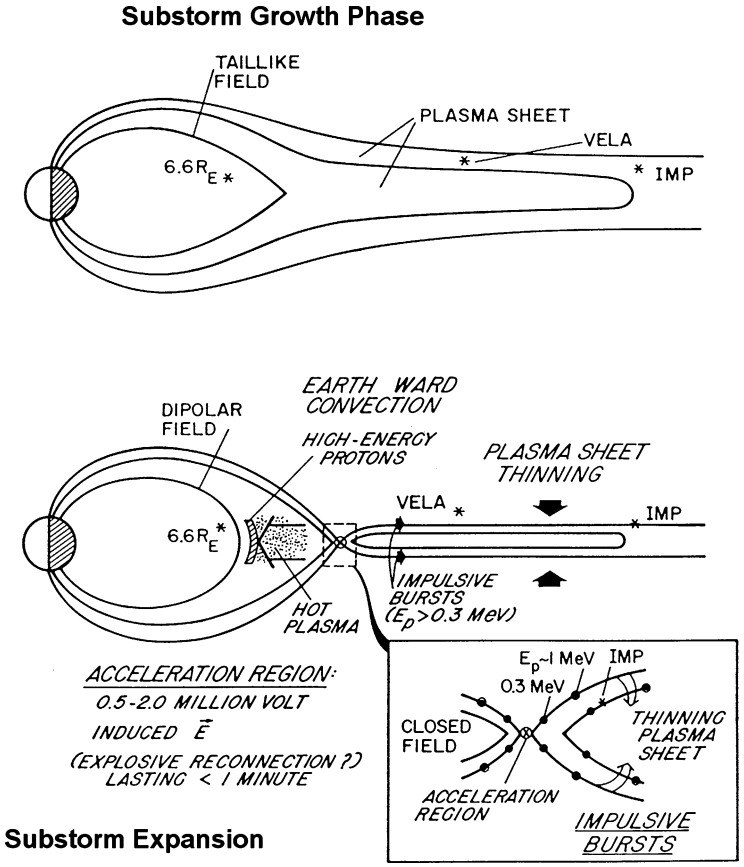

Fig. 2 Schematic of the magnetotail during substorm expansion, including major acceleration sites: the reconnection site and the collapsing field region earthward of the reconnection site. After Baker et al. (1979)

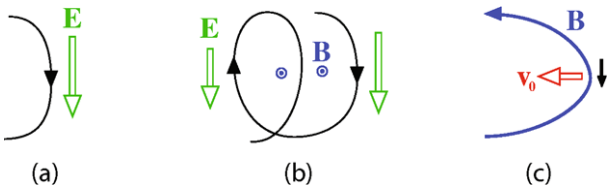

Fig. 3 Characteristic acceleration mechanisms in large-scale dawn-dusk electric fields in the magnetotail: (**a**) direct acceleration along the electric field, (**b**) betatron acceleration, (**c**) current sheet acceleration (Lyons 1984) or Fermi acceleration of type A or B (Northrop 1963). *Black lines* indicate particle orbits. The *black arrow* in (**c**) shows a particle velocity component along the magnetic field, while the *red arrow* indicates field line motion

inertia or nongyrotropy (Hesse and Winske 1998; Hesse et al. 2002). In the auroral acceleration the parallel electric field may be associated with similar kinetic effects or with small charge imbalance as in double layers. Dispersive Alfvén waves may also sustain a parallel component of the auroral electric field. These main auroral acceleration mechanism are considered in Sect. 5.

Betatron acceleration (Fig. 3(b)) involves gyromotion in spatially, or temporally, varying electromagnetic fields, such that the energy gain during one half of a gyration exceeds the loss during the other half. In the adiabatic limit, when the magnetic moment $\mu = W_\perp/B$ is conserved, the gain in perpendicular energy $W_\perp$ then simply follows from an increase in B along the drift path of the particle.

The third acceleration mechanism, illustrated in Fig. 3(c), is sometimes called "current sheet acceleration" (Lyons and Speiser 1982; Lyons 1984). In the adiabatic limit this process may also be understood as first order Fermi acceleration of type B (Northrop 1963). It results from a sling shot effect: a particle crossing the neutral sheet along an earthward convecting field line gains momentum in the earthward direction. If its initial velocity is small compared to the convection speed v_0, it becomes ejected at the speed $2v_0$ and the energy gained is $2mv_0^2$. However, when the speeds are comparable, or the particle velocity is larger than the convection velocity, the energy change is not as easily obtained and may, in the non-adiabatic limit, involve chaotic scattering, as discussed in Sect. 2.2.

Fermi acceleration of type B appears to be different from type A, which is associated with particles trapped between approaching magnetic mirrors. However, the distinction between the two types of first order Fermi acceleration is not as clear as it might seem. Earthward convecting flux tubes also become shorter, such that adiabatic particles that bounce between mirror points can also be considered as experiencing Fermi acceleration of type A (Northrop 1963). If the second adiabatic invariant is conserved during this motion, the energy gain then can be inferred from this invariant (Sect. 2.3).

The different acceleration processes are not mutually exclusive. For instance, the direct acceleration along the electric field is an important part of current sheet acceleration. In any case the energy gain is given by the path integral $q \int \mathbf{E} \cdot d\mathbf{s}$, where q is the particle charge and $d\mathbf{s}$ is the path element. Thus the spatial and temporal properties of the electric field play the key role in the acceleration. The relevant electric field may even be ideal (i.e. given by $-\mathbf{v} \times \mathbf{B}$, where $\mathbf{v}$ is the fluid velocity), such as the localized electric field associated with flow bursts and dipolarization events (Sect. 4), whereas in other cases, such as auroral acceleration, the localization of non-ideal parallel electric fields, distributed along auroral magnetic field lines or concentrated in thin double layers, may be important (Sect. 5).

In simplified views of magnetospheric convection it is frequently assumed that, for southward IMF (interplanetary magnetic field), the solar wind imposes a general cross-tail (dawn-dusk) electric field onto the magnetotail, which would cause earthward convection and also be the source of particle acceleration. However, taking a cross-tail voltage difference of, say, 100 kV, a tail diameter of 40 $R_E \approx 250{,}000$ km, and an equatorial magnetic field $B_{z0} \approx 1$–2 nT, implies a quasi-steady earthward convection speed near the equatorial plane of 200–400 km/s. Such speeds are observed only a few percent of the time during short intervals (Baumjohann et al. 1990; Angelopoulos et al. 1992). These events are commonly referred to as bursty bulk flows (BBFs) (Angelopoulos et al. 1992). Although they are rare, BBFs appear to transport most of the energy and magnetic flux in the plasma sheet (Angelopoulos et al. 1994), even during "Steady Magnetospheric Convection" (SMC) events (Sergeev et al. 1996a).

Thus, quasi-steady convection in the plasma sheet might play a role in earthward transport and heating only under sufficiently quiet conditions. Nevertheless, models with uniform background electric field provide a good means of exploring typical particle behavior and setting a base against which to compare more sophisticated space and time dependent models. This will be discussed further in Sect. 2, which illuminates basic acceleration processes through simplified analytic approaches. Section 3 deals with processes in the vicinity of a reconnection site, based particularly on particle simulations. Section 4 is devoted to "energetic particle injections," that is, rapid energetic particle flux increases in the near tail and

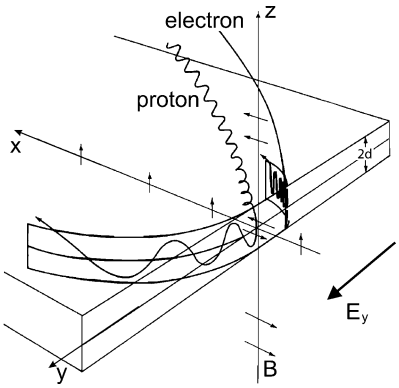

Fig. 4 Typical Speiser orbits for protons and electrons. The figure is adapted from Speiser (1965)

near geosynchronous orbit, which are related to acceleration from inductive electric fields associated with impulsive dipolarization events. Section 5 describes processes that intensify particle precipitation from the tail into the ionosphere through electric fields in the auroral acceleration region with emphasis on the role of parallel electric fields generated by quasi-stationary or Alfvénic processes.

2 Basic Acceleration Processes: Analytic Approaches

2.1 Introduction

Although, as we will demonstrate later, a realistic and quantitative evaluation of substorm acceleration requires three-dimensional, time-dependent models, significant insight into the acceleration mechanisms can already be gained from analytic approaches in simplified magnetic field models including a quasi-static (typically dawn to dusk) electric field. This is the main topic of the present section.

The key region for particle energization is the magnetotail current sheet (CS), which in the simplest case can be described by two components: the main component $B_x(z)$, which changes sign in the neutral plane $z = 0$, and the small component B_z directed normally to the CS. The particle motion in such a CS, including a cross-tail electric field, was first addressed by Ted Speiser (1965, 1967). He found that charged particles, gyrating along field lines towards the central region of the CS, make a half gyration around B_z, while oscillating around the neutral sheet, and then leave the CS along the field lines to the same or the opposite hemisphere. Typical Speiser orbits are shown in Fig. 4. (Due to mirroring closer to Earth this kind of orbit can occur repeatedly.)

In the presence of a dawn-dusk electric field, E_y, ions gain energy during the gyration in the neutral sheet, due to a displacement along the electric field. They pass the distance of the order of two gyroradii along the field E_y and the energy gained during this motion can be estimated as $\sim 2mc^2(E_y/B_z)^2$ (see, e.g., Lyons and Speiser 1982; Cowley and Shull 1983). For typical magnetotail parameters most ions follow Speiser trajectories.

Electrons do not follow this scenario and their acceleration mechanisms can be viewed differently. Due to their small mass, they can be considered as standard guiding-center particles, except in regions of very small magnetic field such as the vicinity of a neutral line (see Sect. 3). Electrons make a number of bounce oscillations between magnetic mirror points and their adiabatic invariants (first and second) are approximately conserved. The presence

of a large-scale dawn-dusk electric field results in earthward convection. This convection brings particles to regions with larger values of the equatorial magnetic field and shorter field lines. Correspondingly they gain energy from the combined effect of betatron (mostly for nearly equatorial particles) and Fermi (mostly for mirroring particles) mechanisms (Lyons 1984; Zelenyi et al. 1990).

Earthward convection in the magnetotail is generally not a steady process. The tail is characterized by a multitude of various transient processes (Baumjohann et al. 2007; Sharma et al. 2008): CS flapping motion (e.g., Sergeev et al. 2006; Petrukovich et al. 2006; Zelenyi et al. 2009 and references therein), bursty bulk flows (e.g., Angelopoulos et al. 1993; Panov et al. 2010 and references therein), plasmoids (e.g., Zong et al. 2004 and references therein) and dipolarization fronts (e.g., Runov et al. 2009 and references therein) may produce large scale inductive electric fields, which can become an effective tool for particle acceleration (Birn et al. 2004b; Ashour-Abdalla et al. 2011). Nevertheless, characteristic features of the quasi-stationary models discussed in this section, can also be found in dynamic cases (see Sect. 4).

Electromagnetic turbulence is often observed in the magnetotail (see review Zimbardo et al. 2010 and references therein). These fast (tens of seconds) microscale (less than a ion gyroradius) fluctuations of magnetic and electric fields (produced by various plasma instabilities) can violate particle adiabaticity. Turbulence driven variations of the magnetic field thus can result in the generation of inductive electric fields that may also accelerate (effectively unmagnetized) particles in a non-adiabatic fashion (Milovanov and Zelenyi 2001; Ono et al. 2009; Artemyev et al. 2009; Perri et al. 2011). Lower frequency (ULF) waves are also considered to be the main acceleration mechanism operating in the ring current/radiation belt region (discussed in the following chapter).

2.2 Ion Dynamics and Resonant Acceleration

This section is devoted to the description of ion dynamics and resonant acceleration in a simple CS geometry. In the Earth's magnetotail CSs with a transverse spatial scale L_z of only a few ion gyroradii are often observed (e.g., Artemyev et al. 2010b; Petrukovich et al. 2011 and references therein). Ion dynamics in such CSs cannot be described by the adiabatic approximation, implying the conservation of the magnetic moment, and may even be regarded as chaotic (Gray and Lee 1982). However, within the chaotic regime some domains of regular dynamics can also be found, one of them corresponds to the Speiser orbits (Chen and Palmadesso 1986). Below we present a theoretical approach into the description of characteristic features.

We consider ion dynamics in the central region of a two-dimensional CS, assuming a linear variation of B_x and uniform B_z, described by a vector potential $A_y \sim B_0(z^2/L_z) - B_z x$ (B_0 is the amplitude of the B_x component). The ion motion then can be described by the Hamiltonian:

$$H = \frac{1}{2m}p_x^2 + \frac{1}{2m}p_z^2 + \frac{1}{2m}\left(p_y - \frac{e}{c}A_y\right)^2. \tag{1}$$

Because H does not depend on y in the simplified 2D case we can set $p_y = 0$ by choosing the origin of the coordinate x. Now we introduce dimensionless variables: $\mathbf{p} \to \mathbf{p}/mv_0$, $H \to H/mv_0^2$, $x \to x(L_z\rho_0)^{-1/2}$, $z \to z(L_z\rho_0)^{-1/2}$, where v_0 is a typical particle velocity and $\rho_0 = mv_0c/eB_0$ is a typical particle gyroradius. Thus, the expression for H can be reduced to

$$H = \frac{1}{2}p_x^2 + \frac{1}{2}p_z^2 + \frac{1}{2}\left(\kappa x - \frac{1}{2}z^2\right)^2, \tag{2}$$

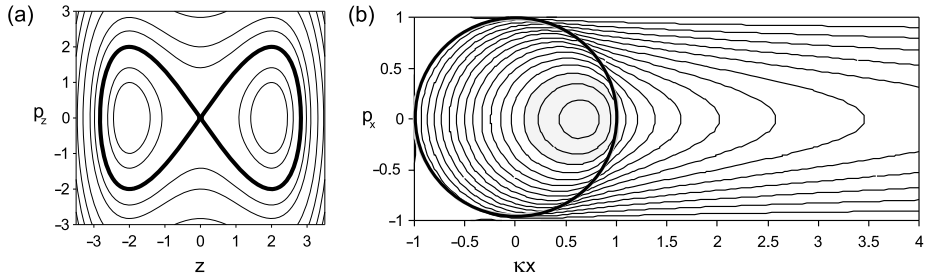

Fig. 5 Phase portrait of fast (**a**) and slow (**b**) motions. The separatrix is shown by *black bold curve*

where κ is the square root of the ratio between field line curvature radius and gyroradius at $z = 0$ (Büchner and Zelenyi 1989), which can be written as

$$\kappa = |B_z/B_0|\sqrt{L_z/\rho_0}. \tag{3}$$

For typical magnetotail parameters (ion temperature ~3–5 keV, magnetic field components $B_z \sim$ 1–2 nT, $B_0 \sim$ 10–20 nT) one finds $\kappa \ll 1$ for ions (Runov et al. 2006). Therefore one can separate the motion into two components, a fast oscillations of (z, p_z) and a slow evolution of $(\kappa x, p_x)$. The Hamiltonian of the fast motion $h_z = H - \frac{1}{2}p_x^2$ depends on the slowly varying parameter κx.

Phase diagrams of the fast motions (Fig. 5(a)) for fixed κx demonstrate two types of closed trajectories: oscillations around the neutral plane $z = 0$ (see also Fig. 4), and gyrations around field lines above and below the neutral plane without crossing $z = 0$. The curve in the phase space that separates these two types of trajectories is called the separatrix.

The area bounded by closed trajectories in the phase plane (z, p_z) can be considered as a quasi-adiabatic invariant of motion (Sonnerup 1971)

$$I_z = \frac{1}{2\pi}\oint p_z dz = \frac{1}{2\pi}\oint \left(h_z - \frac{1}{2}\left(\kappa x - \frac{1}{2}z^2\right)^2\right)^{1/2} dz. \tag{4}$$

Hereinafter we use notation "quasi-adiabatic" to separate invariants I_z (and I_x) from classical adiabatic invariants of guiding-center theory. I_z explicitly depends on the slow variables $(\kappa x, p_x)$ and is approximately conserved during the slow evolution of the Hamiltonian system. Therefore the lines of constant I_z determine the trajectories of particles in the phase plane of the slow variables (Fig. 5(b)). Each point in this plane corresponds to some trajectory in the fast variable plane (z, p_z) and the black bold circle in Fig. 5(b) with $\kappa x > 0$ corresponds to the separatrix. When a particle crosses the half-circle in the $(\kappa x, p_x)$ plane it changes the character of its motion. The separatrix crossing also leads to a jump of the quasi-adiabatic invariant (Neishtadt 1986; Cary et al. 1986),

$$\Delta I_z = -\frac{4}{\pi}\kappa p_x^* \ln(2\sin\pi\xi) \tag{5}$$

where p_x^* is the momentum at the separatrix and $\xi \in [0, 1]$ is a fast variable characterizing the particular point of the separatrix crossing in the (z, p_z) plane.

So far we have neglected the electric field. If a uniform electric field E_y is present, one can simply use a coordinate transformation into a frame that moves with the speed cE_y/B_z in the x direction. In this frame the electric field vanishes and the results obtained above can

still be applied. Now consider the motion in the rest frame. During their half-rotation around B_z in the neutral plane particles gain energy from the displacement along the electric field E_y. Due to jumps ΔI_z the particles are scattered in the CS and do not necessarily leave the system (Büchner and Zelenyi 1989; Zelenyi et al. 2000). The scattered particles only gain some fraction (on average about one half) of $2mc^2(E_y/B_z)^2$. Such particles may move along quasi-trapped orbits and stay trapped in the vicinity of CS. After a few CS encounters the particle motion becomes chaotized and the energy gain becomes enhanced thermal energy of this particle population. However, there are exceptions from such a chaotization scenario.

Each interaction of a particle with the CS consists of two jumps of the quasi-adiabatic invariant (at the entrance to and the exit from the CS). Therefore, the system can contain a class of orbits where these two jumps compensate each other. These orbits are called resonant and were numerically found by Burkhart and Chen (1991) and by Büchner (1991). A detailed analytical description of resonant orbits was given by Ashour-Abdalla et al. (1993), generalized later by Zelenyi et al. (2007).

The sum of entrance jump $\Delta I_{z,1} = -\frac{4}{\pi}\kappa p_x^* \ln(2\sin\pi\xi)$ and exit jump $\Delta I_{z,2} = \frac{4}{\pi}\kappa p_x^* \times \ln(2\sin\pi(\xi+\delta\xi))$ depends mostly on the phase gain during the particle semirotation around B_z between these two consequent separatrix crossings:

$$\Delta I_{z,\Sigma} = \Delta I_{z,1} + \Delta I_{z,2} = \frac{4}{\pi}\kappa p_x^* \ln\left|\cos(\pi\delta\xi) + \sin(\pi\delta\xi)\tan(\pi\xi)\right|. \tag{6}$$

If the gained phase $\pi\delta\xi = \pi N$ (N is an integer), then the total jump becomes identically equal to zero. The expression for $\pi\delta\xi$ only weakly depends on I_z and can be found by integration over the slow variable κx (Büchner and Zelenyi 1989). Expanding $\pi\delta\xi$ near $I_z = 0$ we get $\delta\xi = CH^{1/4}/\kappa + O(I_z)$, where $C = \text{const}$. Therefore, for a fixed value of κ we obtain an expression for the resonance in velocity space, $H \sim N^4$ (Burkhart and Chen 1991).

In realistic cases κ is a function of coordinates ($\kappa \sim B_z(x)$) within the magnetotail and the condition for resonance in configurational space becomes $\kappa(x) \sim 1/N$ (Ashour-Abdalla et al. 1993; Zelenyi et al. 2007). Thus, the condition $\kappa \sim 1/N$ can be satisfied for some special regions within the magnetotail $x = x_N$, $N = 1, 2, \ldots$ (Fig. 6(a)), where $\kappa(x_N) \sim 1/N$. If we take into account that the gained energy $W = 2mc^2(E_y/B_z)^2$ also depends on x then we can find the elegant resonance scaling in the magnetotail. Combining $\kappa \sim B_z W^{-1/4} \sim 1/N$ and $W \sim B_z^{-2}$ we easily obtain $W_N \sim N^{4/3}$ (Ashour-Abdalla et al. 1993; Grigorenko et al. 2010). This universal law does not depend on the particular magneto-plasma configuration (once it is assumed 2D) and can work for any profile $B_z(x)$.

Resonant particles do not experience chaotic scattering and most of the energy acquired during their interaction with the CS is along the magnetic field. Therefore, the group of resonant particles leaving the CS forms a spatially localized accelerated beam (beamlet) with a specific velocity distribution in the form of a "lima bean, which has been reproduced in numerical simulations (Lyons and Speiser 1982; Cowley and Shull 1983). Beamlets with such velocity distributions are often observed in the PSBL as beams of almost monoenergetic particles moving along the field lines towards the Earth (Eastman et al. 1984; Grigorenko et al. 2007, 2010). In addition, such beamlets can be observed in the auroral region: on a time vs energy diagram these observations take the form of a chain of count (or phase density) maxima (Keiling et al. 2004; Sauvaud and Kovrazhkin 2004). Each island from this chain corresponds to an individual resonance x_N. This picture can also be well reproduced by numerical modeling (Ashour-Abdalla et al. 1994, 2005). Both experimental and numerical data conform rather well with the analytical scaling $\ln W \sim (4/3)\ln N$ (Fig. 6(b)). Thus, the theory of quasi-adiabatic ion motion and resonant acceleration in a CS is consistent with the observed mostly field-aligned energetic particle beams.

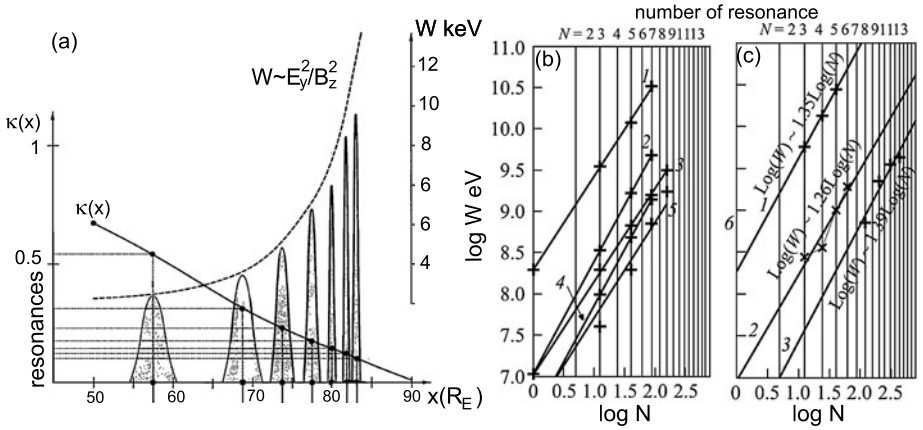

Fig. 6 (**a**) Distribution of the resonance regions and gained energy along the tail, showing also the scaling $W \sim B_z^{-2}$; adapted from Ashour-Abdalla et al. (1995). (**b**) Scaling $\ln W \sim (4/3) \ln N$ for various numerical models. (The numbers indicate the corresponding magnetic field model, see details in Zelenyi et al. 2007.) (**c**) Scaling $\ln W \sim (4/3) \ln N$ for experimental data. (The numbers indicate the corresponding observation, see details in Zelenyi et al. 2007.) The figure is adapted from Zelenyi et al. (2007)

2.3 Quasi-adiabatic and Adiabatic Heating During Earthward Convection

The majority of electrons in the Earth's magnetotail can be considered as magnetized particles, corresponding to a value of $\kappa > 1$. Therefore, for a description of electron dynamics, we can apply the standard guiding-center approximation, assuming conservation of the first adiabatic invariant (magnetic moment $\mu = m_e v_\perp^2/2B$) and the second longitudinal invariant $J_\parallel = \oint v_\parallel ds$ (where s is the arc length along a magnetic field line) (Tverskoy 1969).

During earthward convection due to the drift $\sim E_y/B_z$ electrons move to regions with increased field B_z and the length of their bounce path between subsequent mirror points shrinks. In this case both Fermi and betatron mechanisms provide electron energization (Tverskoy 1969; Lyons 1984; Zelenyi et al. 1990). As discussed in Sect. 4, these mechanisms operate even during dynamic magnetotail evolution associated with dipolarization (Birn et al. 2004b; Delcourt 2002; Apatenkov et al. 2007).

Below we consider electron heating during earthward convection in a 2D CS model. We approximate the magnetic field as $B_x(z) = B_0(z/L_z)$ and $B_z(x) = B_n g(x)$, where $g(x) = (-x/L_x)^{-h}$ for $x \le L_x$ and $h = 0.8$ (this value applies to average tail equilibria, see Birn et al. 1977 and references therein, but may differ in dynamic cases). In this case we can write the following relations between the velocity components $(v_\perp, v_\parallel)$ at the observation point, $B_x = 0$, $B_z = B_n$, and $(u_\perp, u_\parallel)$ at the point $B_x = 0$, $B_z = B_n g(x)$ (Tverskoy 1969):

$$u_\perp^2 = g v_\perp^2, \qquad \Phi\left(1 + \frac{v_\parallel^2}{v_\perp^2}\right) = g^{3/2} \Phi\left(1 + \frac{v_\parallel^2}{v_\perp^2}\right), \qquad \Phi(a) = \int_1^a \sqrt{\frac{a-x}{x^2-1}}\, x^2 dx. \quad (7)$$

We set the initial velocity distribution of electrons as an anisotropic Maxwellian distribution with $T_{e\parallel}/T_{e\perp} > 1$ at the point $B_x = 0$, $B_z = B_n$ and then recalculate the distribution moving backwards along the neutral plane towards the deeper tail by using the relations between $(v_\perp, v_\parallel)$ and $(u_\perp, u_\parallel)$. The integration of the obtained velocity distribution provides a profile of the electron temperature as a function of g (Fig. 7(a)). As one can see, the electron

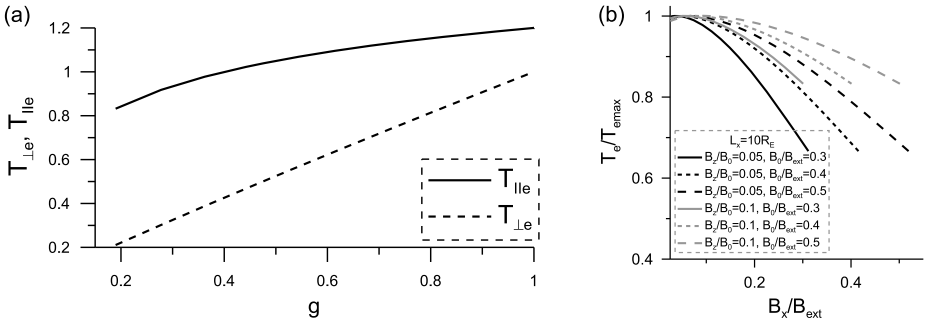

Fig. 7 (**a**) Profiles of electron temperature along the magnetotail. (**b**) Model profiles of electron temperature for various plasma parameters (here B_{ext} is the B_x value in the lobes). In the point $B_z = B_n$ we take electron anisotropy $T_{e\parallel}/T_{e\perp} = 1.2$

temperature $T_{e\perp}$ grows with increasing $B_z \sim g(x)$ more substantially than $T_{e\parallel}$ does. This effect was noticed for the first time by Tverskoy (1969), who demonstrated that for particles with the distant mirror points the energy grows as $B_z^{2/5}$ while for particles moving around the neutral plane the energy grows proportional to B_z.

Obtaining the velocity distribution in the neutral plane (i.e. for each x) one can map this distributions along field lines to obtain the temperature profile $T_e(z) = \frac{1}{3}(T_{e\parallel}(z) + 2T_{e\perp}(z))$ along a vertical cut with $B_z = B_n$, which can be presented as a dependency of $T_e(z)$ on $B_x(z)$ along the $B_z = B_n$ cut (Artemyev et al. 2011). The corresponding theoretical profiles are shown in Fig. 7(b). The decrease of T_e towards the CS boundary in the model profiles conforms very well with spacecraft observations (Artemyev et al. 2011). The electron anisotropies inferred from this model for larger distances (smaller g values) are typically not observed during quiet times (e.g., Stiles et al. 1978). This result stems mainly from our simplified model in which B_x is independent of x. This affects the location of mirror points and thereby the parallel heating. More realistic models that include x variations do not show such large anisotropies.

The discussion above referred to systems which can be described by the guiding-center approach ($\kappa > 1$). However, a similar theory can be developed for particles with $\kappa < 1$ (Zelenyi et al. 1990; Vainshtein et al. 2005). Here for simplicity we use the same CS geometry. The Hamiltonian of charged particles in the system with $B_z = B_z(x)$ and $\mathbf{E} = E_y\mathbf{e}_y$ in dimensionless variables, introduced in the section above, has the following form

$$H = \frac{1}{2}p_x^2 + \frac{1}{2}p_z^2 + \frac{1}{2}\left[\kappa a(x) - \frac{1}{2}z^2 - \kappa\tau\right]^2 \tag{8}$$

where

$$a(x) = \int_{x_0}^{x} \left(B_z\left(x'\right)/\bar{B}_z\right)dx', \qquad \tau = (cE_y/v_0\bar{B}_z)t \tag{9}$$

and $\bar{B}_z$ is some typical value of $B_z(x)$. If we assume that τ is a slow time and the parameter κ is small, we obtain the quasi-adiabatic invariant I_z depending on $(\kappa a(x) - \kappa\tau, p_x)$ for the fast components (z, p_z) of motion. The conservation of I_z prescribes the shape of the trajectory in the $(\kappa x, p_x)$ plane. However, due to the presence of the electric field ($\partial H/\partial\tau \neq 0$), particles additionally drift in the plane $(\kappa x, p_x)$. Because the evolution of the trajectory is much slower than the particle motion in the plane $(\kappa x, p_x)$ (i.e. $cE_y/v_0\bar{B}_z \ll 1$), the area

bounded by the trajectory in the plane $(\kappa x, p_x)$ is conserved during this slow drift. Therefore we can introduce the second quasi-adiabatic invariant $I_x = \oint p_x dx$ (the analogous of $J_\parallel = \oint v_\parallel ds$). The conservation of I_x allows us to describe particle heating during earthward convection of quasi-adiabatic particles (thermal ions in the magnetotail).

One can represent the Hamiltonian of the fast motion $h_z = \frac{1}{2}p_z^2 + \frac{1}{2}(\kappa a(x) - \frac{1}{2}z^2 - \kappa\tau)^2$ as a function of I_z and $\kappa a(x) - \kappa\tau$. Then $H = \frac{1}{2}p_x^2 + h_z(\kappa a(x) - \kappa\tau, I_z)$ and one can get an expression for $I_x = I_x(H, I_z, \tau)$ (Zelenyi et al. 1990; Vainshtein et al. 2005). Due to the conservation of $I_x = I_x(H, I_z, \tau)$ and I_z, the energy H increase with time τ. One can easily estimate the rate of the energy growth for two limiting cases: large values of $I_z \sim 1$ and small values of $I_z \ll 1$. Particles with large value of I_z represent so called regular (or trapped) trajectories (Chen and Palmadesso 1986; Büchner and Zelenyi 1989; Zelenyi et al. 2000) and spend all time inside CS without separatrix crossings. For such particles one can obtain $I_x \sim H/\langle da/dx\rangle$ (Zelenyi et al. 1990). Taking into account $da/dx = B_z/\bar{B}_z$ we obtain $H \sim B_z$. This law of energy growth with the increase of B_z is similar to the one provided by the betatron mechanism for electrons. However, when particle gain enough energy they cross the separatrix and the approximation of large I_z becomes violated. For particles with small I_z one can obtain $H \sim B_z^{2/5}$ (Zelenyi et al. 1990; Vainshtein et al. 2005). Therefore, for ions with distant mirror points (small I_z) we obtain the same law of energization as for electrons. This is not surprising because such particles spend most of the time in the region outside the CS where the motion is magnetized even for the quasi-adiabatic ions.

2.4 Turbulent Acceleration

We described above mechanisms of charged particle acceleration in the magnetotail that operate even under steady conditions. However, an important additional role could be played by turbulent acceleration. The accelerating agent in this case is the inductive electric field $\nabla \times \mathbf{E}_{ind} = -c^{-1}\partial\mathbf{B}/\partial t$, generated by magnetic field variations. These variations can be produced by a multitude of hot plasma instabilities in the magnetotail, such as kink and sausage modes (Lapenta and Brackbill 1997; Daughton 1998), tearing modes (see Schindler 2006; Divin et al. 2007; Zelenyi et al. 2008b, and references therein), lower-hybrid modes (see Daughton 2003, and references therein), ballooning modes (see Golovchanskaya and Maltsev 2005; Pritchett and Coroniti 2010 and references therein). All of these modes may lead to the formation of turbulent electromagnetic fields, as observed by spacecraft (see Hoshino et al. 1994; Petrukovich 2005; Zimbardo et al. 2010 and references therein). Although all of these instabilities saturate within their nonlinear regime, the resulting state is not a steady one. It represents a so-called "NESS"—near equilibrium steady state (Zelenyi and Milovanov 2004), which is steady only on average, but could have active intrinsic dynamics. This phenomenon is characteristic for open systems with persistent energy influx.

The most straightforward way to set up a numerical model of turbulent fields is to represent it as an ensemble of plane electromagnetic waves propagating at different directions (Veltri et al. 1998; Zelenyi et al. 2008a; Artemyev et al. 2009). Initial phases of these waves are chosen as random parameters. For simplification one can also assume that all waves have linear dispersion $v_\phi = \omega_\mathbf{k}/|\mathbf{k}| = \text{const}$, where $\omega_\mathbf{k}$ and $\mathbf{k}$ are wave frequencies and wave numbers. The wave magnitude $\delta B(\mathbf{k}) = C(1 + (\mathbf{kl})^2)^{-\alpha}$ and $\mathbf{l}$ is the vector of correlation length. The power index $\alpha = 7/8$ was chosen on the basis of various experimental observations (Hoshino et al. 1994; Petrukovich 2005). We use this value of α for our 3D calculations, while for a 2D case α will be set to $\alpha = 5/8$ (Chiaravalloti et al. 2006).

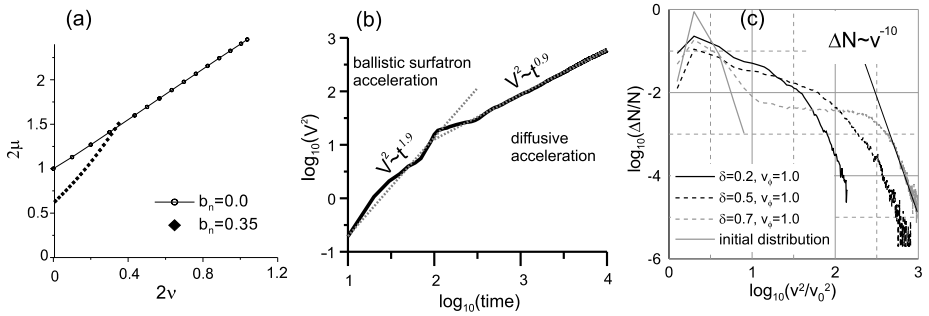

Fig. 8 (**a**) μ as a function of ν for two value of the background magnetic field $b_n = B_{0z}/\bar{B}$. Each point corresponds to some value of v_ϕ. Figure is adapted from Zelenyi et al. (2008a). (**b**) Energy of particle ensemble as a function of time. (**c**) Energy distribution of accelerated ions. The parameters $\delta = \sqrt{\langle \delta \mathbf{B}^2 \rangle}/B_0$ and v_ϕ are normalized by the thermal velocity of the cold incoming particle beam, v_0. Figure is adapted from Artemyev et al. (2009)

2.4.1 2D Model

First we consider a system with a simplified 2D geometry; the 3D case will be discussed in the next section. Particle transport and acceleration takes place mostly in the vicinity of the neutral plane, where the main (sign-changing) component of the magnetic field $B_x \sim z$ is small. The particle motion in such a simplified geometry can then be investigated by taking only the perpendicular magnetic field component into account, given by $\mathbf{B} = B_{0z}\mathbf{e}_z + \delta B_z(x, y, t)\mathbf{e}_z$ (Zelenyi et al. 2008a).

We integrate the nonrelativistic equations of motion ($m\dot{\mathbf{v}} = q\mathbf{E} + q[\mathbf{v} \times \mathbf{B}]/c$ and $\dot{\mathbf{r}} = \mathbf{v}$). Particle velocities are normalized to the initial average velocity of a particle ensemble v_0, time is normalized to the gyrofrequency in the field $\bar{B} = \sqrt{\langle \delta B_z^2 \rangle}$ (averaged over the space), spatial scales are normalized to the gyroradius $\mathbf{r} \to \mathbf{r}/\rho$, $\mathbf{k} \to \mathbf{k}\rho$, where $\rho = mcv_0/q\bar{B}$. Further details can be found in Veltri et al. (1998), Zelenyi et al. (2008a), and Artemyev et al. (2009). We integrate numerically 10^6 trajectories and obtain the displacements in coordinate and velocity space averaged over the particle ensemble: $R^2(t) = \langle |\mathbf{r}(t) - \mathbf{r}_0|^2 \rangle$ and $V^2(t) = \langle |\mathbf{v}(t) - \mathbf{v}_0|^2 \rangle$. It is straightforward (as done by many transport theories) to approximate these terms by power laws: $R^2(t) \propto t^{2\mu}$ and $V^2(t) \propto t^{2\nu}$. Both transport indices are intrinsically coupled in a realistic plasma system. Energization (transport in velocity space) is impossible without particle motion in the configurational space (Zelenyi et al. 2008a; Perri et al. 2009).

Let us first consider an even simpler case without average background magnetic field, $B_{0z} = 0$. The dependence of ν on μ is presented in Fig. 8(a). As one can see, there is a strong correlation between particle acceleration and particle transport. In static magnetic configurations ($v_\phi = 0$) particles do not gain energy ($\nu = 0$) and spatial transport acquires the character of a classical Brownian diffusion with $2\mu = 1$. With increasing ν the spatial transport also intensifies, according to the simple dependence $\mu \approx \nu + 1/2$ (also supported by some analytical considerations, Milovanov 2001).

For the case with background magnetic field, also shown in Fig. 8(a), the situation is somewhat different. For a static case, $\nu \to 0$, as before, but spatial transport is suppressed to a subdiffusion limit ($\mu < 1/2$). These results are important for finite size systems, like the Earth's magnetotail, when spatial scales impose a natural limit on particle energization.

The results for ν were obtained in an asymptotical regime $t \to \infty$. However, the time dependence $V^2(t)$ has more complicated fine structure. As shown in Fig. 8(b), at the initial

stage of acceleration one can obtain $\nu \approx 1$. This is the regime of almost ballistic acceleration. Fast acceleration requires that particles spend sufficient time in the region without magnetic field and with a nonzero value of the electric field. This situation can be realized for particles that interact in a resonance manner with the particular wave from the turbulent ensemble. In this case particles are accelerated in a "surfatron" regime (Neishtadt et al. 2009; Artemyev et al. 2010a) being in resonance with a particular wave only at certain times, while other waves provide only magnetic background turbulence. The surfatron mechanism provides acceleration of particles moving along the electric field while being trapped (or captured) inside a local potential minimum in the region of suppressed magnetic field. In the case of particle resonance the trapping results from a balance between the Lorentz forces of the background magnetic field and that provided by the magnetic field of the wave. However, the surfatron mechanism can be realized in many other configurations. For example, surfatron acceleration in the vicinity of an X-line, described in Sect. 3, results from trapping provided by the potential well of the polarization electric field in the boundary layer between the current sheet and the lobe. When particles gain sufficient energy the probability of capture into resonance with a single wave decreases (Neishtadt et al. 2009; Artemyev et al. 2010a). This is a second acceleration regime when particle begin to interact with the entire ensemble. In this regime fluctuations of the electromagnetic field can be considered as random and acceleration acquires a diffusive character.

2.4.2 3D Model

Now we consider particle acceleration in a more realistic 3D case, potentially relevant for magnetotail acceleration (Artemyev et al. 2009; Perri et al. 2011). In this case particles can be efficiently accelerated only in the vicinity of the neutral sheet. The residence time of a given particle in the central region of the CS is strongly limited (Speiser 1965; Orazberdyev and Trakhtengerts 1973). In the simplest case of CS configuration it is of the order of $\sim mc/qB_z$. The turbulence level also significantly influences the time which a particle spends near the CS (Greco et al. 2002; Artemyev et al. 2009). However, particles can gain relatively large amounts of energy even for such "unfavorable" conditions.

To model particle acceleration in a turbulent CS we use a configuration with $\mathbf{B}_0 = B_0 \tanh(z/L_z)\mathbf{e}_x + B_{0z}\mathbf{e}_z$ and add 3D turbulence $\delta\mathbf{B}$ described in Veltri et al. (1998), and Artemyev et al. (2009). At the boundary of the CS ($z = \pm 3L_z$) we launch cold ion beams propagating towards the neutral plane. Particles move along field lines and penetrate into the central region of the CS. In the vicinity of the neutral sheet these particles interact with the turbulence and leave the CS following usual Speiser orbits. Accelerated particles are collected to obtain the resulting energy distribution at system boundaries (Fig. 8(c)). The acceleration regime has a diffusive character (Artemyev et al. 2009).

As one can see in Fig. 8(c), resulting distributions acquire a tail of high-energy particles. The average energy of an ensemble increases by more than an order of magnitude. Therefore this mechanism can be considered as a candidate for particle acceleration during moderately disturbed periods in the magnetotail.

2.5 Analytical Models of X-line Acceleration

Magnetotail magnetic reconnection is the one of main sources of particle (electron and ion) energization. Numerical simulations represent a very effective approach to reveal the important general characteristics of this widespread physical process (see, e.g., Pritchett 2006; Drake et al. 2006; Birn and Hesse 2010). However, analytical methods which are more

"transparent" physically still keep their value as a relatively easy and straightforward way to understand the various "subtle" features of the reconnection phenomenon.

Analytical models of particle energization related to reconnection may be divided into two groups: stationary models and dynamical models. The first group includes various models of electron and ion acceleration in the X-line magnetic field with a constant electric field. The second group concentrates on the study of particle acceleration during the appearance of an X-line and its subsequent evolution.

Dynamics of heavy ions and light electrons in the vicinity of an X-line are quantitatively different. In the Earth's magnetotail energy release related to magnetic reconnection cannot provide acceleration of ions up to relativistic energies, however electrons are easily reaching the relativistic limit.

The distribution of the electromagnetic field in the vicinity of a stationary X-line can be represented in the following simple form: magnetic field is $\mathbf{B} = B_0(z/L_z)\mathbf{e}_x + B_0(x/L_x)\mathbf{e}_z$ and electric field is $\mathbf{E} = E_0\mathbf{e}_y$. The spatial scales L_z and L_x differ according to the stretched configuration of the magnetotail. The theory of particle acceleration in such geometry is rather straightforward and has been developed by many authors since the 70-ies (Bulanov and Sasorov 1976; Burkhart et al. 1990; Vekstein and Priest 1995; Divin et al. 2010).

We consider the motion of nonrelativistic protons (m_p, $q > 0$) and relativistic electrons (m_e, $q_e = -q < 0$) and introduce dimensionless variables for protons ($\mathbf{v} \to \mathbf{v}/v_0$, $t \to t\Omega_p$, $\mathbf{r} \to \mathbf{r}\Omega_p/v_0$, $\alpha_{x,z} = v_0/(L_{x,z}\Omega_p)$, where $\Omega_{p,e} = qB_0/m_{p,e}c$, v_0 is the typical particle velocity) and for electrons ($\mathbf{p} \to \mathbf{p}/m_e c$, $\mathbf{v} = \mathbf{p}/\gamma$, $t \to t\Omega_e$, $\mathbf{r} \to \mathbf{r}\Omega_e/c$, $\delta_{x,z} = c/(L_{x,z}\Omega_e)$, where $\gamma = \sqrt{1+\mathbf{p}^2}$), and dimensionless parameters $u_{Dp} = cE_0/v_0B_0$, $u_{De} = E_0/B_0$. From the conservation of the momentum along the y-axis one can obtain $v_y = u_{Dp}t + (\alpha_z z - \alpha_x x)$ and $p_y = -u_{De}t - (\delta_z z - \delta_x x)$. For particles accelerated in the vicinity of the X-line these expressions can be reduced to $v_y \approx u_{Dp}t$ and $p_y \approx -u_{De}t$. Equations of motion along x and z can be written taking into account $\gamma \approx |\mathbf{p}| \approx u_{De}t$ (this holds only for high-energy particles, see Bulanov and Sasorov 1976; Burkhart et al. 1990; Vekstein and Priest 1995):

$$\begin{array}{ll} \text{protons} & \text{electrons} \\ \begin{cases} \ddot{x} = \alpha_x u_{Dp} t x \\ \ddot{z} = -\alpha_z u_{Dp} t z, \end{cases} & \begin{cases} u_D t\ddot{x} + u_D\dot{x} = \delta_x x \\ u_D t\ddot{z} + u_D\dot{z} = -\delta_z z. \end{cases} \end{array}$$

One can obtain the solution of this system for protons ($x_p(t) \sim \mathrm{Bi}(t\alpha_x^{1/3}u_{Dp}^{1/3})$, $z_p(t) \sim \mathrm{Bi}(-t\alpha_x^{1/3}u_{Dp}^{1/3})$, where Bi is the Airy wave function) and for electrons ($x_e(t) \sim \mathrm{I}_0(2\sqrt{t\delta_x/u_{De}})$ and $z_e(t) \sim \mathrm{J}_0(2\sqrt{t\delta_z/u_{De}})$, where J_0 and I_0 are Bessel functions of real and complex arguments, correspondingly).

The coordinate $x(t)$ grows with time exponentially both for electrons and protons and the particle motion in this direction becomes unstable. Energy gain in such systems is possible only during a time interval $t_p \sim (\alpha_x u_{Dp})^{-1/3}$ and $t_e \sim u_{De}/\delta_x$. After this time particles leave the acceleration region (vicinity of X-line). Therefore, the maximum energy gain possible for such a "steady reconnection" regime follows as $\frac{1}{2}v_{y,\max}^2 \approx \frac{1}{2}(u_{Dp}t_p)^2 = \frac{1}{2}(u_{Dp}^2/\alpha_x)^{2/3}$ for ions and $\gamma_{e,\max} \approx u_{De}t_e = u_{De}^2/\delta_x$ for electrons.

The complementary dynamical approach considers the effects related to the formation of the X-line. This process can be described as the growth of an ion tearing mode. Following the ideas by Galeev et al. (1978), we assume that the initial stage of the tearing mode has an explosive character. Then we can write $\mathbf{B} = B_0(z/L_z)\mathbf{e}_x + B_0\lambda(t)(x/L_x)\mathbf{e}_z$ and $\mathbf{E} = E_0\dot{\lambda}(t)\mathbf{e}_y$, where $\lambda(t) = (t - t_{\max}/t_0)/(1 - t/t_0)$, t_0 is the time scale of the tearing growth

and $t_{\max} < t_0$ is the duration of the first stage of tearing. Dimensionless equations of motion in this case take a form (see Zelenyi et al. 1984, 1990):

$$\begin{array}{ll} \text{protons} & \text{electrons} \\ \begin{cases} \ddot{x} = \alpha_x u_{Dp} \lambda^2(t) x \\ \ddot{z} = -\alpha_z u_{Dp} \lambda^2(t) z, \end{cases} & \begin{cases} \ddot{x} + (\dot{\lambda}(t)/\lambda(t))\dot{x} = (\delta_x/u_{De})x \\ \ddot{z} + (\dot{\lambda}(t)/\lambda(t))\dot{z} = -(\delta_z/u_{De})x. \end{cases} \end{array}$$

Solutions of these equations for protons and for electrons are: $x_p(t) \sim (1 - t/t_0)^{A_\pm/2}$ and $x_e(t) \sim (1 - t/t_0) I_1(\sqrt{\delta_x/u_{D_e}}(1 - t/t_0))$, where $A_\pm = 1 \pm \sqrt{1 + 4\alpha_x u_{Dp}(t_0 - t_{\max})}$. For protons $x_p \sim (1 - t/t_0)^{A_-/2} \to \infty$ as $t \to t_0$ in agreement with Zelenyi et al. (1984). Thus, the proton motion becomes unstable and protons can spend only a limited time interval, t_p, in the vicinity of the X-line in a framework of the dynamical model as well as in the steady case. From equation $x(t_p)\alpha_x \sim 1$ one can obtain $t_p \sim t_0(1 - \alpha_x^{-2/A_-})$ and the maximum energy gain of protons can be estimated as $\frac{1}{2} v_{y,\max}^2 \sim \frac{1}{2}(u_{Dp}\lambda(t_p))^2$.

For electrons the situation is very different. Their motion in the dynamic case appears to be stable: $x_e(t) \sim (1 - t/t_0) I_1(\sqrt{\delta_x/u_{D_e}}(1 - t/t_0)) \to 0$ as $t \to t_0$. Therefore, electrons can spend all available time $t_{\max}$ in the acceleration region (vicinity of the X-line) and gain maximum possible energy $\gamma_{e,\max} \approx u_{De}\lambda(t_{\max}) = u_{De}$.

The analytical considerations described above can be applied to find the expressions for energy distributions of protons $F_p(\varepsilon)$ and electrons $F_e(\varepsilon)$. For the case of stationary X-line these distributions were obtained by Bulanov and Sasorov (1976): $F_p(\varepsilon) \sim (2\varepsilon/v_{y,\max}^2)^{1/8} \exp\{-(2\varepsilon/v_{y,\max}^2)^{3/4}\}$ and $F_e(\varepsilon) \sim \exp\{-(\varepsilon/\gamma_{e,\max})^{1/2}\}$. Energy distribution of protons due to acceleration by dynamical X-line was obtained by Galeev (Galeev 1979): $F_p(\varepsilon) \sim (2\varepsilon/v_{y,\max}^2)^{1-A_+/2}$.

In this section we considered only direct particle acceleration from the electric field along an X-line. However, the acceleration during magnetic reconnection includes many other mechanisms (e.g., betatron acceleration in the pileup region, surfatron acceleration, etc.), which can contribute to the energy gain of ions and electrons; these mechanisms will be discussed in Sect. 3.

2.6 Summary

In this section we have provided insights into typical particle orbits and acceleration mechanisms that operate in the magnetotail current sheet, using simplified models to obtain quantitative estimates of energy gains. These mechanisms include X-line and current sheet acceleration and scattering as well as betatron and Fermi acceleration associated with temporal or spatial variations of the underlying electromagnetic fields. Quasi-steady approaches were complemented by models of turbulent acceleration. Analytical calculations can be a very powerful tool complementing numerical methods discussed in the following sections. A number of additional realistic effects influencing energetic particle distributions, including magnetic shear (Bulanov 1980), incoming particles (Zelenyi et al. 1984, 1990), betatron effects far from the X-line (Vainshtein et al. 2005; Hoshino 2005), can also be investigated using simple and elucidating analytical calculations.

3 Acceleration in the Vicinity of the Reconnection Site

In Sect. 2 we have used simplified analytical approaches to investigate basic acceleration processes, which also included an analytic approach to acceleration in the vicinity of an

X-line. In Sect. 4 we will focus on consequences of near-tail reconnection, particularly in relation to magnetospheric substorms. However, reconnection may occur almost anywhere along the tail, with and without relation to substorms, and be the cause of particle acceleration. In this section we focus on the acceleration mechanisms in the immediate vicinity of a tail reconnection site. After a brief discussion of observations (Sect. 3.1) we present insights from particle-in-cell (PIC) simulations (Sect. 3.2), followed by a summary and short discussion of open problems (Sect. 3.3).

3.1 Observations in the Magnetotail

The supra-thermal particle acceleration by reconnection has been extensively discussed in the terrestrial magnetosphere based on *in situ* plasma observations. In the early satellite observations, energetic particle bursts in the magnetotail have been reported (Sarris et al. 1976; Hones 1979), and those bursts have been identified to be associated with magnetic reconnection (Baker and Stone 1977; Terasawa and Nishida 1976; Moebius et al. 1983).

In the course of magnetic reconnection in the Earth's magnetotail, cold lobe plasma situated outside the current sheet can be transported into the current sheet, and then ions and electrons are heated up to a few keV and several 100 eV, respectively. Roughly, the heated ion thermal velocity is known to be about the Alfvén speed defined by the lobe magnetic field (B_{lobe}) and the density in the current sheet (n_{ps}). This suggests that reconnection and the thermalization of the reconnection outflow is an important (perhaps dominant) factor in heating the ion plasma sheet population. However, the same argument fails in explaining the observed electron temperatures, which are lower than the ion temperatures by a factor of 5–7. Therefore plasma sheet heating, together with the particle entry mechanisms, remains an unsolved problem.

The heated plasma does not necessarily have a Maxwellian distribution function and often shows non-gyrotropic distributions (Hoshino et al. 1998), because the scale length of the current sheet in the vicinity of the reconnection region is of the order of an ion gyro-radius, and because the mean free path is much larger than the scale length of reconnection. In addition to non-Maxwellian features, more importantly, supra-thermal particles, whose energies significantly exceed the thermal energy, can be efficiently generated in the reconnection region. In the Earth's magnetotail, non-thermal electrons can be accelerated to at least several 100 keV (e.g., Øieroset et al. 2002), and energetic electrons reaching $\sim$1 MeV are believed to be generated in strong reconnection events. Non-thermal ions during reconnection have been reported by several satellite observations as well (e.g., Moebius et al. 1983), but the literature on energetic ion observations (outside of geosynchronous orbit) is limited.

Figure 9 shows the electron energy spectrum in and around the diffusion region of reconnection observed by the Wind satellite in the mid tail (Øieroset et al. 2002). The low-energy distribution can be fitted by a Maxwellian distribution with 400 eV, while the non-thermal high-energy electrons can be seen at least up to 300 keV. The non-thermal electron spectra can be approximated by a power law distribution of $f \propto E^{-s}$ with the power law index $s = 4.8$–5.7. The observation of the high-energy particles is difficult due to the very low fluxes of energetic particles, but the maximum attainable energy in the tail reconnection is known to reach up to about 1 MeV. On the other hand, the available potential energy across the reconnection region can be estimated as

$$e\phi \simeq 200\left(\frac{v_A}{500\ \mathrm{km/s}}\right)\left(\frac{B_{lobe}}{20\ \mathrm{nT}}\right)\left(\frac{M}{0.1}\right)\left(\frac{L}{30R_E}\right)\ \mathrm{keV}, \tag{10}$$

where M is the reconnection rate, L is the scale length of the magnetotail cross-section, and B_{lobe} is the typical lobe magnetic field. Therefore, the maximum attainable energy observed

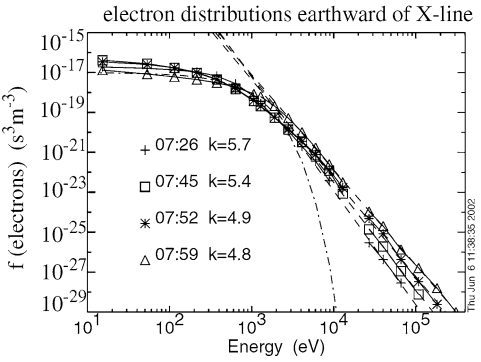

Fig. 9 Electron energy spectra observed just on the earthward side of an X-type region. The power-law indexes k of four different time periods are shown in the plot. Adapted from Øieroset et al. (2002)

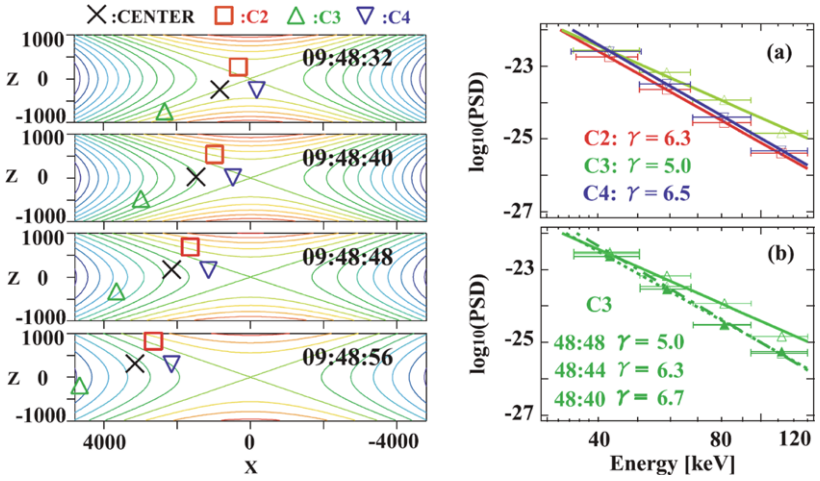

Fig. 10 The *left-hand panel* represents the locations of three Cluster satellites C2, C3 and C4 of four different time periods, while the *right-hand panel* shows the energy spectra at the peak enhancement time (*top*) and that of C3 for three different time periods (*bottom*). The power-law indexes γ are shown in the plot. Adapted from Imada et al. (2007)

in the tail seems to exceed the available potential energy. Note that the length of the active reconnection region is probably less than the size of the tail cross-section, and in such a case the available potential energy should be even smaller than the above estimation.

Figure 10 shows multi-point satellite observations of reconnection by the four Cluster satellites, indicating in detail the locations of energetic electron enhancements (Imada et al. 2007). The left-hand panels show the positions of three satellites, C2, C3 and C4, which are calculated based on a model magnetic field assuming that the reconnecting magnetic field can be described by $\mathbf{B} = B_{lobe}(\alpha(x/\lambda_x)\mathbf{e_z} + \tanh(z/\lambda_z)\mathbf{e_x})$. The free parameters of B_{lobe}, α, λ_x, and λ_z can be fitted by using the four-spacecraft data. The right-hand top panel shows the electron energy spectrum integrated over pitch angles at the peak enhancement time of energetic electrons, that is, the spectrum for C2 is taken at 0948:40, C3 at 0948:48 and C4 at 0948:39. The γ values represent the power law indexes, which may vary by many effects such as the activity of reconnection, the position from the X-type neutral point and so on. Taking into account these effects, one can say that the observed power law indexes from 5.0 to 6.3 are basically consistent with other observations in magnetotail (e.g., Øieroset et

al. 2002). Since the satellite C3 has the hardest spectrum among the three satellites, let us look carefully at the relationship between the energetic electron spectrum and the position of satellite C3 in the reconnection region. The satellite C3, which is indicated by the triangle symbol, is situated outside the separatrix of reconnection at the time of 0948:32, and enters into the downstream region of reconnection after 0948:40. The hardest electron spectrum of C3 at 0948:48 corresponds to the magnetic field pile-up region, namely the region between the X-type neutral point and the O-type point. This result is consistent with Geotail observations analyzed by superposed epoch analysis of the reconnection region by Imada et al. (2005). They concluded that the electrons are accelerated by the gradient/curvature B drift in the magnetic pileup region as well as by the direct acceleration in the diffusion region.

The relationship between the enhancement of energetic electron fluxes and magnetic islands has been also studied. Chen et al. (2008) found that energetic electrons have peak fluxes at sites of compressed density within small magnetic islands. Retinò et al. (2008) showed that the enhancement of energetic electron flux is associated with flux rope coalescence, and discussed that not only the direct acceleration by the reconnection electric field in the diffusion region but also the betatron acceleration with non-adiabatic pitch-angle scattering is an import agent for electron acceleration. This effect will be further discussed in Sect. 4 in relation to injection events in the near tail.

3.2 Simulation Studies of Reconnection

In order to understand the particle acceleration in reconnection, the nonlinear time evolution of a thin current sheet has been studied by many different research groups (e.g., Hoshino et al. 2001; Drake et al. 2003; Pritchett 2008; Oka et al. 2010) using particle-in-cell (PIC) simulations. Basically they assumed a Harris current sheet as the initial condition where the thickness of current sheet is of the order of an ion inertia length, as suggested by the satellite observation in the tail. Several important acceleration mechanisms have been proposed, operating in various different regions: (1) the X-type region, which basically coincides with the magnetic diffusion region, (2) magnetic field pileup region where the reconnection jets interact with the pre-existing plasmas at rest, (3) the magnetic island formed in a long current sheet, (4) the coalescence region of two magnetic islands, and (5) the boundary layer between the lobe and the plasma sheet.

One of the most important processes is the Speiser particle motion in the vicinity of the X-type region, discussed in Sect. 2. At the X-type region of reconnection, the charged particles, which are transported from the lobes by $E \times B$ drift motion, can be accelerated along the reconnection electric field (E) parallel to the electric current. During the acceleration, the particles can be ejected from the weak magnetic field region due to the Lorentz force of the reconnecting magnetic field. The energy gain by the Speiser motion depends on the electromagnetic field structure in the vicinity of the X-type region, and if the domain size of weak magnetic field region (i.e., magnetic diffusion region) were large, the particles can be efficiently accelerated by staying long inside the magnetic diffusion region. The core populations of ions and electrons can be accelerated to the order of the standard Alfvén velocity ($B/\sqrt{4\pi n_{ps} m_i}$) and the electron Alfvén velocity ($B/\sqrt{4\pi n_{ps} m_e}$), respectively (e.g., Shay et al. 2001).

Both ions and electrons can follow Speiser acceleration in the X-type region, but the electron Speiser acceleration can only occur very close to the X-line where electrons are unmagnetized. The thickness of this region is of the order of the electron inertia length (c/ω_{pe}). Due to the smallness of this acceleration region, other acceleration processes are needed to explain the observed large non-thermal electron fluxes. As reported by Cluster

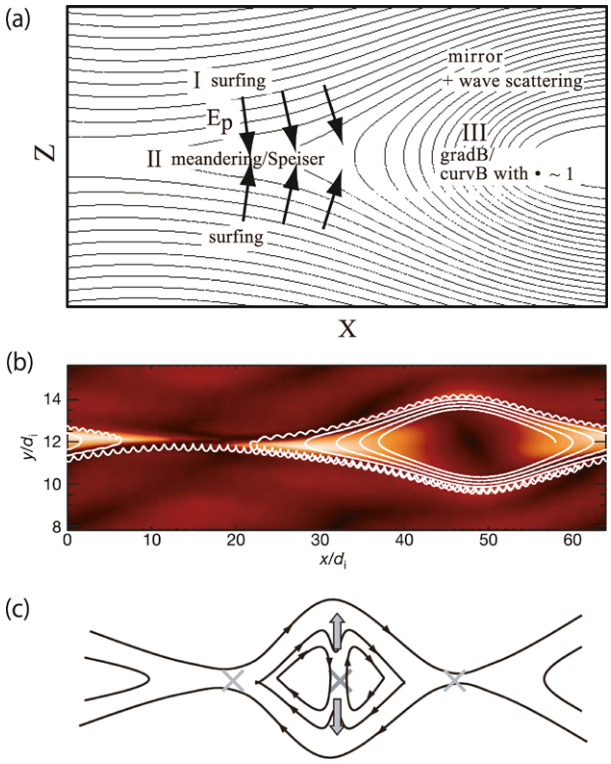

Fig. 11 Several particle acceleration models proposed based on Particle-In-Cell (PIC) simulations. (**a**) the multi-step acceleration model with the Speiser motion in the diffusion region, the chaotic, gradient/curvature B drift motion in the magnetic field pileup region, and the surfing/surfatron acceleration in the boundary, (**b**) the magnetic island acceleration during the contracting motion, showing an electron path (*white contour*) on the background of the electric field (*color*), and (**c**) the island merging/coalescence acceleration where a strong reconnection electric field is initiated due to the coalescence instability. Adapted from Hoshino (2005), Drake et al. (2006), and Oka et al. (2010)

observations (Imada et al. 2007), in addition to the Speiser/meandering particle acceleration in the X-type region, energetic electrons can be further accelerated in the magnetic field pileup region produced by compression of the reconnection outflow. Hoshino et al. (2001) demonstrated in PIC simulation that electron acceleration first occurs near the X-type region, and those pre-accelerated electrons are further accelerated during ∇B and/or curvature B drift motion around the magnetic pileup region.

During this stage, if the particle is magnetized in the magnetic field, the adiabatic invariant $v_\perp^2/B$ is conserved and the energy gain is limited to the change of the magnetic field across the pileup magnetic field region. However, if the gyro-radius of those accelerated electrons is almost equal to the curvature radius of the reconnecting magnetic field [i.e., the κ value, Eq. (3) in Sect. 2.2, is the order of unity], the energetic electrons exhibit a chaotic behavior during the acceleration, and the electrons can be scattered toward larger pitch angles due to a centrifugal force perturbing the particle gyro-motion in a weak magnetic field region (Büchner and Zelenyi 1989; Delcourt et al. 1996). This scattering process has a tendency to trap particles inside the plasma sheet, which in turn contributes to the preferential acceleration of hot electrons. For magnetic reconnection in a thin current sheet, this process can play an important role in the non-thermal electron acceleration. These processes are envisioned in Fig. 11(a), as the meandering/Speiser (II) and the grad B/curv B with $\kappa \sim 1$ (III).

It is noteworthy that a polarization electric field develops in the boundary layer between the current sheet and the lobe for thin current sheet reconnection. The polarization electric field is induced in association with the Hall reconnection (e.g., Birn et al. 2001; Nagai et al. 2001). Hoshino (2005) demonstrated by using a particle-in-cell simulation

that electrons can be trapped by the electrostatic potential well of the polarization electric field, and during the trapping phase the electrons can gain their energies from the convection/inductive reconnection electric field (i.e., the dawn-to-dusk electric field in tail coordinates) through the so-called surfing/surfatron acceleration (e.g., Sagdeev and Shapiro 1973). The polarization electric field is enhanced for driven reconnection with additional Poynting flux injected from the lobe boundary, and then the production of energetic electrons increases.

Not only the X-type and magnetic field pileup regions but also magnetic islands bounded by two X-type reconnection regions may involve another important particle acceleration mechanism. For a long current sheet, many X-type regions can be simultaneously generated during reconnection, with magnetic islands bounded by two X-type regions at each end. The magnetic islands continue growing and the magnetic field lines start shrinking. During this contracting motion of islands, the particles gain energy by reflecting from the ends of the contracting magnetic islands (Drake et al. 2006). Figure 11(b) shows an electron trajectory within a contracting island. The electron can gain the energy from the electric field driving the contracting motion of the magnetic island during each turn/reflection in the current sheet.

Another interesting acceleration process occurs during multi-island coalescence stage. The coalescence is the process of the merging of two magnetic islands through reconnection (Finn and Kaw 1977). Since two magnetic islands with parallel currents undergo Lorentz forces that attract each other, the reconnection electric field can be strongly enhanced due to the contraction motion (Pritchett and Wu 1979). Recently electron energization of coalescence has been studied in detail by PIC simulations, and it is reported that magnetic reconnection during coalescence of the magnetic islands leads to efficient energization of electrons (Pritchett 2008; Oka et al. 2010). The schematic illustration of this process is shown in Fig. 11(c). Note that the flow directions generated by the coalescence are north- and southward in the tail coordinates, with the direction of the electric field from dusk to dawn, opposite to the dawn-to-dusk direction of the original reconnection field at the X-type region. Therefore, the combined acceleration of the original X-type and the coalescence reconnection may modify the simple estimation of the available potential energy given in Eq. (10).

3.3 Summary and Unresolved Issues

The non-thermal electron acceleration in the magnetotail has been extensively studied by combining sophisticated satellite observations and numerical simulations. Most of the observed characteristics of electron acceleration by reconnection can be successfully reproduced by particle-in-cell (PIC) simulations. This acceleration is a complex problem, and several different mechanisms seem to contribute to electron energization in the vicinity of a reconnection region. To understand what controls the electron acceleration efficiency, Imada et al. (2011) studied statistically reconnection characteristics, using Geotail data, and found that the electrons are efficiently accelerated in a thin current sheet during fast reconnection events.

Compared to the electron acceleration, the observational and computational studies of ion acceleration are limited, and our understanding is not matured to conclude whether or not the reconnection in the vicinity of an X-type region is a strong ion accelerator. Since ions in general are not magnetized in the reconnection region, one may postulate that ion acceleration could happen more easily than electron acceleration, but the issue of ion acceleration is still controversial. In fact, some observations reported ion acceleration during a reconnection event (e.g., Moebius et al. 1983), but other observations found no enhancement of energetic

ion fluxes in reconnection events even though electron acceleration was clearly observed (e.g., Øieroset et al. 2002). Where and how ion acceleration can be generated remains an open issue.

The situation is different in the near tail, and in particular at geosynchronous orbit, where a wealth of observations have demonstrated the occurrence of energetic ion flux increases (injections) together with energetic electron injections. The characteristics and present understanding of such events are discussed in the following section.

4 Substorm Injections

Substorm injections are rapid flux increases of energetic particles in the range of a few tens of keV to hundreds of keV. The fluxes can rise by more than an order of magnitude over a time of a few minutes or less. They tend to be closely related to substorm onset and are best documented by geosynchronous observations (Parks et al. 1968; Lezniak et al. 1968; Arnoldy and Chan 1969), but do also occur farther out and, more rarely, inside of geosynchronous orbit. In Sect. 4.1 we first present some characteristic observations, followed in 4.2 by insights into the acceleration mechanisms obtained particularly from test particle simulations in time dependent electromagnetic fields.

4.1 Observations

The distinction between dispersionless injections, occurring simultaneously over a wide range of energies, and dispersed events led to the idea of an "injection boundary" (McIlwain 1974; Mauk and McIlwain 1974), which bounds the region where fluxes become simultaneously enhanced at different energies. Energetic particles observed outside of this region get there by energy-dependent azimuthal drift and hence appear dispersed in energy, with electrons drifting eastward (Arnoldy and Chan 1969; Pfitzer and Winckler 1969) and ions drifting westward (Bogott and Mozer 1973). Full 360 degree azimuthal drifts (or even multiple such drifts) of energetic particles, injected locally on the nightside, may also lead to "drift echos" (Belian et al. 1978), consisting of dispersed secondary peaks of the particle fluxes.

Observations indicate a close correlation of changes in the energetic particle fluxes with local magnetic field changes (Lezniak and Winckler 1970; Swanson 1978). For periods typically 1–2 hours prior to the onset of substorms, electron distributions, observed in the premidnight sector, become peaked along the direction of the local magnetic field. These "cigar-like" anisotropies (Baker and Higbie 1978) are accompanied by a local tail-like magnetic field. At substorm onset an abrupt transition usually occurs from the cigar-shaped distributions to pancake-shaped distributions. This is associated with powerful enhancements of energetic particle fluxes extending up to several hundred keV in energy. The anisotropy sequence is thought to be due to the buildup and subsequent release of stresses in the magnetotail; a loss of $\sim 90^\circ$ pitch angle particles through dayside magnetopause interaction might also play a role (Baker and Higbie 1978). The association between injection properties and magnetic field changes was further supported by characteristic changes in the orientation of the symmetry axis of hot electron pressure anisotropy (Thomsen et al. 1996; Birn et al. 1997b), which also indicate a rapid dipolarization following a stretching during the substorm growth phase.

Many hundreds of substorm sequences have been studied from geostationary orbit platforms (Baker and Higbie 1978; Baker et al. 1979, 1981). A particularly clear example is

presented in Fig. 12, studied in detail by Baker et al. (1981). At approximately 0100 UT on December 29, 1976, a large injection of energetic (>30 keV) particles was observed by Los Alamos instrumentation onboard spacecraft 1976-059 at geostationary orbit. This particle enhancement was closely associated with the onset of a major substorm (also at 0100 UT) identified by sharp negative bays in the H components of magnetic records at Leirvogur (Iceland) and Narssarssuaq (Greenland) and by the occurrence of a positive H component bay at 0100 UT in the mid-latitude magnetogram record at M'Bour.

The substorm expansion onset (and concomitant particle flux increase) was preceded (between 2330 and 0100 UT) by a pronounced stretching of the magnetic field into a tail-like configuration and by a development of highly cigar-like (field-aligned) electron distributions at geostationary orbit. DMSP auroral images, taken during the course of the growth and expansion phases of this substorm, as well as ground riometer data, showed clearly that there was no measurable substorm activity as the magnetosphere developed its very stressed, growth-phase configuration prior to substorm expansion onset. These results supported the concept of a storage of energy (growth phase) prior to its rapid release at substorm onset. IMP 8 satellite observations in the high southern magnetotail lobe at $\sim 35 R_E$ geocentric radial distance (top panel of Fig. 12) provided strong corroborative evidence of this storage and subsequent release of magnetic energy.

The lower two panels of Fig. 12 summarize inferred magnetic field and electron anisotropy information for this event. Notice, in particular, the systematic and progressive development of θ_B and C2 throughout this period: θ_B (the field line tilt from a northward GSM coordinate direction) went from an approximately nominal dipole value ($\theta_B \sim 20°$) to an extremely tail-like value ($\theta_B \sim 90°$) with the magnetic field essentially parallel to the magnetic equatorial plane. This magnetic topology is more characteristic of the distant plasma sheet than of the near-Earth magnetosphere. Near the substorm onset at 0100 UT, θ_B rapidly returned to a much more dipolar value.

A systematic study of dispersionless injections, observed during the full year 1990 by the geosynchronous spacecraft 1989-046 (Birn et al. 1997b), revealed further characteristics:

(1) Dispersionless ion and electron injections tend to occur simultaneously near midnight ($p+e$ events), but may be offset by a few minutes away from midnight, such that ion injections precede electron injections ($p \rightarrow e$ events) prior to midnight with the opposite past midnight ($e \rightarrow p$ events) (Birn et al. 1997b). Even farther away from midnight they may occur without being accompanied by significant injections of the other species, even before the dispersion becomes measurable. Figure 13 shows a $p \rightarrow e$ event obtained from the geosynchronous spacecraft 1989-046 on April 13, 1990. The left panels show electron (top) and ion (bottom) fluxes as function of time. Interestingly, the increases of the lower energy electron fluxes (< 20 keV), obtained by the "Magnetospheric Plasma Analyzer" (MPA) (Bame et al. 1993), precede those above 40 keV by several minutes and follow more closely the higher-energy ion fluxes, obtained by the "Synchronous Orbit Particle Analyzer" (SOPA) (Belian et al. 1992). No significant flux increases are observed for ions below 40 keV.

(2) The flux enhancements are limited in energy range, from a few keV to hundreds of keV for electrons and a few tens of keV to hundreds of keV for ions. This is illustrated by the right panels in Fig. 13, showing electron (top) and ion (bottom) distribution functions obtained by MPA ($E < 40$ keV) and SOPA ($E > 40$ keV) for the same event (Birn et al. 1997a, 1997b). The figure further illustrates electron flux increases in the range from ~5 keV to ~80 keV, coinciding with the ion flux increases above 40 keV, followed ~7 minutes later by more energetic electron flux increases above ~20 keV. The survey of Birn et al. (1997b) also showed that, on average, the particle flux increases resulted in

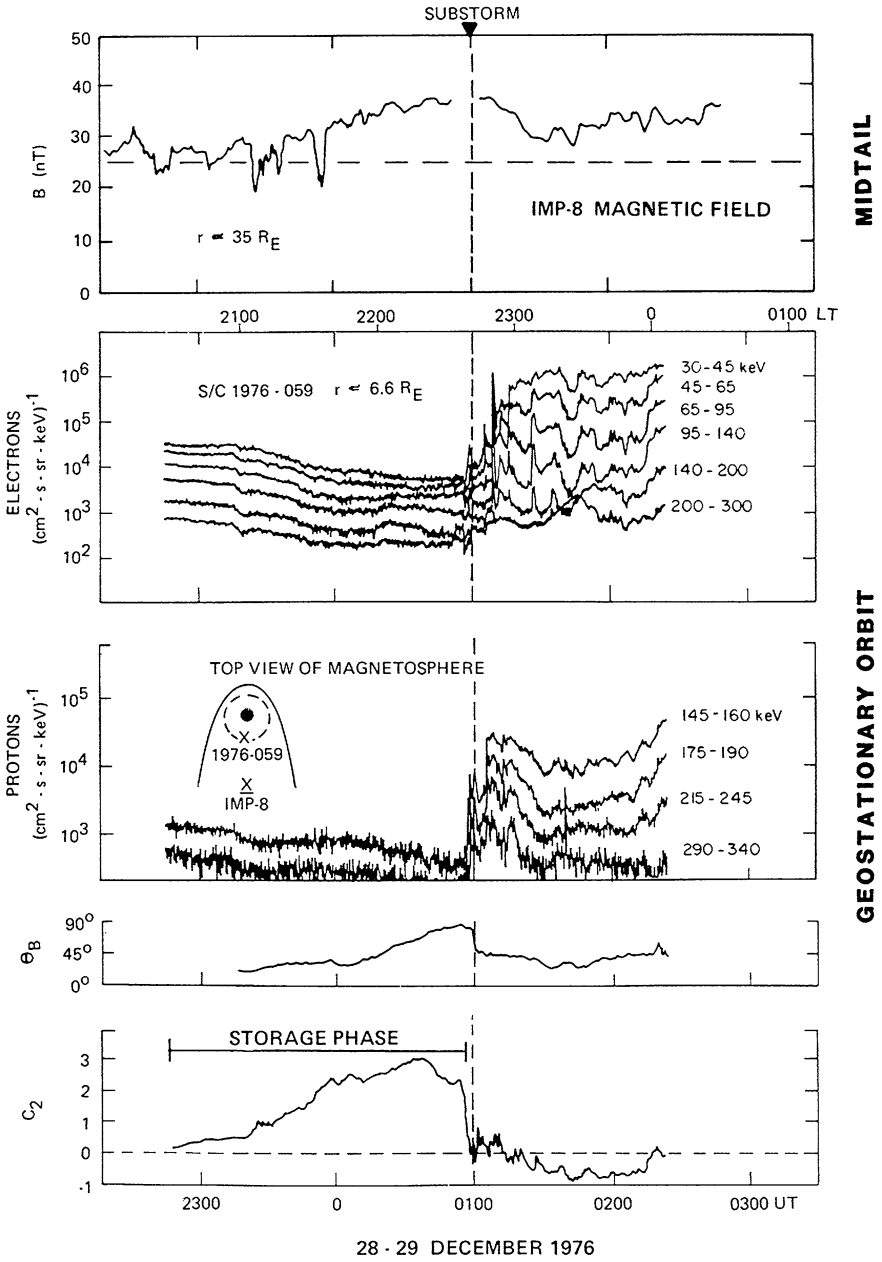

Fig. 12 Characteristic field and particle flux changes during a substorm on December 29, 1976. The *top panel* shows the mid-tail ($\sim 35R_E$) IMP 8 magnetic field magnitude. The *second and third* panel show energetic electron and ion (presumed to be proton) fluxes obtained at geosynchronous orbit by the Los Alamos spacecraft 1976-059. The *lower two panels* indicate the inferred magnetic field orientation and the electron anisotropy parameter C2. After Baker et al. (1981)

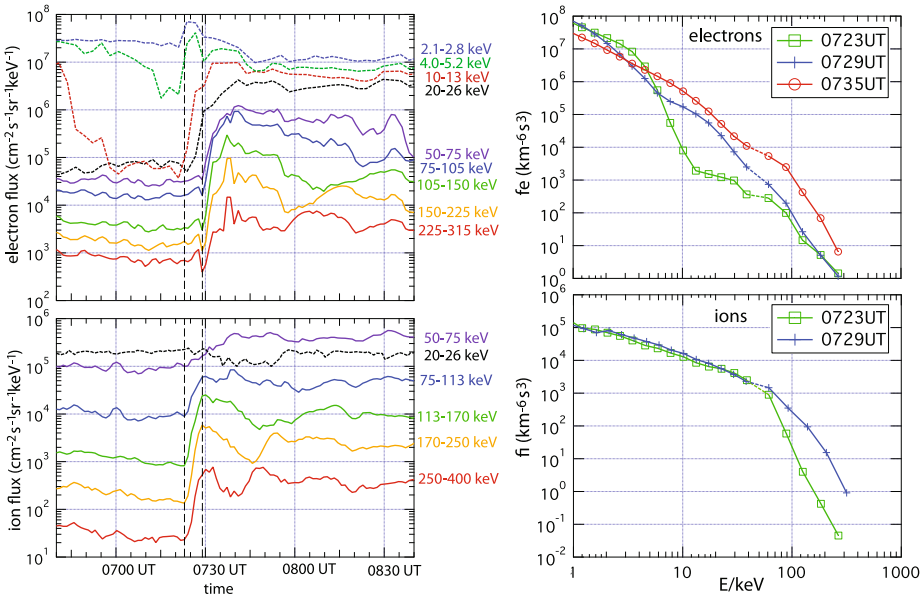

Fig. 13 (*Left panels*) Electron and ion fluxes, (right panels) electron and ion distribution functions, obtained from the geosynchronous spacecraft 1989-046 on April 13, 1990. The *color-coded contours in the left panels* represent various energies as indicated. *Solid lines* represent fluxes obtained by SOPA and *dotted lines* fluxes obtained by MPA. The *dashed vertical lines* indicate injection onset times for ions and electrons. The energy distributions *on the right* are comprised of MPA measurements for $E < 50$ kEV and SOPA measurements for $E > 50$ keV. Modified after Birn et al. (1997a, 1997b)

temperature, or rather, average energy, increases from ∼1 keV to ∼2 keV for electrons, and ∼10 keV to ∼16 keV for ions; the latter almost entirely due to flux increases above 40 keV.

While most of the injection events show flux increases only up to a few hundred of keV, some events may reach energies of 1 MeV or higher. The impulsive nature of several such events was documented by multiple proton drift echos (e.g., Belian et al. 1978; Baker et al. 1979). These events appear to occur particularly under strong solar wind driving, when the magnetosphere becomes more stressed.

4.2 Simulations and Interpretations

The observations of energetic particle injections at geosynchronous orbit put stringent conditions on the possible acceleration site and mechanisms. The fact that dispersionless injections are observed near 6.6 R_E is inconsistent with a direct source from acceleration at a reconnection site, which is commonly inferred to be close to 15–20 R_E distance or even beyond. The clear association with magnetic field dipolarization shows the importance of induced electric fields. The limited azimuthal range of dispersionless injections and the details of energy-dispersed observations demonstrates a strong azimuthal localization of the acceleration region (Reeves et al. 1991).

Insights into, and clarification of the relative importance of acceleration mechanisms have been obtained particularly from investigating test particle orbits in time dependent electromagnetic fields, simulating substorm effects in the near tail. Li et al. (1998) and Zaharia et al. (2000) successfully modeled dispersionless injections and subsequent drift echos

by tracing electron drift orbits in the equatorial plane, using assumed localized, earthward propagating electric field pulses, $E_y(x, y, t)$, in fixed magnetic fields. These models did not incorporate the self-consistent change of the magnetic field (dipolarization) associated with the spatial variation of E_y. A more self-consistent approach was used by Birn et al. (1997a, 1998, 2004b) and, more recently, by Ashour-Abdalla et al. (2011), who used the electric and magnetic fields from MHD simulations of magnetotail reconnection, earthward flow, and magnetic field collapse, to trace ion and electron test particles. As these models included both the magnetic reconnection site and the dipolarizing region, they also permitted to investigate their relative importance.

In the following we present results primarily from Birn et al. (1997a, 1998, 2004b, 2012), which provide higher spatial and temporal resolution than the simulations by Ashour-Abdallah et al. (2011). (Also, in the latter case, electrons were traced only from a source region just earthward of the reconnection site.) The test particle simulations are based on three-dimensional, time-dependent electric and magnetic fields of simulations of magnetotail reconnection (Birn and Hesse 1996; Birn et al. 2011). Full orbits were integrated for the ions. Although electrons satisfy the adiabatic drift approximation in the inner tail near geosynchronous orbit, their history shows that a significant portion resides on magnetic field lines that have undergone reconnection, so that in the past the electrons have encountered the vicinity of the reconnection site, where the drift approximation breaks down. Birn et al. (2004b) therefore employed a combination of full orbits and drift orbits (using the conservation of the first adiabatic invariant μ) with a switch from one to the other based on the adiabaticity parameter κ [Eq. (3) in Sect. 2]. Particles were traced backwards in time from selected locations until they reached a boundary of the simulation box or the initial state. Liouville's theorem of the conservation of phase space density f along a phase space trajectory was then employed to calculate f at the final destination from the initial and boundary values that were chosen to be consistent with the MHD moments. For further details we refer to Birn et al. (2004b).

4.2.1 Acceleration Mechanisms and Source Regions

In this section we illustrate source regions and acceleration mechanisms by characteristic orbits of ions and electrons. Although protons, and even more so heavier ions, are essentially nonadiabatic in the dynamic near tail region during substorms, while electrons are adiabatic over most of their orbits, the source regions and acceleration mechanisms are quite equivalent. We demonstrate these by a typical orbit of each species.

Figure 14 illustrates typical orbits of accelerated protons and electrons. Figure 14a shows characteristic electron and proton orbits, projected into the x, y plane, overlaid on snapshots of the cross-tail electric field (color). The electric field exhibits the properties of a spatially localized, earthward propagating flow burst. As shown by Birn et al. (2011), this is associated with an enhancement of B_z (dipolarization front). The instantaneous locations of protons and electrons are shown as orange and yellow dots, respectively. The red dashed contours show the instantaneous location of the near-Earth X-line ($B_z = 0$ line). The time unit is 10 s. Figure 14b shows the temporal evolution of the kinetic energy of the particles (red for the electron, orange for the proton). The particles were traced backwards in time from selected locations at $t = 132$, choosing a final energy of 80 keV and pitch angles of 85°.

Both particles show complementary behavior with similar energization. The electron, which satisfied the drift approximation during the final part of the orbit, drifts eastward toward the acceleration site from the dusk flank plasma sheet. When it reaches the region

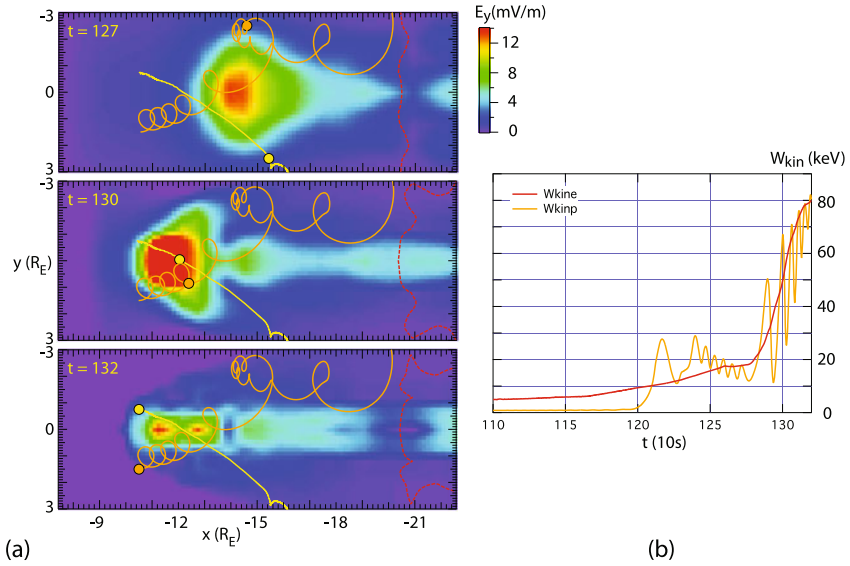

Fig. 14 (**a**) Snapshots of the cross-tail electric field (*color*) from an MHD simulation of tail reconnection and earthward flow (Birn et al. 2011), with overlaid trajectories of a proton (*orange*) and electron (*yellow*), accelerated to a final energy of 80 keV. The instantaneous locations of protons and electrons are shown as *orange and yellow dots*, respectively. The *red dashed contours* show the instantaneous location of the near-Earth X-line ($B_z = 0$). The time unit is 10 s. (**b**) Temporal evolution of the kinetic energy of the two particles (*red*: electron; *orange*: proton). After Birn et al. (2012)

of strong electric field it participates in the earthward collapse and experiences primarily betatron acceleration, associated with the increase of B_z under conservation of the magnetic moment μ.

The proton does not satisfy the drift approximation, and the full orbit was integrated throughout. Nevertheless, its acceleration is quite similar. It initially drifts toward the acceleration region from the dawn flank, exhibiting "Speiser orbits" (see Sect. 2.1), that is, bounces along field lines with mirroring closer to Earth and half-gyration around the B_z field near the equatorial plane (only the last part of such an orbit is shown). At $t \sim 122$ this part of the orbit is close to the neutral line and the proton experiences acceleration in the direction of the electric field, as discussed in Sect. 2. However, about half of that energy is lost during the eastward motion after exit from that region. Subsequently, the proton essentially gyrates around the increasing magnetic field dominated by B_z and becomes accelerated by the fact that the energy gain during the westward part of the orbit exceeds the energy loss during the eastward motion (which is the essence of betatron acceleration). Thus the mechanism and the net energy gain is quite similar to that of the electron, although the proton does not conserve its magnetic moment. The dominant acceleration stems from this last part of the evolution (Fig. 14(b)).

In the case of Fig. 14 the ion and electron originate from the dawn and dusk central plasma sheet. An alternative source region consists of particles on closed field lines with equatorial crossing points tailward of the reconnection site. When these field lines undergo reconnection the particles that are earthward of the reconnection site become trapped on the shortened field line (while the others become ejected with the plasmoid) and undergo betatron and Fermi acceleration on the collapsing field lines. This is illustrated by Fig. 15 for an electron orbit with a final energy of 80 keV and a final pitch angle of 15° in the equatorial

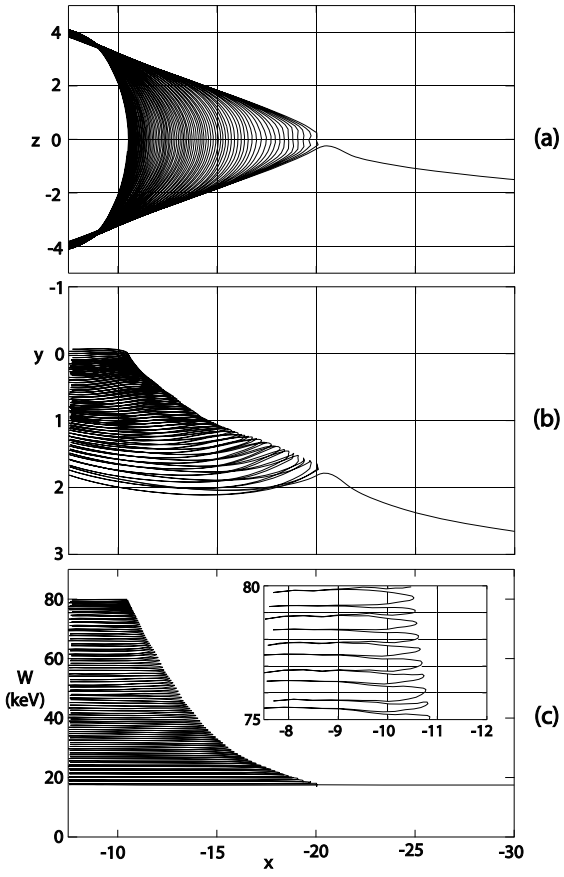

Fig. 15 Characteristic electron acceleration at small pitch angles: (**a**) projection of the orbit into the x, z plane; (**b**) projection into the x, y plane; (**c**) electron energy as function of x with an insert showing an enlargement of the last part. After Birn et al. (2012), based on test particle studies in MHD fields (Birn et al. 2011)

plane, again integrated in the fields of Birn et al. (2011). Figures 15(a)–(b) show projections of the electron orbit into the x, z and x, y plane, respectively. Figure 15(c) shows the electron energy as function of x. The initial orbit follows field lines with equatorial crossing points tailward and dusk-ward of the reconnection site. As the field line undergoes reconnection the electron becomes trapped earthward of the neutral line. (Only the very last portion of the orbit tailward of the reconnection site is shown.) Subsequently it participates in the earthward collapse and the associated acceleration. In this example the electron motion is mostly field aligned. As shown by Fig. 15(c), and particularly the insert, the acceleration takes place in many steps during neutral sheet crossings. This acceleration can be interpreted equally well as current sheet acceleration (in the adiabatic limit), Fermi acceleration of type B, or direct acceleration due to dawnward drift opposite to the electric field.

In summary, we find two typical source regions for accelerated particles: the near-tail plasma sheet flank regions and the closed field line region with equatorial crossing points tailward of the reconnection site. There can also be very effective acceleration of particles that are originally on open field lines (lobes). However, due to their very low density, they cannot contribute significantly to the flux enhancement observed in the near tail and at geosynchronous orbit. The primary acceleration mechanisms for both species can be understood as betatron and first-order Fermi acceleration of type B (Northrop 1963), although ions do not conserve adiabatic invariants during acceleration. Due to pitch angle scattering

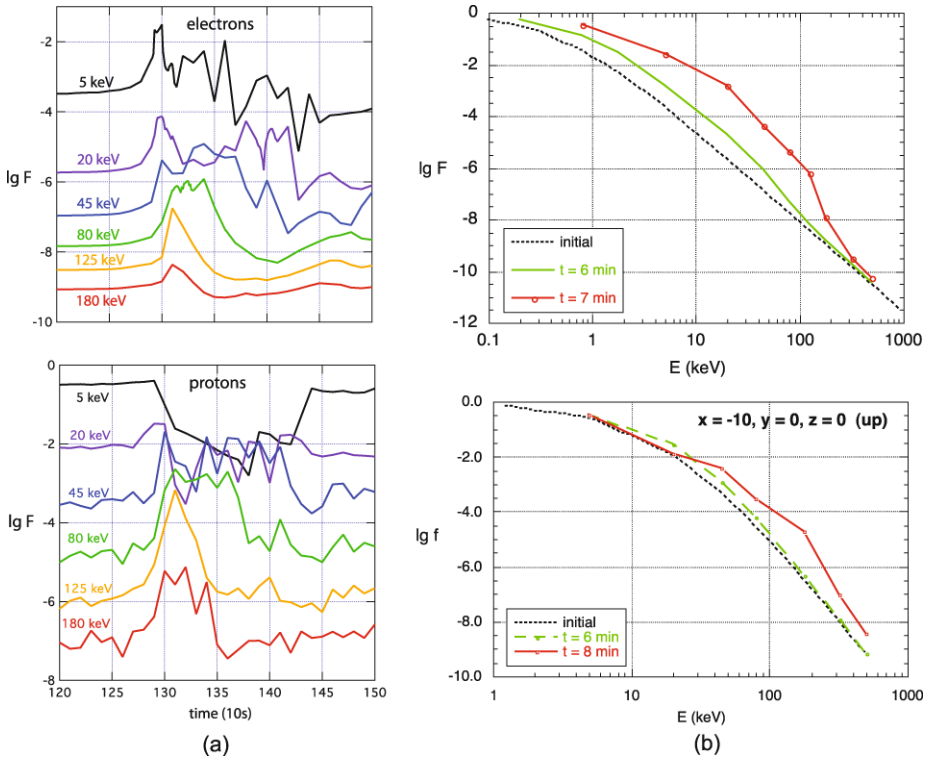

Fig. 16 Test particle results on energetic particle fluxes and phase space distributions: (**a**) Electron (*top*) and proton fluxes (*bottom*) at $x = -10.5$, $y = 0$, $z = 0$ as function of time; after Birn et al. (2012), based on test particle orbits in the simulation of Birn et al. (2011); (**b**) energy distributions of electrons (*top*) and protons (*bottom*), obtained at $x = -10$, $y = 0$, $z = 0$ in the simulation of Birn and Hesse (1996); after Birn et al. (1997a, 2004b)

during neutral sheet crossings, individual ions and electrons may actually experience both during their history.

4.2.2 Temporal and Energy-Dependent Characteristics

In this section we present some temporal and spatial properties of ion and electron fluxes inferred from the test particle simulations. Figure 16 illustrates results on the temporal evolution and energy dependence of energetic particle fluxes. Figure 16a shows fluxes of 15° pitch angle electrons and protons as function of time, based again on test particle orbits in the simulation fields of Birn et al. (2011), which correspond to the electric field and orbits shown in Fig. 14. The fluxes are obtained at the location $x = -10.5$, $y = 0$, $z = 0$. Obviously at this location the flux increases are consistent with the observed fast, simultaneous, (approximately) dispersionless ion and electron injections. The slight inverse dispersion of the electron fluxes shown in Fig. 16(a) (increases at lower energy precede those at higher energy) is of the order of 2 Alfvén times, that is, approximately 10–20 s. This would not show in many observations that have a time resolution of only ∼1 min. However, larger in-

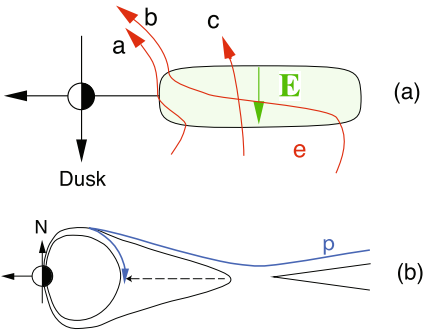

Fig. 17 Schematic of typical orbits relevant for the limited energy range of injections: (**a**) Electron orbits in the equatorial plane (or equatorial crossing points for low pitch angle orbits) at different energies; (**b**) low-energy (few keV) proton orbit in the x, z plane; the *dashed arrow* indicates the collapse of a field line from the vicinity of the reconnection site to a near-Earth location during the bounce of the ion. After Birn et al. (2012)

verse dispersions of electron fluxes are frequently observed also (see Fig. 13). Figure 16(a) also illustrates that the flux increases extend to lower energies for electrons, whereas ion fluxes at energies below 20 keV actually decrease, which is also often observed (Birn et al. 1997b). Figure 16(b), taken from an earlier set of test particle simulations (Birn et al. 1997a, 2004b), shows the characteristic change in electron and ion distribution functions, which again confirms the limitation of the energy range of particle flux increases.

4.3 Summary and Discussion

In summary, test particle orbits in the dynamic fields of MHD simulations have very successfully reproduced qualitatively, and even quantitatively, significant injection features:

(1) The fast rise of the fluxes by one or even up to two orders of magnitude, which is simultaneous and dispersionless in a central region around midnight. The acceleration and the flux changes are strongly tied to the changes in the, predominantly dawn-dusk, electric field. The fast rise of E_y associated with dipolarization events determines the rise of the energetic particle fluxes. A more gradual increase of E_y enables an increase of electron fluxes at lower energy (a few keV) that may precede the rise at higher, hundreds of keV, fluxes.

(2) The limitations of the energy range of flux increases of a few keV to hundreds of keV for electrons, and a few tens of keV to hundreds of keV for protons. Major contributing effects are illustrated in Fig. 17(a), representing the equatorial drift of a near 90° pitch angle, or the equatorial crossing points of a low pitch angle, electron. Basically, the energy dependency results from a competition between Fermi/betatron acceleration from the transport towards Earth and the acceleration from cross-tail drift in the direction opposite to the electric field. The high-energy limit is largely associated with the maximum energy gain from crossing the region of enhanced electric field (orbit c). Properties near the inner edge of the acceleration region depend on the energy. Higher-energy electrons (orbit a) spend a shorter distance in the acceleration region and therefore gain relatively less energy than lower-energy electrons (orbit b). This explains why, at certain locations, flux increases at higher energies may be lower and shorter than those at lower energies, as visible in Fig. 16(a).

(3) A main reason for the difference between the lower limits of flux enhancements for ions and electrons is illustrated in Fig. 17(b). At keV energies the main source region

of both ions and electrons is the plasma sheet with field lines that extend beyond the reconnection site and undergo reconnection. An electron exhibits many bounces after the field line has undergone reconnection, as shown in Fig. 15, and may therefore gain a significant amount of energy from Fermi/betatron acceleration. For few-keV ions, however, the bounce period and the field evolution time are comparable. Therefore, at these energies, an ion that undergoes a similar reconnection history may after the first mirroring be on a field line that has already moved close to Earth, so that the particle essentially circumvents the acceleration region of enhanced electric field. This is a likely reason why ion injections have a higher low-energy limit than electrons.

In this section we have focused particularly on substorm injections, which are probably the most extensively studied acceleration events in the magnetosphere. The main element that governs the acceleration is the $-\mathbf{v} \times \mathbf{B}$ electric field, associated with a spatially and temporally localized flow burst. This underlying mechanism is similar to that invoked for dipolarization events that do not necessarily lead to a full substorm (Runov et al. 2009) but may be associated with energetic particle flux enhancements, nevertheless (Sergeev et al. 2009). Differences appear to exist in size, magnitude, and particularly depth of penetration toward Earth but the associated acceleration mechanisms can be expected to be similar to those identified in this section for substorm injections.

An interesting question remains: what is the cause of the occasional events that show injections of one or several MeV particles. One conclusion can be drawn from the fact that in the simulations the maximum energy gain is related to the cross-tail electric field, integrated along the particle path across the acceleration region. (In a conventional steady state model, as discussed in Sect. 2, this energy gain would correspond to a potential difference. However, in the present case the electric field is not a potential field but an induced field associated with the localized collapse of a section of the tail.) Thus, higher energy gains require stronger, or more extended, electric fields. Consistent with that conclusion is the fact that MeV proton events occur under strongly stressed conditions with higher impact from the solar wind.

5 Auroral Acceleration

5.1 Introduction

As mentioned earlier, magnetotail activity is the major cause of auroral displays. The major mechanisms that couple the two regions are the current systems, particularly the field-aligned currents and associated particle precipitation, strongly influenced by parallel electric fields. The physical processes responsible for the formation of the large spectrum of terrestrial auroral forms have been studied intensively from ground and by in-situ measurements performed by rockets and spacecraft. The investigation of the energy source and transport in the auroral regions is carried out coherently with the evaluation of atomic processes responsible for the visible and UV auroral emissions. The wealth of auroral forms is organized in catalogues and categories helping to a systematic evaluation of the main auroral characteristics. The substorm cycle and the morphology of discrete auroral arcs at meso- and microscales remain, however, outstanding unsolved problems. Although the two topics are necessarily coupled, in the following we will mainly discuss auroral acceleration processes in discrete arcs.

A new challenge of this field of research is to extract the features of auroral acceleration processes that have a universal dimension. Indeed, data gathered by the Hubble Space Telescope and by planetary satellite missions reveal new features of the auroral emissions

on magnetized planets like Saturn (see e.g. Belenkaya et al. 2011; Bunce et al. 2008; Gérard et al. 2004; Grodent et al. 2010; Stallard et al. 2008) and Jupiter (see, e.g., Brandt et al. 2010; Clarke et al. 1998; Gladstone et al. 2007; Nichols et al. 2009; Vogt et al. 2011). The auroral forms on other planets have similarities but also significant differences with respect to the terrestrial aurora (see, e.g., Clarke et al. 2005). Recent in-situ data confirm that auroral forms are also present on non-magnetized planets with remnant crustal magnetic field, like Mars (Leblanc et al. 2008; Lundin et al. 2006). The auroral acceleration of particles excites instabilities, like the cyclotron maser instability, producing typical radio emissions (Gurnett et al. 2002). These radio emissions are believed to be signatures that could trace auroral acceleration of particles on Jupiter-like exoplanets (Nichols 2011). The ISSI book (Paschmann et al. 2003) devoted to the terrestrial aurora is one of the key references in the field and reviews almost exhaustively all the aspects of auroral physics. In this section we focus on the much narrower field of auroral acceleration and describe its specificity in the context of plasma acceleration processes in the Universe. Although many questions persist, the investigation of the auroral acceleration of particles reveals fundamental plasma processes whose role in space plasma dynamics just begins to be fully appreciated.

Observations from rockets and spacecraft have revealed that magnetospheric electrons/ions, accelerated Earthward/anti-Earthward, carry the upward field-aligned (FA) current of the auroral current circuit (ACC). The downward FA current of the ACC is carried mainly by ionospheric electrons and by a limited fraction of precipitating ions. The "upward/downward" FA current topology is found at large scales, typical for the auroral oval (Anderson et al. 2008; Iijima and Potemra 1976; Kamide 1982; Ohtani et al. 2010; Weimer 2001) as illustrated in Fig. 18, as well as at microscales associated with discrete auroral arcs (Boström 1964; Hasunuma et al. 2008; Marklund et al. 1997; Marklund 2009) as shown in Fig. 19.

The scale invariance and self-similarity of the upward/downward FA currents may be a hallmark of the acceleration process itself or it can be linked to the properties of the magnetospheric generator feeding the auroral circuit (see, e.g., Borovsky 1993; Galperin 2002; de Keyser and Echim 2010). The energy carried by the precipitated electrons is transferred at ionospheric altitudes to ions and neutral atoms and excites luminous auroral emissions by atomic processes.

In-situ measurements of energy spectra of downgoing electrons have revealed two classes of auroral acceleration signatures: (i) monoenergetic, characterized by an enhanced flux in a narrow energy band and (ii) broadband, corresponding to higher fluxes over a broad band of energy (typically between 100 eV and 10 keV, see also Fig. 20). The two different signatures likely pertain to two classes of acceleration mechanisms. The monoenergetic spectra, also called "inverted-V" events (for a discussion see Newell 2000), result from quasi-static Earthward acceleration of electrons through a field-aligned electric field. There is increasing evidence that the broadband spectra result from acceleration of electrons imprinted by the interaction with dispersive Alfvén waves (see, e.g., Chaston et al. 2003a). An illustration of typical spectra for each class is shown in Fig. 20. The two types of auroral acceleration can be detected simultaneously; the broadband feature is often observed close to the edges of the inverted-V structure and of the auroral oval, at the boundary with the polar cap (see, e.g., Fig. 20 and Chaston et al. 2003a; Marklund et al. 2011). Magnetospheric charged particles having enough initial energy can impact on the upper atmospheric layers without acceleration by a parallel electric field; in this case the luminous emission is faint, generating the so-called diffuse aurora. A statistical survey based on in-situ observations of energy spectra of precipitating particles by DMSP

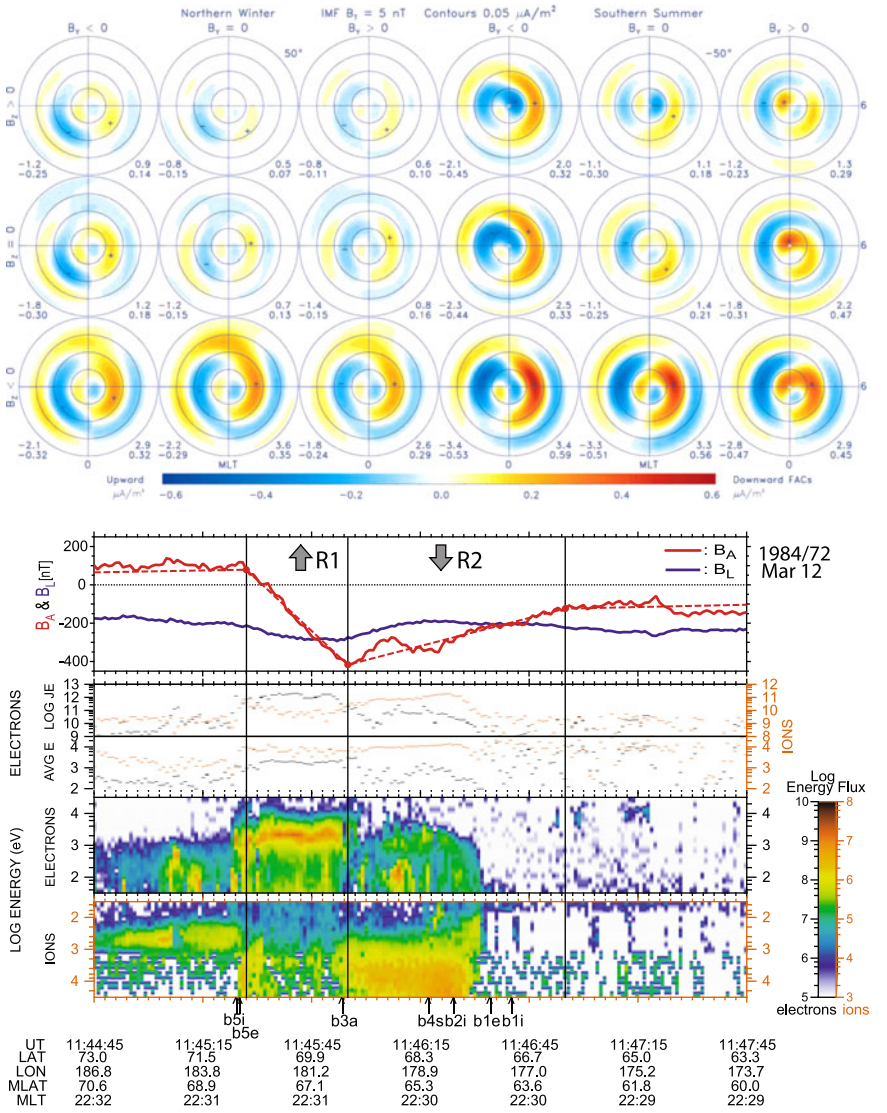

Fig. 18 *Top*: Statistical maps of the large scale pattern of field-aligned currents from observations by MAGSAT and OERSTED satellites from Papitashvili et al. (2002). The field-aligned current density is color coded (*blue*—upward currents, *red*—downward currents). The maps are organized by the IMF clock angle for northern winter (left) and southern summer (right) and are consistent with the early statistical pattern of Region 1 and 2 field-aligned currents (Iijima and Potemra 1978). *Bottom*: example of experimental data confirming the large scale trends outlined in the *top figure*; the panels show data from DMSP spacecraft above the auroral oval in the evening sector and illustrate, from top to bottom, magnetic field perturbation due to FA currents, energy flux and average energy of electrons and ions, energy-time diagrams of electrons and ions. The peak of the electron energy at 3 keV (*fifth panel from top*) is a hallmark of the electrostatic acceleration; one also notes that the large scale upward(R1)/downward(R2) current configuration is clearly evidenced by the electron and ion energy spectra; some precipitation boundaries are also indicated, see Ohtani et al. (2010) for details

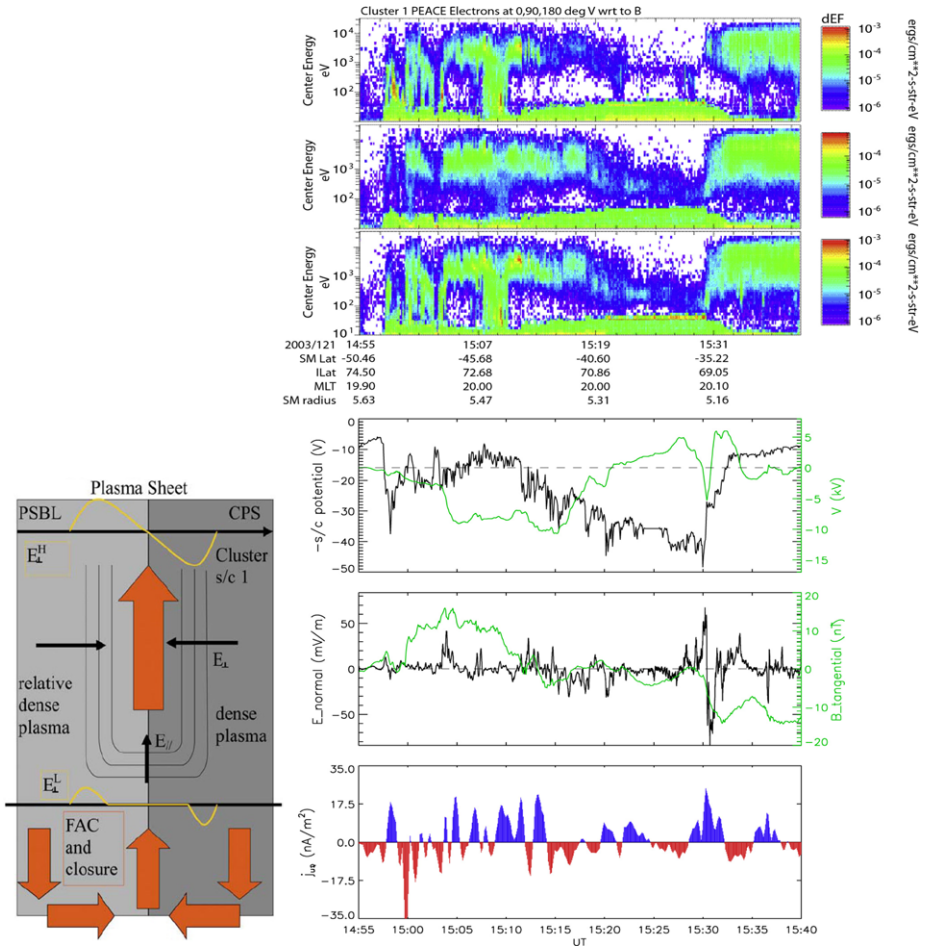

Fig. 19 *Left*: Diagram of the electric circuit associated with a stable discrete auroral arc (from Marklund et al. 2007); *Right*: Cluster data illustrating the "upward/downward" configuration of field-aligned currents associated with a discrete auroral arc; panels show energy spectra of electrons at three pitch angles (0°—meaning upward going, 90°, 180°), spacecraft potential and electric potential, electric field/magnetic field normal/tangent to the arc, field-aligned current density; the discrete arc observed at 15:30 UT is formed at the interface between the central plasma sheet and the plasma sheet boundary layer and corresponds to an upward FA current sheet (in *blue*) embedded into two downward FA current sheets (in *red*); adapted from Marklund et al. (2007)

has revealed that the hemispheric precipitating flux is, surprisingly, dominated (about 70 % of the total flux) by the diffuse aurora (Newell et al. 2009). The monoenergetic aurora carries more energy than the broadband aurora, but the latter plays an increasing role for active conditions (Newell et al. 2009).

5.2 Quasi-stationary Acceleration by Parallel Electric Fields

The energy gain illustrated in Fig. 19 and the upper panel of Fig. 20 is achieved by acceleration of electrons by a field-aligned electric field, $E_{\parallel}$. Theoretical, numerical and observational studies, both in space and in the laboratory, consolidate our understanding on how the

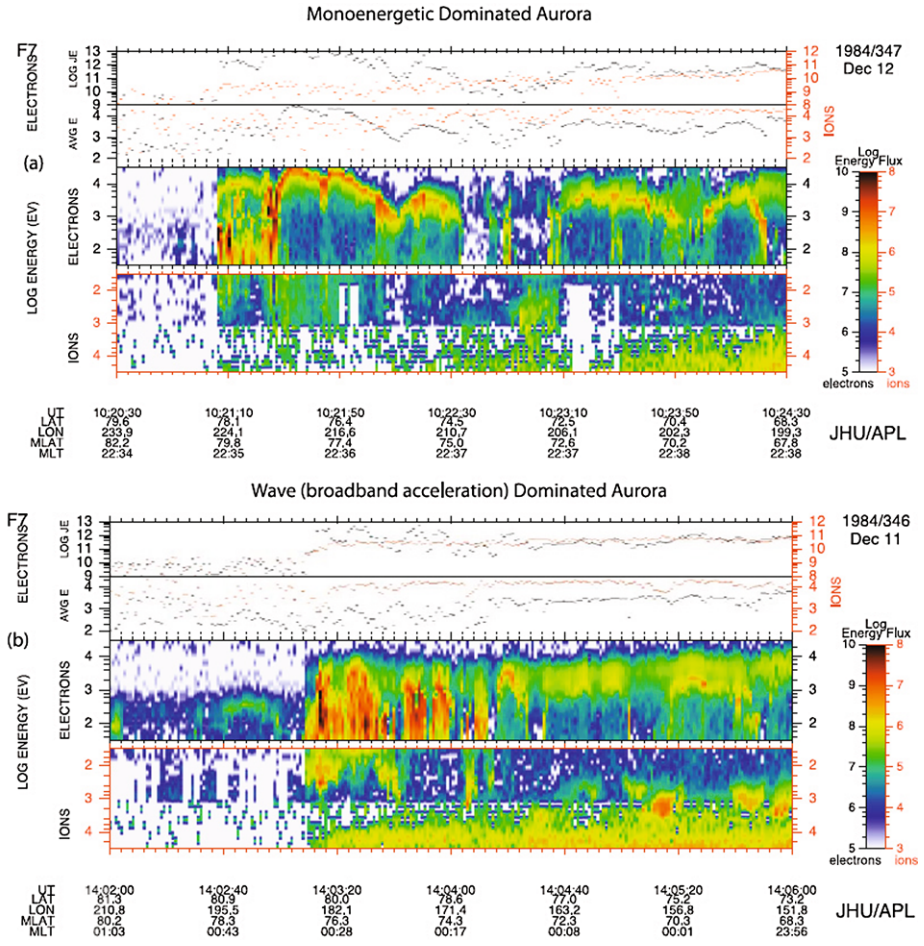

Fig. 20 *Upper panel*: DMSP data illustrating a "monoergetic/inverted-V" spectrum of auroral electrons in the nightside auroral oval; *lower panel*: "broadband" signature of auroral acceleration from DMSP observations. Adapted from Newell et al. (2009)

field-aligned electric field can be formed and sustained in collisionless plasmas immersed in an auroral mirroring magnetic field.

5.2.1 Acceleration by $E_\parallel$ *Distributed Along Large Scales*

By imposing the condition of quasi-neutrality on the charge carried by electrons and ions oscillating in a non-uniform magnetic field between two mirror points, Alfvén and Fälthammar (1963) derived a quantitative expression for the parallel electric field in a low density plasma formed by electrons and ions:

$$E_\parallel = -\frac{1}{|e|}\left[\frac{W_{i\parallel}W_{e\perp} - W_{e\parallel}W_{i\perp}}{4B(W_{i\parallel} + W_{e\parallel})}\right]\left(\frac{dB}{ds}\right) \tag{11}$$

where s is the coordinate along the magnetic field line, $W_\parallel = \frac{1}{2}mv_\parallel^2$, $W_\perp = \frac{1}{2}mv_\perp^2$, e and i refer to electrons and ions, respectively. The relationship (11) is derived under the strongly simplified assumption that the plasma is monoenergetic. From (11) it follows that $E_\parallel = 0$ if and only if the magnetic field is uniform or the pitch angle distributions of the monoenergetic ions and electrons are strictly identical. When this restrictive condition is not satisfied a field-aligned electric field is distributed along the magnetic field line; its local amplitude at each point along the line of magnetic force is determined by (11). Alfvén and Fälthammar argued that in a low density plasma and a mirroring magnetic field the field-aligned potential drop forms "before any appreciable current can flow."

In (11) only a magnetospheric population populates the flux tube and therefore $E_\parallel$ is perhaps overestimated, as shown later (Lemaire and Scherer 1973; Chiu and Schulz 1978). Persson (1966) derived a formal expression of the parallel electric field for a collisionless electron plasma as a solution of the Vlasov equation for the velocity distribution function (VDF) of species α:

$$\frac{\partial g_\alpha}{\partial t} + \left[\frac{q_\alpha}{m_\alpha}(\mathbf{E} + \mathbf{v}\times\mathbf{B}) + m_\alpha \mathbf{a}_g\right]\cdot\nabla_v g_\alpha + \mathbf{v}\cdot\nabla_r g_\alpha = 0. \tag{12}$$

In a one-dimensional geometry, the parallel component of the electric field is then given by (Persson 1966):

$$E_\parallel = -\frac{m_\alpha}{|e|}\left[\frac{v_\perp}{2B}\frac{dB}{ds}\left(v_\perp\frac{\partial g_\alpha}{\partial v_\parallel} - v_\parallel\frac{\partial g_\alpha}{\partial s}\right) - v_\parallel\frac{\partial g_\alpha}{\partial s}\right]\left(\frac{\partial g_\alpha}{\partial v_\parallel}\right)^{-1}. \tag{13}$$

This relation is valid under additional restrictive assumptions about the velocity distribution function g_α, imposing that: (i) the right hand side of (13) does not depend on $v_\perp$ and $v_\parallel$, (ii) the electric field derived for the VDF of electrons (g_e) and ions (g_i) is the same and (iii) the zero order moments of g_i and g_e satisfy the quasi-neutrality condition. A Vlasov solution satisfying the conditions (i)–(iii) is difficult to find for realistic velocity distribution functions (Boström 2003). Persson (1966) was able to provide tractable solutions only in the case of a mono-energetic ("well-defined energy") plasma population, similar to the solution of Alfvén and Fälthammar. Nevertheless, these pioneering works frame the general context for the kinetic treatment of parallel electric field in the magnetosphere and the auroral regions.

The first order moment of the Vlasov equation (12) gives the momentum equation for each plasma species and also provides an expression of the parallel electric field as a function of macroscopic properties:

$$E_\parallel = -\frac{1}{en}\left(\frac{\partial p_\parallel}{\partial s} + mn\overline{v_\parallel}\frac{\partial \overline{v_\parallel}}{\partial s} + \frac{p_\perp - p_\parallel}{B}\frac{\partial B}{\partial s}\right) \tag{14}$$

where n, $p_\parallel$, $p_\perp$, $\overline{v_\parallel}$ are the standard moments of the VDF of each species (see Stark et al. 2011 as well as Echim et al. 2011 for a discussion on the kinetic and fluid approach). The first term in (14) corresponds to the parallel pressure, the second gives a measure of electron inertial effects, the third one is related to the magnetic mirror force. Note that the parallel component of the electric field given in (14) has been computed in the context of the one-fluid theory and the generalized Ohm's law by Rönnmark (1999) and Hull et al. (2003).

A case study by Stark et al. (2011) evaluates quantitatively the relative contributions of the three terms in (14). This study is based on a particular configuration of the auroral electric potential with a prescribed potential jump/double layer and distributed parallel electric

field outside the jump, along the magnetic line of force (Boström 2003, 2004). Closer to the ionosphere the ionospheric electron pressure is the main contributor to the small parallel field; within the potential jump mirroring effects, as well as pressure effects due to magnetospheric electrons are dominant. In the magnetospheric part of the field line, the parallel component of the electric field is distributed over large distances and is mainly sustained by the magnetospheric parallel pressure gradient. The formation of distributed parallel electric field structures is difficult to be proved beyond any doubt by experimental observations in the auroral regions. However, observations of particle signatures consistent with U-shaped and S-shaped profiles of the electric equipotential lines are interpreted as hallmarks of distributed parallel electric fields (see, e.g., Janhunen et al. 2001; Marklund et al. 2011).

5.2.2 *Acceleration by Intense* $E_{\parallel}$ *Confined in Double Layers*

A double layer (DL) is defined, following Block (1978), as "consisting of two equal but oppositely charged space charge layers." A discussion by Boström (2003, 2004) evidences the connections between the double layer theory and the early plasma physics concepts, as the Langmuir theory of particle dynamics in a discharge tube (Mott-Smith and Langmuir 1926). When the DL is immersed into a background magnetic field, the electric field has a parallel component. Therefore DLs are plasma structures where the MHD approximation breaks down. Double layers have been first evidenced, generated and studied in the laboratory (for a review see Block 1978 and Charles 2007). It was suggested that they could play a role for the auroral acceleration of particles (see Alfvén and Fälthammar 1963; Block 1978, 1988). Thermoelectric potential differences and double layers at the contact between cold and hot magnetospheric populations were first advocated by Hultquist (1971) and modeled in various configurations (see, e.g., Lemaire and Scherer 1978; Singh et al. 1987). A general discussion on double layers and their importance in astrophysics may be found in the review by Raadu (1989).

In collisionless geophysical and astrophysical plasmas stationary weak and strong double layers are solutions of the Vlasov–Poisson equations. Analytical solutions can sometimes be found (e.g., Schamel and Bujarbarua 1983) but more often numerical solutions are provided, like those found for the auroral double layers by, e.g., Ergun et al. (2002b), Singh and Khazanov (2005) and Main et al. (2006, 2010). The thickness of the accelerating double layers is in general of the order of the Debye length. The double layer is "weak" when its total potential drop is smaller than, or of the order of, kT_e/e (Raadu and Rasmussen 1988). In a multicomponent plasma, as is the case in the auroral regions where populations of magnetospheric and ionospheric origin interact mutually, a double layer can be simultaneously weak and strong, depending on which population is taken for reference (Ergun et al. 2004). Outside the weak double layer the parallel electric field is small, almost equal to zero, and the plasma is electrically quasi-neutral: for instance in a plasma in isothermal hydrostatic equilibrium in a gravitational field $(n^+ - n^-)/n^- \approx 4 \times 10^{-37}$; in the polar wind $(n^+ - n^-)/n^- \approx 4 \times 10^{-9}$.

Parallel electric fields are difficult to measure in space, the direct detection of weak/strong double layers confined to thin sheaths is even more challenging. In spite of some controversy (Bryant et al. 1992; Borovsky 1992), experimental observations and numerical simulations lead to a deeper understanding of the role of double layers for auroral acceleration, particularly for the upward current branch of the auroral circuit. Careful investigation of electric field data from Polar and FAST satellites provides direct and indirect evidence for the formation of parallel electric fields and double layers (e.g. Mozer and Kletzing 1998; Ergun et al. 2002a; Hull et al. 2003).

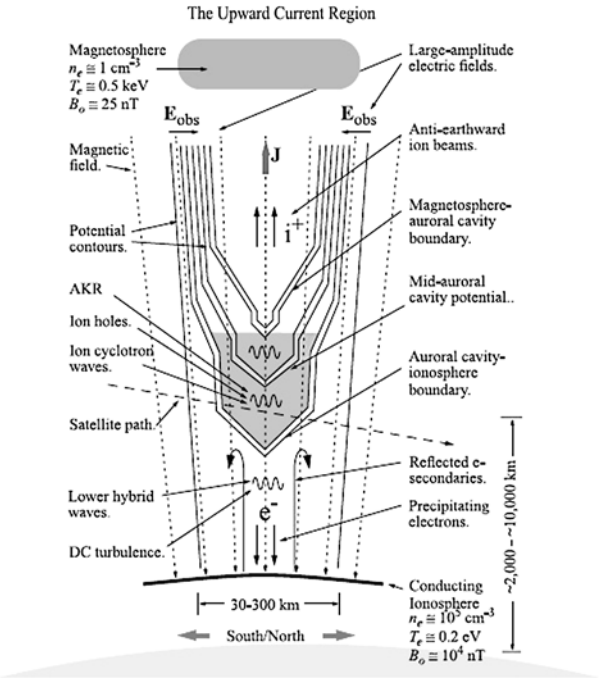

Fig. 21 Diagram sketching a possible configuration of the auroral upward current region. *Dashed contours* depict the magnetic field lines; *solid lines* illustrate electric equipotentials. The cartoon, adapted from Ergun et al. (2004) and a sketch by Carlson et al. (1998), illustrates the possible localization of a double layer structure at lower altitudes, at the contact between the auroral cavity with the ionosphere, as well as at higher altitudes, corresponding to the interface of the cavity with the magnetosphere. The cartoon also identifies possible location of several types of auroral plasma waves

A diagram illustrating a simplified possible configuration of the upward current region, including the formation of DL structures, is shown in Fig. 21. Strong double layers are believed to be formed at the interface between the ionospheric upper layers and the auroral cavity and also at the interface of the latter with the magnetosphere. A possible intermediate DL, inside the auroral cavity itself, has been advocated by Ergun et al. (2004). The auroral cavity is a region located between roughly 2 to 4 R_E where the plasma density decreases drastically (Calvert 1981) due to the excavation of the cold thermal ionospheric plasma by parallel acceleration of ionospheric ions (Paschmann et al. 2003) and/or ion heating by cyclotron waves (Wahlund et al. 1992; Norqvist et al. 1996). Experimental reports based on in-situ measurements from spacecraft advocate the detection of strong double layers at the ionospheric boundary of the auroral cavity (Chust et al. 1998; Ergun et al. 2004). These instances of auroral DLs have intense parallel electric fields, of the order of 100–200 mV/m or more and spatial scales of the order of a Debye length (a few kilometers in the auroral plasma). Vlasov solutions (Main et al. 2006) and PIC simulations (Main et al. 2010) describe double layer structures that are in agreement with the auroral observations and confirm that these structures are quasistable; the stability conditions depend on the ratio between hot and cold electrons contributing to the DL equilibrium and/or the temperature of the cold population (Main et al. 2010).

5.2.3 *Current Voltage Relationship, Magnetosphere-Ionosphere Coupling with Quasi-static* $E_\parallel$ *and Current Continuity*

The adiabatic motion of particles between the magnetospheric generator and the auroral ionosphere relates the field-aligned current density, $j_\parallel$, and the flux of precipitating energy, ε_{em}, to the field-aligned potential drop between the magnetosphere and ionosphere, $\Delta\Phi = \Phi_i - \Phi_m$ (Knight 1973; Lemaire and Scherer 1973). The relationship $j_\parallel = j_\parallel(\Delta\Phi)$ is known

as the current-voltage relation (CVR), or Ohm's law, for the auroral electric circuit. It has been computed by several authors for $\Delta\Phi$ monotonically decreasing with altitude and a magnetospheric generator described by various VDF: Maxwellian (Knight 1973; Lemaire and Scherer 1973) biMaxwellian (Fridman and Lemaire 1980), or kappa (Pierrard 1996), see also the review by Pierrard et al. (2007). Note that experimental investigators mostly test the linearized CVR relationship (Knight 1973; Lyons et al. 1979).

The CVR is a main element of stationary models describing the coupling and particle acceleration between the magnetosphere and the auroral ionosphere. These models use the current continuity in the topside ionosphere as the mathematical kernel that couples the properties of the magnetospheric generator feeding the energy of the auroral circuit, and the parameters of the high latitude ionosphere, where the auroral arcs form (Lyons 1981; Chiu and Schulz 1978; Roth et al. 1993; Echim et al. 2007). It has been shown that convergent magnetospheric electric fields fitted to experimental data sustain arc-like, narrower structures in the auroral ionosphere (Lyons 1981). Based on the qualitative arguments of Roth et al. (1993), numerical magnetosphere-ionosphere (M-I) coupling models demonstrate quantitatively that magnetospheric plasma interfaces play the role of auroral generators of discrete arcs (Echim et al. 2007; de Keyser and Echim 2010). The magnetospheric interfaces in these studies are modeled as general Vlasov equilibria satisfying the coupled Vlasov-Maxwell system of equations (Roth et al. 1996). Similar conclusions were obtained by Birn et al. (2004a) for the auroral effects of thin current sheets. Two-dimensional quasi-stationary magnetosphere-ionosphere models based on ad-hoc magnetospheric electric fields were proposed by Chiu and Schulz (1978), Chiu and Cornwall (1980), and Chiu et al. (1981). A recent discussion of the electrostatic magnetosphere-ionosphere coupling and the role of the CVR can be found in de Keyser and Echim (2010).

In Fig. 22 we illustrate results obtained from the quasi-stationary modeling of the magnetosphere-ionosphere coupling based on a magnetospheric plasma interface as auroral generator. This interface consists of a thin current layer, identified in Cluster observations as a tangential discontinuity (TD). On the one hand the generator, observed in-situ by Cluster, is modeled by a Vlasov-Maxwell solution, on the other hand the electrodynamic properties of the associated discrete auroral are provided by M-I coupling modeling compared with observations by DMSP (Vaivads et al. 2003; Echim et al. 2009). The relative good agreement between models and simultaneous satellite observations above and below the auroral acceleration region support the scenario of a quasistatic acceleration of auroral electrons by a parallel electric field. Note however that in this model the altitude profile of the parallel electric field remains unspecified. Indeed, the only assumption made on the field-aligned potential drop is that it varies monotonically with the altitude. This condition can be satisfied by distributed as well as by confined (double layer) parallel electric fields. More efforts, in terms of modeling and observations are needed in order to reveal the geometry, the structure and the dynamics of quasistatic fields powering aurora.

5.3 Auroral Acceleration by $E_{\parallel}$ Sustained by Dispersive Alfvén Waves

The quasi-static scenario for the auroral acceleration of down-going electrons can describe large scale auroral features (Lyons 1980; Chiu and Cornwall 1980) but also fine scale, discrete arcs with typical widths of the order of 1–15 kilometer (Lyons 1981; Echim et al. 2008, 2009). It is believed that the very fine structure of auroral arcs, of the order of 100 meter, which is roughly equal to the typical electron inertial length in the topside ionosphere, is related to Alfvénic acceleration processes. There is a wealth of wave activity in the terrestrial auroral magnetosphere and ionosphere, however it is only

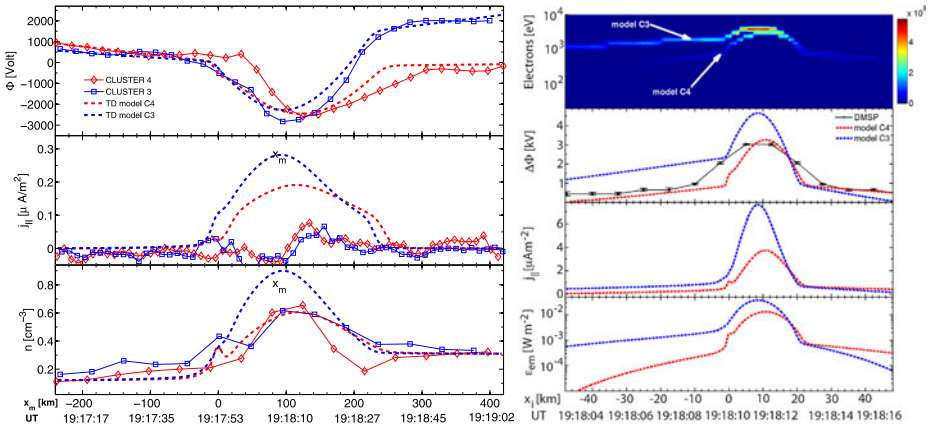

Fig. 22 *Left*: comparison between Cluster observations (*squares*) and Vlasov-Maxwell modeling results (*dashed lines*) of a tangential discontinuity (TD) as the auroral generator above the acceleration region; the panels show the electric potential as a function of the coordinate normal to the plasma interface, the field-aligned current density, the plasma density; *Right*: electrodynamics of the auroral arc below the acceleration region from simulations and observations; the panels show: a synthetic energy spectrum of precipitating electrons resulting from acceleration in the parallel electric field, the field-aligned potential drop corresponding to the two generator models derived for Cluster observations, the *solid black line* corresponds to the field aligned potential drop derived form DMSP observations of an auroral arc in conjunction with the interface observed by Cluster; parallel current density and the integrated flux of precipitating energy are also shown. Adapted from Echim et al. (2009)

recently that quantitative estimation of the Poynting flux carried by the Alfvén waves has been made in the auroral regions (Wygant et al. 2000). In this section we discuss acceleration of particles by parallel electric fields and therefore we focus on Dispersive Alfvén Waves (DAW), a class of waves that received increased attention and experimental support during the last decade. Depending on the kinetic properties of the electron population, DAW may be divided into: (i) Inertial Alfvén Waves (IAW), present in low β plasma[1] when the electron thermal velocity is less than the Alfvén velocity $v_{Te} < v_A$, where $v_A = B_0/\sqrt{\mu_0 \rho}$, and (ii) Kinetic Alfvén Waves (KAW) present in intermediate beta plasma[2] when $v_{Te} > v_A$ (Lysak and Lotko 1996). Since the magnetic field intensity (B_0) and mass density (ρ) vary with altitude, it is expected that the two types of waves act at different altitudes along the auroral field lines (Stasiewicz et al. 2000; Lysak and Song 2003).

As pointed out by Stéfant (1970) dispersive Alfvén waves carry a parallel electric field. The latter is produced at frequencies below ion cyclotron and when the wavelength perpendicular to the background magnetic field is comparable to the ion gyroradius at electron temperature (or ion acoustic gyroradius), $R_c = \sqrt{m_i K T_e / e B_0}$, or to the ion gyroradius, $R_{Lp} = \sqrt{m_i K T_i / e B_0}$, or to the electron inertial length, $\lambda_e = \sqrt{m_e / n_e \mu_0 e^2}$ (Lysak and Lotko 1996; Seyler and Wu 2001; Seyler and Liu 2007). The general properties of dispersive Alfvén waves are derived from a two fluid description of auroral plasma, based on the continuity

[1] The low β regime is defined by the condition, $\beta = 2\mu_0 n K T_e / B_0^2 < m_e / m_i$.

[2] $m_e / m_i < \beta < 1$.

and momentum conservation equations for each species α:

$$\frac{\partial n_\alpha}{\partial t} + \nabla \cdot (n_\alpha \mathbf{u}_\alpha) = 0, \tag{15}$$

$$\frac{\partial \mathbf{u}_\alpha}{\partial t} + \mathbf{u}_\alpha \cdot (\nabla \mathbf{u}_\alpha) = \frac{e_\alpha}{m_\alpha}(\mathbf{E} + \mathbf{u}_\alpha \times \mathbf{B}) - \left(\frac{1}{m_\alpha n_\alpha}\right) \nabla \cdot \underline{\mathbf{P}}_\alpha \tag{16}$$

where the tensor pressure $\underline{\mathbf{P}}_\alpha$ is included in the last term of the momentum equation (16). Equations (15)–(16) are coupled to the Maxwell's equations:

$$\nabla \cdot \mathbf{B} = 0, \tag{17}$$

$$\nabla \times \mathbf{E} + \frac{\partial \mathbf{B}}{\partial t} = 0, \tag{18}$$

$$\varepsilon_0 \nabla \cdot \mathbf{E} = \sum_\alpha e_\alpha n_\alpha, \tag{19}$$

$$\frac{1}{\mu_0} \nabla \times \mathbf{B} - \varepsilon_0 \frac{\partial \mathbf{E}}{\partial t} = \sum_\alpha \mathbf{j}_\alpha. \tag{20}$$

The displacement current in Ampère's equation (20) is in general neglected (Goertz and Boswell 1979). A general expression of the parallel electric field from the equations (15)–(20) is given by Thompson and Lysak (1996), Stasiewicz et al. (2000), and Paschmann et al. (2003):

$$E_\parallel = \left(R_c^2 - \lambda_e^2 \frac{1 + k_\perp^2 R_c^2}{1 + k_\perp^2 \lambda_e^2}\right) \frac{\partial}{\partial s} (\nabla_\perp \cdot \mathbf{E}_\perp) \tag{21}$$

where s is the coordinate in the direction of the magnetic field. Equation (21) reveals the dependence of the Alfvénic parallel electric field on the plasma parameters and the perpendicular electric wave field. In the inertial limit, when λ_e is large, the second term dominates and the parallel electric field accelerates the electrons in the direction of the field-aligned current. The ratio between the two terms in (21) is equal to $R_c/\lambda_e = \sqrt{\beta_e(m_i/m_e)}$, thus in cold plasmas the electron inertia is dominant, contrary to warm plasma where the electron pressure dominates. In auroral plasma the boundary between the two regimes was estimated by Lysak and Carlson (1981) to be at an altitude of about 4–5 R_E. Chaston et al. (2003b) discussed the opposite limit of the inertial and kinetic effects from (21), suggesting that the acceleration of electrons in the warm case may be less efficient than in the colder case as illustrated by Fig. 23.

One outstanding problem for the auroral acceleration by DAW is the relative rapid damping of the kinetic waves at small scales. Thus, short wavelength DAW would not be able to travel longer distances from their source (Chaston et al. 2008) and a mechanism is required to replenish efficiently the energy at smaller scales all along the magnetic flux tube. Such a mechanism could be wave phase mixing (Lysak and Song 2000), the feedback from the ionosphere (Streltsov and Lotko 2004), or plasma instabilities (Génot et al. 2004; Singh et al. 2007). Recent observations, modeling, and statistical analysis (Chaston et al. 2008, 2011) evidence that in Alfvénic aurora the perpendicular magnetic fluctuations scale according to a power-law with the spectral index $-7/3$. Similar statistical trends were found by Lund (2010) for FAST auroral observations and Uritsky et al. (2002) for global images of the aurora. Tam et al. (2010) and Tam and Chang (2011) revealed the multifractal

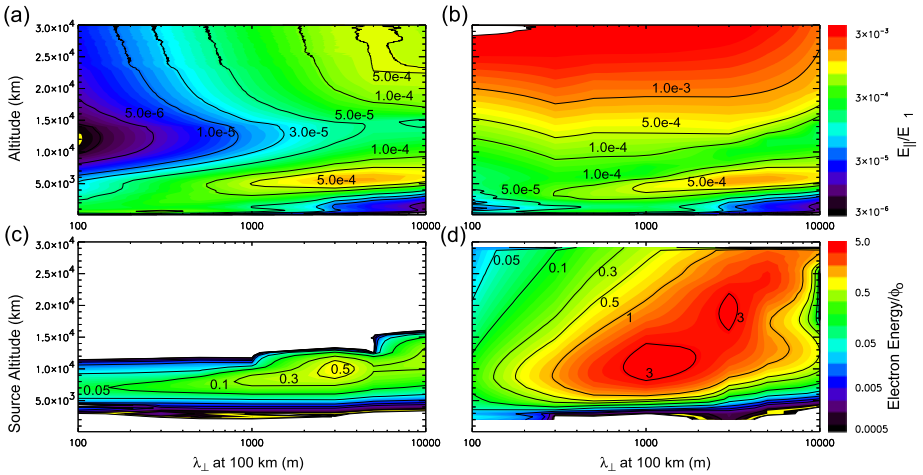

Fig. 23 Simulation results showing in the *upper panels* the ratio $E_\parallel/E_\perp$ derived from (21) and in the *lower panels* the electron energy gain injected into the respective wavefields. Data is shown in normalized units and the two-dimensional maps are represented as function of $\lambda_\perp$, the wave transverse scale in the ionosphere, and the altitude. *Left panels* illustrate pure kinetic (warm plasma) effects; *right panels* illustrate the pure inertial (cold plasma) case. This figure is adapted from Chaston et al. (2003b)

spectrum of the auroral electric field turbulence detected from in-situ auroral rocket observations. These findings suggest the presence of a turbulent cascade of the energy transfer in the auroral regions (Fig. 24), a mechanism that could possibly explain the coupling between scales in Alfvénic aurora. The energy cascade is similar to the one in Kolmogorov turbulence; in the case of aurora the cascade is sustained by mutual interaction between direct and reflected (from the ionosphere) waves. Dissipation is achieved through field-aligned acceleration of electrons by the parallel electric field; essentially this is a Landau damping process (Chaston et al. 2008). The driving mechanism is related to large-scale fluctuations in the magnetosphere; the cascade transports the energy between scales and along magnetic field lines, it thus provides the power of the Alfvénic aurora. The cascade is non-homogeneous, FAST data reveal hallmarks of intermittency, i.e. localized burst of energy dissipation, also observed from rocket measurements of the auroral magnetic field (Chaston et al. 2008; Tam et al. 2010).

5.4 Summary

Auroral acceleration of particles is revealed by optical emissions in the upper atmosphere and by in-situ measurements of particle spectra at high-latitudes. In this section we have reviewed acceleration mechanisms based on parallel electric fields, which may also be relevant in an broader astrophysical context. Two types of auroral acceleration mechanisms have been discussed: (i) the quasistatic acceleration by distributed or confined quasi-stationary parallel electric fields and (ii) the time dependent acceleration by dispersive Alfvén waves.

The adiabatic motion of electrons and ions with different pitch angle distribution sustains a parallel electric field distributed along the auroral magnetic field lines. A similar effect is due to a long range distributed parallel pressure gradient. The structure of the electric potential in this case is consistent with U-shaped and S-shaped equipotentials coupling the magnetospheric generator of the auroral arcs to the ionospheric load. Specific auroral

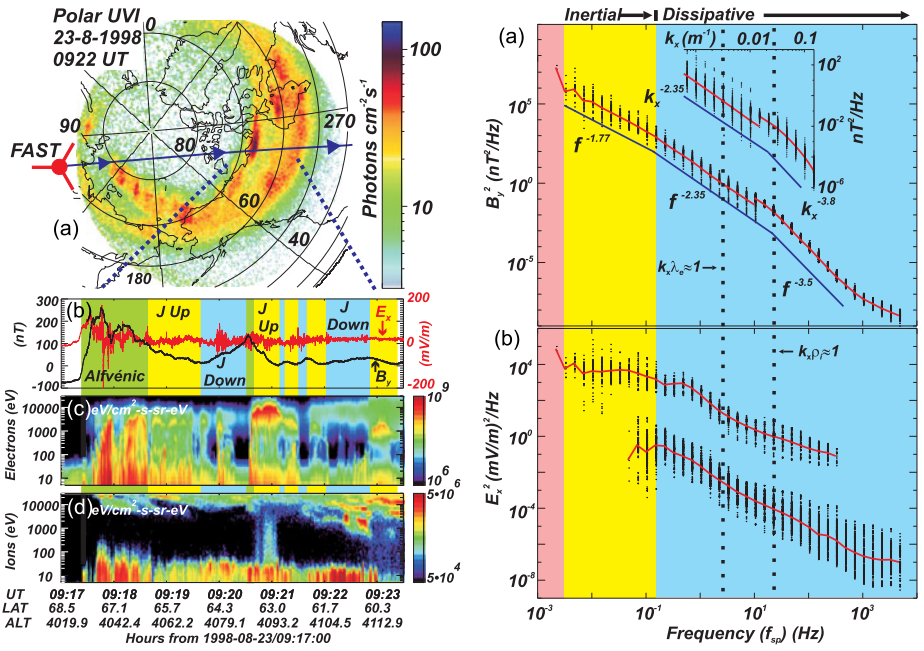

Fig. 24 *Left*: (**a**) Polar UV observations of aurora in the Northern hemisphere; the FAST orbit is illustrated, (**b**) orthogonal components of the electric and magnetic field recorded by FAST traversing the aurora with indications of the respective field-aligned currents; (**c**) Electron energy spectrum from FAST, showing signatures of Alfvénic and monoenergetic (quasistatic) acceleration; (**d**) ion spectrogram from FAST; *Right*: Inertial and dissipative range of the magnetic (**a**) and electric (**b**) spectrum of turbulence detected by FAST. The magnetic field turbulence shows spectral similarities with turbulence in the solar wind and magnetosheath, suggesting scale coupling with large scale magnetospheric processes; the electric field spectrum of turbulence is less structured. This figure is adapted from Chaston et al. (2008)

processes, like the formation of density cavities, drive the formation of more intense and localized auroral parallel electric fields in double layer structures. The strong density gradient at the interfaces of the auroral cavities with the ionosphere and the magnetosphere is the region where the double layers are more likely to be formed. In-situ observations and numerical simulations provide evidence for the existence and stability of auroral double-layers and their role for particle acceleration. Quasi-stationary models for the coupling between a magnetospheric generator and the auroral arc in the high latitude ionosphere are based on a current-voltage relation linking the field aligned current density with the total field-aligned potential drop. These models describe the characteristics of the auroral arc and of the accelerated spectrum of particles as a function of the properties of the magnetospheric generator.

Alfvén waves with small perpendicular wavelength are dispersive. Two regimes of the dispersive Alfvén waves are relevant for auroral acceleration and sustain a parallel electric field: inertial and kinetic Alfvén waves. Each class of waves is important for a specific domain of plasma parameters: inertial waves are active in low β plasmas, kinetic effects are dominant in warm, intermediate β plasmas. The coupling between scales is crucial for the energy supply at smaller scales, relevant for discrete arcs in Alfvénic aurora. Recent observations and modeling provide evidence for an energy cascade carrying the energy from larger to smaller scales.

Quasistatic and Alfvénic acceleration are key elements of the auroral processes. Recent statistical studies quantify the relative role of the two mechanisms for the global precipitating energy budget at high latitudes. The energy input from auroral acceleration processes is complemented by diffusive auroral precipitation of non-accelerated particles. Quasistatic and Alfvénic aurora have a comparable contribution to the total ionospheric budget of input energy. Satellite observations suggest that the quasistatic acceleration is more efficient during quiet conditions; the role of Alfvénic processes is increased when the magnetosphere is active.

Acknowledgement The work of A.A. and L.Z. was supported by RFBR (No. 10-02-93114), grants of Leading Schools NIII-3200.2010.2. J.B. acknowledges support by NASA SR&T and MMS grants. M.E. acknowledges support from the Belgian Office for Science (Belspo), grant MO/35/031 and from the European Space Agency, PECS contract 98049/2007(KEEV). The authors thank the International Space Science Institute (ISSI) and the organizing committee for support and the opportunity to participate in the ISSI Workshop on Particle Acceleration in Cosmic Plasmas.

References

S.I. Akasofu, *Polar Magnetospheric Substorms* (Reidel, Dordrecht, 1968)

H. Alfvén, C. Fälthammar, *Cosmical Electrodynamics* (Clarendon Press, Oxford, 1963)

B.J. Anderson, H. Korth, C.L. Waters, D.L. Green, P. Stauning, Statistical Birkeland current distributions from magnetic field observations by the Iridium constellation. Ann. Geophys. **26**, 671–687 (2008). doi:10.5194/angeo-26-671-2008

V. Angelopoulos, W. Baumjohann, C.F. Kennel, F.V. Coroniti, M.G. Kivelson, R. Pellat, R.J. Walker, H. Lühr, G. Paschmann, Bursty bulk flows in the inner central plasma sheet. J. Geophys. Res. **97**, 4027 (1992)

V. Angelopoulos, C.F. Kennel, F.V. Coroniti, R. Pellat, H.E. Spence, M.G. Kivelson, R.J. Walker, W. Baumjohann, W.C. Feldman, J.T. Gosling, Characteristics of ion flow in the quiet state of the inner plasma sheet. Geophys. Res. Lett. **20**, 1711–1714 (1993). doi:10.1029/93GL00847

V. Angelopoulos, C.F. Kennel, F.V. Coroniti, R. Pellat, M.G. Kivelson, R.J. Walker, C.T. Russell, W. Baumjohann, W.C. Feldman, J.T. Gosling, Statistical characteristics of bursty bulk flow events. J. Geophys. Res. **99**, 21257–21280 (1994)

S.V. Apatenkov, V.A. Sergeev, M.V. Kubyshkina, R. Nakamura, W. Baumjohann, A. Runov, I. Alexeev, A. Fazakerley, H. Frey, S. Muhlbachler, P.W. Daly, J. Sauvaud, N. Ganushkina, T. Pulkkinen, G.D. Reeves, Y. Khotyaintsev, Multi-spacecraft observation of plasma dipolarization/injection in the inner magnetosphere. Ann. Geophys. **25**, 801–814 (2007)

R.L. Arnoldy, K.W. Chan, Particle substorms observed at the geostationary orbit. J. Geophys. Res. **74**, 5019 (1969)

A.V. Artemyev, L.M. Zelenyi, H.V. Malova, G. Zimbardo, D. Delcourt, Acceleration and transport of ions in turbulent current sheets: formation of non-Maxwellian energy distribution. Nonlinear Process. Geophys. **16**, 631–639 (2009)

A.V. Artemyev, A.I. Neishtadt, L.M. Zelenyi, D.L. Vainshtein, Adiabatic description of capture into resonance and surfatron acceleration of charged particles by electromagnetic waves. Chaos **20**(4), 043128 (2010a). doi:10.1063/1.3518360

A.V. Artemyev, A.A. Petrukovich, R. Nakamura, L.M. Zelenyi, Proton velocity distribution in thin current sheets: Cluster observations and theory of transient trajectories. J. Geophys. Res. **115**, A12255 (2010b). doi:10.1029/2010JA015702

A.V. Artemyev, L.M. Zelenyi, A.A. Petrukovich, R. Nakamura, Hot electrons as tracers of large-scale structure of magnetotail current sheets. Geophys. Res. Lett. **38**, L14102 (2011). doi:10.1029/2011GL047979

M. Ashour-Abdalla, J.P. Berchem, J. Büchner, L.M. Zelenyi, Shaping of the magnetotail from the mantle—global and local structuring. J. Geophys. Res. **98**, 5651–5676 (1993). doi:10.1029/92JA01662

M. Ashour-Abdalla, L.M. Zelenyi, V. Peroomian, R.L. Richard, Consequences of magnetotail ion dynamics. J. Geophys. Res. **99**, 14891–14916 (1994). doi:10.1029/94JA00141

M. Ashour-Abdalla, L.M. Zelenyi, V. Peroomian, R.L. Richard, J.M. Bosqued, The mosaic structure of plasma bulk flows in the Earth's magnetotail. J. Geophys. Res. **100**, 19191–19210 (1995). doi:10.1029/95JA00902

M. Ashour-Abdalla, J.M. Bosqued, M. El-Alaoui, V. Peroomian, L.M. Zelenyi, R.J. Walker, J. Wright, A stochastic sea: The source of plasma sheet boundary layer ion structures observed by Cluster. J. Geophys. Res. **110**(A9), A12221 (2005). doi:10.1029/2005JA011183

M. Ashour-Abdalla, M. El-Alaoui, M.L. Goldstein, M. Zhou, D. Schriver, R. Richard, R. Walker, M.G. Kivelson, K.J. Hwang, Observations and simulations of non-local acceleration of electrons in magnetotail magnetic reconnection events. Nat. Phys. **7**, 360–365 (2011). doi:10.1038/nphys1903

D.N. Baker, E.C. Stone, Observations of energetic electrons /E no less than about 200 keV/ in the earth's magnetotail—plasma sheet and fireball observations. J. Geophys. Res. **82**, 1532–1546 (1977). doi:10.1029/JA082i010p01532

D.N. Baker, P.R. Higbie, E.W. Hones Jr., R.D. Belian, High-resolution energetic particle measurements at 6.6R_E: 3. Low-energy electron anisotropies and short-term substorm predictions. J. Geophys. Res. **83**, 4863 (1978)

D.N. Baker, R.D. Belian, P.R. Higbie, E.W. Hones Jr., High-energy magnetospheric protons and their dependence on geomagnetic and interplanetary conditions. J. Geophys. Res. **84**, 7138 (1979)

D.N. Baker, R.D. Belian, P.R. Higbie, E.W. Hones Jr., Global properties of the magnetosphere during a substorm growth phase: A case study. J. Geophys. Res. **86**, 8941 (1981)

S.J. Bame, R.D. Belian, P.R. Higbie, E.W. Hones Jr., Magnetospheric plasma analyzer for spacecraft with constrained resources. Rev. Sci. Instrum. **64**, 1026 (1993)

W. Baumjohann, G. Paschmann, H. Lühr, Characteristics of high-speed ion flows in the plasma sheet. J. Geophys. Res. **95**, 3801 (1990)

W. Baumjohann, A. Roux, O. Le Contel, R. Nakamura, J. Birn, M. Hoshino, A.T.Y. Lui, C.J. Owen, J. Sauvaud, A. Vaivads, D. Fontaine, A. Runov, Dynamics of thin current sheets: Cluster observations. Ann. Geophys. **25**, 1365–1389 (2007)

E.S. Belenkaya, S.W.H. Cowley, J.D. Nichols, M.S. Blokhina, V.V. Kalegaev, Magnetospheric mapping of the dayside UV auroral oval at Saturn using simultaneous HST images, Cassini IMF data, and a global magnetic field model. Ann. Geophys. **29**, 1233–1246 (2011). doi:10.5194/angeo-29-1233-2011

R.D. Belian, D.N. Baker, P.R. Higbie, E.W. Hones Jr., High-resolution energetic particle measurements at 6.6r_e: 2. High-energy proton drift echos. J. Geophys. Res. **83**, 4857 (1978)

R.D. Belian, G.R. Gisler, T. Cayton, R. Christensen, High Z energetic particles at geosynchronous orbit during the great solar proton event of October, 1989. J. Geophys. Res. **97**, 16897 (1992)

J. Birn, M. Hesse, Details of current disruption and diversion in simulations of magnetotail dynamics. J. Geophys. Res. **101**, 15345 (1996)

J. Birn, M. Hesse, Energy release and transfer in guide field reconnection. Phys. Plasmas **17**(1), 012109 (2010). doi:10.1063/1.3299388

J. Birn, R.R. Sommer, K. Schindler, Self-consistent theory of the quiet magnetotail in three dimensions. J. Geophys. Res. **82**, 147–154 (1977)

J. Birn, M.F. Thomsen, J.E. Borovsky, G.D. Reeves, D.J.M.R.D. Belian, M. Hesse, Substorm ion injections: Geosynchronous observations and test particle orbits in three-dimensional dynamic MHD fields. J. Geophys. Res. **102**, 2325 (1997a)

J. Birn, M.F. Thomsen, J.E. Borovsky, G.D. Reeves, D.J. McComas, R.D. Belian, Characteristic plasma properties of dispersionless substorm injections at geosynchronous orbit. J. Geophys. Res. **102**, 15345 (1997b)

J. Birn, M.F. Thomsen, J.E. Borovsky, G.D. Reeves, D.J. McComas, R.D. Belian, M. Hesse, Substorm electron injections: Geosynchronous observations and test particle simulations. J. Geophys. Res. **103**, 9235 (1998)

J. Birn, J.F. Drake, M.A. Shay, B.N. Rogers, R.E. Denton, M. Hesse, M. Kuznetsova, Z.W. Ma, A. Bhattacharjee, A. Otto, P.L. Pritchett, Geospace Environmental Modeling (GEM) magnetic reconnection challenge. J. Geophys. Res. **106**, 3715–3720 (2001). doi:10.1029/1999JA900449

J. Birn, K. Schindler, M. Hesse, Thin electron current sheets and their relation to auroral potentials. J. Geophys. Res. **109**(A18), A02217 (2004a). doi:10.1029/2003JA010303

J. Birn, M.F. Thomsen, M. Hesse, Electron acceleration in the dynamic magnetotail: Test particle orbits in three-dimensional MHD simulation fields. Phys. Plasmas **11**, 1825 (2004b). doi:10.1063/1.1704641

J. Birn, R. Nakamura, E.V. Panov, M. Hesse, Bursty bulk flows and dipolarization in MHD simulations of magnetotail reconnection. J. Geophys. Res. **116**, A01210 (2011). doi:10.1029/2010JA016083

J. Birn, R. Nakamura, E.V. Panov, M. Hesse, S. Zaharia, Particle acceleration in dipolarization events. J. Geophys. Res. (2012, submitted)

L.P. Block, A double layer review. Astrophys. Space Sci. **55**, 59–83 (1978). doi:10.1007/BF00642580

L.P. Block, Acceleration of auroral particles by magnetic-field aligned electric fields. Astrophys. Space Sci. **144**, 135–147 (1988). doi:10.1007/BF00793177

F.H. Bogott, F.S. Mozer, Nightside energetic particle decreases at the synchronous orbit. J. Geophys. Res. **78**, 8119 (1973)

J.E. Borovsky, Double layers do accelerate particles in the auroral zone. Phys. Rev. Lett. **69**, 1054–1056 (1992). doi:10.1103/PhysRevLett.69.1054

J.E. Borovsky, Auroral arc thicknesses as predicted by various theories. J. Geophys. Res. **98**, 6101–6138 (1993). doi:10.1029/92JA02242
R. Boström, A model of the auroral electrojects. J. Geophys. Res. **69**, 4983–4999 (1964). doi:10.1029/JZ069i023p04983
R. Boström, Kinetic and space charge control of current flow and voltage drops along magnetic flux tubes: Kinetic effects. J. Geophys. Res. **108**, 8004 (2003). doi:10.1029/2002JA009295
R. Boström, Kinetic and space charge control of current flow and voltage drops along magnetic flux tubes: 2. Space charge effects. J. Geophys. Res. **109**(A18), A01208 (2004). doi:10.1029/2003JA010078
P.C. Brandt, B.H. Mauk, D.G. Mitchell, J.F. Carbary, C.P. Paranicas, Birth and acceleration of energetic particles and relation to current systems: Aurorae and radio emissions at Earth, Saturn and Jupiter, in *European Planetary Science Congress 2010* (2010), p. 440
D.A. Bryant, R. Bingham, U. de Angelis, Double layers are not particle accelerators. Phys. Rev. Lett. **68**, 37–39 (1992). doi:10.1103/PhysRevLett.68.37
J. Büchner, Correlation-modulated chaotic scattering in the Earth's magnetosphere. Geophys. Res. Lett. **18**, 1595–1598 (1991). doi:10.1029/91GL01905
J. Büchner, L.M. Zelenyi, Regular and chaotic charged particle motion in magnetotaillike field reversals. I—Basic theory of trapped motion. J. Geophys. Res. **94**, 11821–11842 (1989). doi:10.1029/JA094iA09p11821
S.V. Bulanov, The energy spectrum of particles accelerated near a singular magnetic field line. Sov. Astron. Lett. **6**, 206 (1980)
S.V. Bulanov, P.V. Sasorov, Energy spectrum of particles accelerated in the neighborhood of a line of zero magnetic field. Sov. Astron. **19**, 464–468 (1976)
E.J. Bunce, C.S. Arridge, J.T. Clarke, A.J. Coates, S.W.H. Cowley, M.K. Dougherty, J.C. Gérard, D. Grodent, K.C. Hansen, J.D. Nichols, D.J. Southwood, D.L. Talboys, Origin of Saturn's aurora: Simultaneous observations by Cassini and the Hubble Space Telescope. J. Geophys. Res. **113**, A09209 (2008). doi:10.1029/2008JA013257
G.R. Burkhart, J. Chen, Differential memory in the Earth's magnetotail. Geophys. Res. Lett. **96**, 14033 (1991). doi:10.1029/91JA01137
G.R. Burkhart, J.F. Drake, J. Chen, Magnetic reconnection in collisionless plasmas—prescribed fields. J. Geophys. Res. **95**, 18833–18848 (1990). doi:10.1029/JA095iA11p18833
W. Calvert, The auroral plasma cavity. Geophys. Res. Lett. **8**, 919–921 (1981). doi:10.1029/GL008i008p00919
C.W. Carlson, R.F. Pfaff, J.G. Watzin, The Fast Auroral SnapshoT (FAST) mission. Geophys. Res. Lett. **25**, 2013–2016 (1998). doi:10.1029/98GL01592
J.R. Cary, D.F. Escande, J.L. Tennyson, Adiabatic-invariant change due to separatrix crossing. Phys. Rev. A **34**(5), 4256–4275 (1986)
C. Charles, TOPICAL REVIEW: A review of recent laboratory double layer experiments. Plasma Sources Sci. Technol. **16**, 1 (2007). doi:10.1088/0963-0252/16/4/R01
C.C. Chaston, J.W. Bonnell, C.W. Carlson, J.P. McFadden, R.E. Ergun, R.J. Strangeway, Properties of small-scale Alfvén waves and accelerated electrons from FAST. J. Geophys. Res. **108**, 8003 (2003a). doi:10.1029/2002JA009420
C.C. Chaston, J.W. Bonnell, C.W. Carlson, J.P. McFadden, R.J. Strangeway, R.E. Ergun, Kinetic effects in the acceleration of auroral electrons in small scale Alfven waves: A FAST case study. Geophys. Res. Lett. **30**(6), 1289 (2003b). doi:10.1029/2002GL015777
C.C. Chaston, C. Salem, J.W. Bonnell, C.W. Carlson, R.E. Ergun, R.J. Strangeway, J.P. McFadden, The turbulent alfvénic aurora. Phys. Rev. Lett. **100**(17), 175003 (2008). doi10.1103/PhysRevLett.100.175003
C.C. Chaston, K. Seki, T. Sakanoi, K. Asamura, M. Hirahara, C.W. Carlson, Cross-scale coupling in the auroral acceleration region. Geophys. Res. Lett. **382**, L20101 (2011). doi:10.1029/2011GL049185
J. Chen, P.J. Palmadesso, Chaos and nonlinear dynamics of single-particle orbits in a magnetotaillike magnetic field. J. Geophys. Res. **91**, 1499–1508 (1986)
L.J. Chen, A. Bhattacharjee, P.A. Puhl-Quinn, H. Yang, N. Bessho, S. Imada, S. Mühlbachler, P.W. Daly, B. Lefebvre, Y. Khotyaintsev, A. Vaivads, A. Fazakerley, E. Georgescu, Observation of energetic electrons within magnetic islands. Nat. Phys. **4**, 19–23 (2008). doi:10.1038/nphys777
F. Chiaravalloti, A.V. Milovanov, G. Zimbardo, Self-similar transport processes in a two-dimensional realization of multiscale magnetic field turbulence. Phys. Scr. T **122**, 79–88 (2006). doi:10.1088/0031-8949/2006/T122/012
Y.T. Chiu, J.M. Cornwall, Electrostatic model of a quiet auroral arc. J. Geophys. Res. **85**, 543–556 (1980)
Y.T. Chiu, M. Schulz, Self-consistent particle and parallel electrostatic field distributions in the magnetospheric-ionospheric auroral region. J. Geophys. Res. **83**, 629–642 (1978)
Y. Chiu, A. Newman, J. Cornwall, On the structure and mapping of auroral electrostatic potentials. J. Geophys. Res. **86**, 10029–10037 (1981)

T. Chust, P. Louarn, M. Volwerk, H. de Feraudy, A. Roux, J.E. Wahlund, B. Holback, Electric fields with a large parallel component observed by the Freja spacecraft: Artifacts or real signals? J. Geophys. Res. **103**, 215–224 (1998). doi:10.1029/97JA02587

J.T. Clarke, G. Ballester, J. Trauger, J. Ajello, W. Pryor, K. Tobiska, J.E.P. Connerney, G.R. Gladstone, J.H. Waite, L.B. Jaffel, J.C. Gérard, Hubble space telescope imaging of Jupiter's UV aurora during the Galileo orbiter mission. J. Geophys. Res.**103**, null (1998). doi:10.1029/98JE01130

J.T. Clarke, J.C. Gérard, D. Grodent, S. Wannawichian, J. Gustin, J. Connerney, F. Crary, M. Dougherty, W. Kurth, S.W.H. Cowley, E.J. Bunce, T. Hill, J. Kim, Morphological differences between Saturns ultraviolet aurorae and those of Earth and Jupiter. Nature **433**, 717–719 (2005). doi:10.1038/nature03331

S.W.H. Cowley, P. Shull Jr., Current sheet acceleration of ions in the geomagnetic tail and the properties of ion bursts observed at the lunar distance. Planet. Space Sci. **31**, 235–245 (1983)

W. Daughton, Kinetic theory of the drift kink instability in a current sheet. J. Geophys. Res. **103**, 29429–29444 (1998). doi:10.1029/1998JA900028

W. Daughton, Electromagnetic properties of the lower-hybrid drift instability in a thin current sheet. Phys. Plasmas **10**, 3103–3119 (2003). doi:10.1063/1.1594724

J. de Keyser, M. Echim, Auroral and sub-auroral phenomena: an electrostatic picture. Ann. Geophys. **28**, 633–650 (2010). doi:10.5194/angeo-28-633-2010

D.C. Delcourt, Particle acceleration by inductive electric fields in the inner magnetosphere. J. Atmos. Sol.-Terr. Phys. **64**, 551–559 (2002). doi:10.1016/S1364-6826(02)00012-3

D.C. Delcourt, J.A. Sauvaud, R.F. Martin, T.E. Moore, On the nonadiabatic precipitation of ions from the near-Earth plasma sheet. J. Geophys. Res. **1011**, 17409–17418 (1996). doi:10.1029/96JA01006

A.V. Divin, M.I. Sitnov, M. Swisdak, J.F. Drake, Reconnection onset in the magnetotail: Particle simulations with open boundary conditions. Geophys. Res. Lett. **34**, 9109 (2007). doi:10.1029/2007GL029292

A. Divin, S. Markidis, G. Lapenta, V.S. Semenov, N.V. Erkaev, H.K. Biernat, Model of electron pressure anisotropy in the electron diffusion region of collisionless magnetic reconnection. Phys. Plasmas **17**(12), 122102 (2010). doi:10.1063/1.3521576

J.F. Drake, M. Swisdak, C. Cattell, M.A. Shay, B.N. Rogers, A. Zeiler, Formation of electron holes and particle energization during magnetic reconnection. Science **299**, 873–877 (2003). doi:10.1126/science.1080333

J.F. Drake, M. Swisdak, H. Che, M.A. Shay, Electron acceleration from contracting magnetic islands during reconnection. Nature **443**, 553–556 (2006). doi:10.1038/nature05116

T.E. Eastman, L.A. Frank, W.K. Peterson, W. Lennartsson, The plasma sheet boundary layer. J. Geophys. Res. **89**, 1553–1572 (1984). doi:10.1029/JA089iA03p01553

M. Echim, M. Roth, J. De Keyser, Sheared magnetospheric plasma flows and discrete auroral arcs: a quasi-static coupling model. Ann. Geophys. **25**, 317–330 (2007)

M.M. Echim, M. Roth, J. de Keyser, Ionospheric feedback effects on the quasi-stationary coupling between LLBL and postnoon/evening discrete auroral arcs. Ann. Geophys. **26**, 913–928 (2008)

M.M. Echim, R. Maggiolo, M. Roth, J. De Keyser, A magnetospheric generator driving ion and electron acceleration and electric currents in a discrete auroral arc observed by Cluster and DMSP. Geophys. Res. Lett. **361**, L12111 (2009). doi:10.1029/2009GL038343

M.M. Echim, J. Lemaire, Ø. Lie-Svendsen, A review on solar wind modeling: Kinetic and fluid aspects. Surv. Geophys. **32**, 1–70 (2011). doi:10.1007/s10712-010-9106-y

R.E. Ergun, L. Andersson, D.S. Main, Y.J. Su, C.W. Carlson, J.P. McFadden, F.S. Mozer, Parallel electric fields in the upward current region of the aurora: Indirect and direct observations. Phys. Plasmas **9**, 3685–3694 (2002a). doi:10.1063/1.1499120

R.E. Ergun, L. Andersson, D. Main, Y.J. Su, D.L. Newman, M.V. Goldman, C.W. Carlson, J.P. McFadden, F.S. Mozer, Parallel electric fields in the upward current region of the aurora: Numerical solutions. Phys. Plasmas **9**, 3695–3704 (2002b). doi:10.1063/1.1499121

R.E. Ergun, L. Andersson, D. Main, Y.J. Su, D.L. Newman, M.V. Goldman, C.W. Carlson, A.J. Hull, J.P. McFadden, F.S. Mozer, Auroral particle acceleration by strong double layers: The upward current region. J. Geophys. Res. **109**(A18), A12220 (2004). doi:10.1029/2004JA010545

J.M. Finn, P.K. Kaw, Coalescence instability of magnetic islands. Phys. Fluids **20**, 72–78 (1977). doi:10.1063/1.861709

M. Fridman, J. Lemaire, Relationship between auroral electron fluxes and field-aligned electric potential differences. J. Geophys. Res. **85**, 664–670 (1980)

A.A. Galeev, Reconnection in the magnetotail. Space Sci. Rev. **23**, 411–425 (1979). doi:10.1007/BF00172248

A.A. Galeev, F.V. Coroniti, M. Ashour-Abdalla, Explosive tearing mode reconnection in the magnetospheric tail. Geophys. Res. Lett. **5**, 707–710 (1978). doi:10.1029/GL005i008p00707

Y.I. Galperin, Multiple scales in auroral plasmas. Journal of Atmospheric and Solar-Terrestrial. Physics **64**, 211–229 (2002). doi:10.1016/S1364-6826(01)00085-2

V. Génot, P. Louarn, F. Mottez, Alfvén wave interaction with inhomogeneous plasmas: acceleration and energy cascade towards small-scales. Ann. Geophys. **22**, 2081–2096 (2004). doi:10.5194/angeo-22-2081-2004

J.C. Gérard, D. Grodent, J. Gustin, A. Saglam, J.T. Clarke, J.T. Trauger, Characteristics of Saturn's FUV aurora observed with the space telescope imaging spectrograph. J. Geophys. Res. **109**, A09207 (2004). doi:10.1029/2004JA010513

R.G. Giovanelli, A theory of chromospheric flares. Nature **158**, 81–82 (1946)

G.R. Gladstone, S.A. Stern, D.C. Slater, M. Versteeg, M.W. Davis, K.D. Retherford, L.A. Young, A.J. Steffl, H. Throop, J.W. Parker, H.A. Weaver, A.F. Cheng, G.S. Orton, J.T. Clarke, J.D. Nichols, Jupiter's nightside airglow and aurora. Science **318**, 229 (2007). doi:10.1126/science.1147613

C.K. Goertz, R.W. Boswell, Magnetosphere-ionosphere coupling. J. Geophys. Res. **84**, 7239–7246 (1979). doi:10.1029/JA084iA12p07239

I.V. Golovchanskaya, Y.P. Maltsev, On the identification of plasma sheet flapping waves observed by Cluster. Geophys. Res. Lett. **32**, 2102 (2005). doi:10.1029/2004GL021552

P.C. Gray, L.C. Lee, Particle pitch angle diffusion due to nonadiabatic effects in the plasma sheet. J. Geophys. Res. **87**, 7445–7452 (1982). doi:10.1029/JA087iA09p07445

A. Greco, A.L. Taktakishvili, G. Zimbardo, P. Veltri, L.M. Zelenyi, Ion dynamics in the near-Earth magnetotail: Magnetic turbulence versus normal component of the average magnetic field. J. Geophys. Res. **107**, 1267 (2002). doi:10.1029/2002JA009270

E.E. Grigorenko, J.A. Sauvaud, L.M. Zelenyi, Spatial-Temporal characteristics of ion beamlets in the plasma sheet boundary layer of magnetotail. J. Geophys. Res. **112**(A11), A05218 (2007). doi:10.1029/2006JA011986

E.E. Grigorenko, L.M. Zelenyi, M.S. Dolgonosov, J.A. Sauvaud, Spatial and temporal structures in the vicinity of the Earth's tail magnetic separatrix cluster observations, in *The Cluster Active Archive, Studying the Earth's Space Plasma Environment*, ed. by H. Laakso, M. Taylor, C.P. Escoubet (2010), pp. 435–451

D. Grodent, A. Radioti, B. Bonfond, J.C. Gérard, On the origin of Saturn's outer auroral emission. J. Geophys. Res. **115**, A08219 (2010). doi:10.1029/2009JA014901

D.A. Gurnett, W.S. Kurth, G.B. Hospodarsky, A.M. Persoon, P. Zarka, A. Lecacheux, S.J. Bolton, M.D. Desch, W.M. Farrell, M.L. Kaiser, H.P. Ladreiter, H.O. Rucker, P. Galopeau, P. Louarn, D.T. Young, W.R. Pryor, M.K. Dougherty, Control of Jupiters radio emission and aurorae by the solar wind. Nature **415**, 985–987 (2002)

T. Hasunuma, T. Nagatsuma, R. Kataoka, Y. Takahashi, H. Fukunishi, A. Matsuoka, A. Kumamoto, Statistical study of polar distribution of mesoscale field-aligned currents. J. Geophys. Res. **113**, A12214 (2008). doi:10.1029/2008JA013358

M. Hesse, K. Schindler, A theoretical foundation of general magnetic reconnection. J. Geophys. Res. **93**, 5559–5567 (1988)

M. Hesse, D. Winske, Electron dissipation in collisionless magnetic reconnection. J. Geophys. Res. **103**, 26479 (1998)

M. Hesse, M. Kuznetsova, M. Hoshino, The structure of the dissipation region for component reconnection: Particle simulations. Geophys. Res. Lett. **29**, 1563 (2002). doi:10.1029/2001GL014,714

E.W. Hones Jr., Transient phenomena in the magnetotail and their relation to substorms. Space Sci. Rev. **23**, 393–410 (1979). doi:10.1007/BF00172247

M. Hoshino, Electron surfing acceleration in magnetic reconnection. J. Geophys. Res. **110**(A9), A10215 (2005). doi:10.1029/2005JA011229

M. Hoshino, A. Nishida, T. Yamamoto, S. Kokubun, Turbulent magnetic field in the distant magnetotail: Bottom-up process of plasmoid formation? Geophys. Res. Lett. **21**, 2935–2938 (1994). doi:10.1029/94GL02094

M. Hoshino, T. Mukai, T. Yamamoto, S. Kokubun, Ion dynamics in magnetic reconnection: Comparison between numerical simulation and Geotail observations. J. Geophys. Res. **103**, 4509–4530 (1998). doi:10.1029/97JA01785

M. Hoshino, T. Mukai, T. Terasawa, I. Shinohara, Suprathermal electron acceleration in magnetic reconnection. J. Geophys. Res. **106**, 25979–25998 (2001). doi:10.1029/2001JA900052

A.J. Hull, J.W. Bonnell, F.S. Mozer, J.D. Scudder, C.C. Chaston, Large parallel electric fields in the upward current region of the aurora: Evidence for ambipolar effects. J. Geophys. Res. **108**, 1265 (2003). doi:10.1029/2002JA009682

B. Hultqvist, On the production of a magnetic-field-aligned electric field by the interaction between the hot magnetospheric plasma and the cold ionosphere. Planet. Space Sci. **19**, 749 (1971). doi:10.1016/0032-0633(71)90033-X

T. Iijima, T.A. Potemra, The amplitude distribution of field-aligned currents at northern high latitudes observed by Triad. J. Geophys. Res. **81**, 2165–2174 (1976). doi:10.1029/JA081i013p02165

T. Iijima, T.A. Potemra, Large-scale characteristics of field-aligned currents associated with substorms. J. Geophys. Res. **83**, 599–615 (1978). doi:10.1029/JA083iA02p00599
S. Imada, M. Hoshino, T. Mukai, Average profiles of energetic and thermal electrons in the magnetotail reconnection regions. Geophys. Res. Lett. **320**, L09101 (2005). doi:10.1029/2005GL022594
S. Imada, R. Nakamura, P.W. Daly, M. Hoshino, W. Baumjohann, S. Mühlbachler, A. Balogh, H. Rème, Energetic electron acceleration in the downstream reconnection outflow region. J. Geophys. Res. **112**(A11), A03202 (2007). doi:10.1029/2006JA011847
S. Imada, M. Hirai, M. Hoshino, T. Mukai, Favorable conditions for energetic electron acceleration during magnetic reconnection in the Earth's magnetotail. J. Geophys. Res. **116**(A15), A08217 (2011). doi:10.1029/2011JA016576
P. Janhunen, A. Olsson, W.K. Peterson, H. Laakso, J.S. Pickett, T.I. Pulkkinen, C.T. Russell, A study of inverted-V auroral acceleration mechanisms using Polar/Fast Auroral Snapshot conjunctions. J. Geophys. Res. **106**, 18995–19012 (2001). doi:10.1029/2001JA900012
Y. Kamide, The relationship between field-aligned currents and the auroral electrojets—A review. Space Sci. Rev. **31**, 127–243 (1982). doi:10.1007/BF00215281
A. Keiling, H. Rème, I. Dandouras, J.M. Bosqued, G.K. Parks, M. McCarthy, L. Kistler, E. Amata, B. Klecker, A. Korth, R. Lundin, Transient ion beamlet injections into spatially separated PSBL flux tubes observed by Cluster-CIS. Geophys. Res. Lett. **31**, L12804 (2004). doi:10.1029/2004GL020192
L. Knight, Parallel electric fields. Planetary and Space. Science **21**, 741–750 (1973)
G. Lapenta, J.U. Brackbill, A kinetic theory for the drift-kink instability. J. Geophys. Res. **102**, 27099–27108 (1997). doi:10.1029/97JA02140
F. Leblanc, O. Witasse, J. Lilensten, R.A. Frahm, A. Safaenili, D.A. Brain, J. Mouginot, H. Nilsson, Y. Futaana, J. Halekas, M. Holmström, J.L. Bertaux, J.D. Winningham, W. Kofman, R. Lundin, Observations of aurorae by SPICAM ultraviolet spectrograph on board Mars Express: Simultaneous ASPERA-3 and MARSIS measurements. J. Geophys. Res. **113**, A08311 (2008). doi:10.1029/2008JA013033
J. Lemaire, M. Scherer, Plasma sheet particle precipitation: A kinetic model. Planet. Space Sci. **21**, 281–289 (1973)
J. Lemaire, M. Scherer, Field aligned distribution of plasma mantle and ionospheric plasmas. J. Atmos. Sol.-Terr. Phys. **40**, 337–342 (1978)
T.W. Lezniak, J.R. Winckler, Experimental study of magnetospheric motions and the acceleration of energetic electrons during substorms. J. Geophys. Res. **75**, 7075 (1970)
T.W. Lezniak, R.L. Arnoldy, G.K. Parks, J.R. Winckler, Measurement and intensity of energetic electrons at the equator at 6.6 r_e. Radio Sci. **3**, 710 (1968)
X. Li, D.N. Baker, M. Temerin, G.D. Reeves, Simulation of dispersionless injections and subsequent drift echoes of energetic electrons associated with substorms. Geophys. Res. Lett. **25**, 3763 (1998)
E.J. Lund, On the dissipation scale of broadband ELF waves in the auroral region. J. Geophys. Res. **115**(A14), A01201 (2010). doi:10.1029/2009JA014545
R. Lundin, D. Winningham, S. Barabash, R. Frahm, D. Brain, H. Nilsson, M. Holmström, M. Yamauchi, J.R. Sharber, J.A. Sauvaud, A. Fedorov, K. Asamura, H. Hayakawa, A.J. Coates, Y. Soobiah, C. Curtis, K.C. Hsieh, M. Grande, H. Koskinen, E. Kallio, J. Kozyra, J. Woch, M. Fraenz, J. Luhmann, S. McKenna-Lawler, S. Orsini, P. Brandt, P. Wurz, Auroral plasma acceleration above Martian magnetic anomalies. Space Sci. Rev. **126**, 333–354 (2006). doi:10.1007/s11214-006-9086-x
L. Lyons, Generation of large-scale regions of auroral currents, electric potentials and precipitation by the divergence of the convection electric field. J. Geophys. Res. **85**, 17–24 (1980)
L. Lyons, Discrete aurora as the direct result of an inferred high altitude generating potential distribution. J. Geophys. Res. **86**, 1–8 (1981)
L.R. Lyons, Electron energization in the geomagnetic tail current sheet. J. Geophys. Res. **89**, 5479–5487 (1984). doi:10.1029/JA089iA07p05479
L.R. Lyons, T.W. Speiser, Evidence for current sheet acceleration in the geomagnetic tail. J. Geophys. Res. **87**, 2276–2286 (1982)
L. Lyons, D. Evans, R. Lundin, An observed relation between magnetic field aligned electric fields and downward electron energy fluxes in the vicinity of auroral forms. J. Geophys. Res. **84**, 457–461 (1979)
R.L. Lysak, C.W. Carlson, The effect of microscopic turbulence on magnetosphere-ionosphere coupling. Geophys. Res. Lett. **8**, 269–272 (1981). doi:10.1029/GL008i003p00269
R.L. Lysak, W. Lotko, On the kinetic dispersion relation for shear Alfvén waves. J. Geophys. Res. **101**, 5085–5094 (1996). doi:10.1029/95JA03712
R.L. Lysak, Y. Song, The role of alfvén waves in the formation of auroral parallel electric fields, in *Magnetospheric Current Systems*, ed. by S.-I. Ohtani, R. Fujii, M. Hesse, R.L. Lysak (American Geophysical Union, Washington, 2000), p. 147
R.L. Lysak, Y. Song, Kinetic theory of the Alfvén wave acceleration of auroral electrons. J. Geophys. Res. **108**, 8005 (2003). doi:10.1029/2002JA009406

D.S. Main, D.L. Newman, R.E. Ergun, Double layers and ion phase-space holes in the auroral upward-current region. Phys. Rev. Lett. **97**(18), 185001 (2006). doi:10.1103/PhysRevLett.97.185001

D.S. Main, D.L. Newman, R.E. Ergun, Conditions for establishing quasistable double layers in the Earth's auroral upward current region. Phys. Plasmas **17**(12), 122901 (2010). doi:10.1063/1.3520058

G.T. Marklund, On the ionospheric coupling of auroral electric fields. Nonlinear Process. Geophys. **16**, 365–372 (2009)

G. Marklund, T. Karlsson, J. Clemmons, On low-altitude particle acceleration and intense electric fields and their relationship to black aurora. J. Geophys. Res. **102**, 17509–17522 (1997). doi:10.1029/97JA00334

G. Marklund, T. Johansson, S. Lileo, T. Karlsson, Cluster observations of an auroral potential and associated field-aligned current reconfiguration during thinning of the plasma sheet boundary layer. J. Geophys. Res. **112**, A01208 (2007)

G.T. Marklund, S. Sadeghi, J.A. Cumnock, T. Karlsson, P.A. Lindqvist, H. Nilsson, A. Masson, A. Fazakerley, E. Lucek, J. Pickett, Y. Zhang, Evolution in space and time of the quasi-static acceleration potential of inverted-V aurora and its interaction with Alfvénic boundary processes. J. Geophys. Res. **116**(A15), A00K13 (2011). doi:10.1029/2011JA016537

B.H. Mauk, C.E. McIlwain, Correlation of Kp with the substorm-injected plasma boundary. J. Geophys. Res. **79**, 3193 (1974)

C.E. McIlwain, Substorm injection boundaries, in *Magnetospheric Physics*, ed. by B.M. McCormac (Reidel, Norwell, 1974), p. 143

R. McPherron, C. Russell, M. Aubry, Phenomenological model of substorms. J. Geophys. Res. **78**, 3131 (1973)

A.V. Milovanov, Stochastic dynamics from the fractional Fokker-Planck-Kolmogorov equation: Large-scale behavior of the turbulent transport coefficient. Phys. Rev. E **63**(4), 047301 (2001). doi:10.1103/PhysRevE.63.047301

A.V. Milovanov, L.M. Zelenyi, "Strange" Fermi processes and power-law nonthermal tails from a self-consistent fractional kinetic equation. Phys. Rev. E **64**(5), 052101 (2001). doi:10.1103/PhysRevE.64.052101

E. Moebius, M. Scholer, D. Hovestadt, G. Paschmann, G. Gloeckler, Energetic particles in the vicinity of a possible neutral line in the plasma sheet. J. Geophys. Res. **88**, 7742–7752 (1983). doi:10.1029/JA088iA10p07742

H.M. Mott-Smith, I. Langmuir, The theory of collectors in gaseous discharges. Phys. Rev. **28**, 727–763 (1926). doi:10.1103/PhysRev.28.727

F.S. Mozer, C.A. Kletzing, Direct observation of large, quasi-static, parallel electric fields in the auroral acceleration region. Geophys. Res. Lett. **25**, 1629–1632 (1998). doi:10.1029/98GL00849

T. Nagai, I. Shinohara, M. Fujimoto, M. Hoshino, Y. Saito, S. Machida, T. Mukai, Geotail observations of the Hall current system: Evidence of magnetic reconnection in the magnetotail. J. Geophys. Res. **106**, 25929–25950 (2001). doi:10.1029/2001JA900038

A.I. Neishtadt, Change of an adiabatic invariant at a separatrix. Soviet. J. Plasma Phys. **12**, 568–573 (1986)

A.I. Neishtadt, A.V. Artemyev, L.M. Zelenyi, D.L. Vainshtein, Surfatron acceleration in electromagnetic waves with a low phase velocity. JETP Lett. **89**, 441–447 (2009). doi:10.1134/S0021364009090045

P.T. Newell, Reconsidering the inverted-V particle signature: Relative frequency of large-scale electron acceleration events. J. Geophys. Res. **105**, 15779–15794 (2000). doi:10.1029/1999JA000051

P.T. Newell, T. Sotirelis, S. Wing, Diffuse, monoenergetic, and broadband aurora: The global precipitation budget. J. Geophys. Res. **114**(A13), A09207 (2009). doi:10.1029/2009JA014326

J.D. Nichols, Magnetosphere-ionosphere coupling at Jupiter-like exoplanets with internal plasma sources: implications for detectability of auroral radio emissions. Mon. Not. R. Astron. Soc. **414**, 2125–2138 (2011). doi:10.1111/j.1365-2966.2011.18528.x

J.D. Nichols, J.T. Clarke, J.C. Gérard, D. Grodent, K.C. Hansen, Variation of different components of Jupiter's auroral emission. J. Geophys. Res. **114**, A06210 (2009). doi:10.1029/2009JA014051

P. Norqvist, M. André, L. Eliasson, A.I. Eriksson, L. Blomberg, H. Lühr, J.H. Clemmons, Ion cyclotron heating in the dayside magnetosphere. J. Geophys. Res. **1011**, 13179–13194 (1996). doi:10.1029/95JA03596

T.G. Northrop, *The Adiabatic Motion of Charged Particles* (Interscience, New York, 1963)

S. Ohtani, S. Wing, P.T. Newell, T. Higuchi, Locations of night-side precipitation boundaries relative to R2 and R1 currents. J. Geophys. Res. **115**, A10233 (2010). doi:10.1029/2010JA015444

M. Øieroset, R.P. Lin, T.D. Phan, D.E. Larson, S.D. Bale, Evidence for electron acceleration up to ∼300 keV in the magnetic reconnection diffusion region of Earth's magnetotail. Phys. Rev. Lett. **89**(19), 195001 (2002). doi:10.1103/PhysRevLett.89.195001

M. Oka, T.D. Phan, S. Krucker, M. Fujimoto, I. Shinohara, Electron acceleration by multi-island coalescence. Astrophys. J. **714**, 915–926 (2010). doi:10.1088/0004-637X/714/1/915

Y. Ono, M. Nosé, S.P. Christon, A.T.Y. Lui, The role of magnetic field fluctuations in nonadiabatic acceleration of ions during dipolarization. J. Geophys. Res. **114**(A13), 5209 (2009). doi:10.1029/2008JA013918
K. Orazberdyev, V.Y. Trakhtengerts, Certain singularities of particle motion and acceleration in a linearly nonuniform magnetic field with a neutral plane. Radiophys. Quantum Electron. **16**, 21–25 (1973). doi:10.1007/BF01080789
E.V. Panov, R. Nakamura, W. Baumjohann, V.A. Sergeev, A.A. Petrukovich, V. Angelopoulos, M. Volwerk, A. Retinò, T. Takada, K. Glassmeier, J.P. McFadden, D. Larson, Plasma sheet thickness during a bursty bulk flow reversal. J. Geophys. Res. **115**(A14), A05213 (2010). doi:10.1029/2009JA014743
V.O. Papitashvili, F. Christiansen, T. Neubert, A new model of field-aligned currents derived from high-precision satellite magnetic field data. Geophys. Res. Lett. **29**(14), 140000-1 (2002)
G.K. Parks, R.L. Arnoldy, T.W. Lezniak, J.R. Winckler, Correlated effects of energetic zone during magnetospheric substorms. Radio Sci. **3**, 715 (1968)
G. Paschmann, S. Haaland, R. Treumann, *Auroral Plasma Physics*, 1st edn. (Kluwer Academic, Dordrecht, 2003)
S. Perri, A. Greco, G. Zimbardo, Stochastic and direct acceleration mechanisms in the Earth's magnetotail. Geophys. Res. Lett. **36**, 4103 (2009). doi:10.1029/2008GL036619
S. Perri, G. Zimbardo, A. Greco, On the energization of protons interacting with 3-D time-dependent electromagnetic fields in the Earth's magnetotail. J. Geophys. Res. **116**(A15), A05221 (2011). doi:10.1029/2010JA016328
H. Persson, Electric field parallel to the magnetic field in a low-density plasma. Phys. Fluids **9**, 1090–1098 (1966). doi:10.1063/1.1761807
A.A. Petrukovich, Low frequency magnetic fluctuations in the Earth's plasma sheet, in *Astrophysics and Space Science Library*, ed. by A.S. Sharma, P.K. Kaw. Astrophysics and Space Science Library, vol. 321 (2005), p. 145
A.A. Petrukovich, T.L. Zhang, W. Baumjohann, R. Nakamura, A. Runov, A. Balogh, C. Carr, Oscillatory magnetic flux tube slippage in the plasma sheet. Ann. Geophys. **24**, 1695–1704 (2006)
A.A. Petrukovich, A.V. Artemyev, H.V. Malova, V.Y. Popov, R. Nakamura, L.M. Zelenyi, Embedded current sheets in the Earth magnetotail. J. Geophys. Res. **116**, A00125 (2011). doi:10.1029/2010JA015749
K.A. Pfitzer, J.R. Winckler, Intensity correlations and substorm electron drift effects in the outer radiation belt measured with the Ogo3 and ATS 1 satellites. J. Geophys. Res. **74**, 5005 (1969)
V. Pierrard, New model of magnetospheric current-voltage relationship. J. Geophys. Res. **101**, 2669–2676 (1996)
V. Pierrard, G.V. Khazanov, J.F. Lemaire, Current voltage relationship. Journal of Atmospheric and Solar-Terrestrial. Physics **69**, 2048–2057 (2007). doi:10.1016/j.jastp.2007.08.005
P.L. Pritchett, Relativistic electron production during guide field magnetic reconnection. J. Geophys. Res. **111**(A10), 10212 (2006). doi:10.1029/2006JA011793
P.L. Pritchett, Collisionless magnetic reconnection in an asymmetric current sheet. J. Geophys. Res. **113**(A12), A06210 (2008). doi:10.1029/2007JA012930
P.L. Pritchett, F.V. Coroniti, A kinetic ballooning/interchange instability in the magnetotail. J. Geophys. Res. **115**(A14), A06301 (2010). doi:10.1029/2009JA014752
P.L. Pritchett, C.C. Wu, Coalescence of magnetic islands. Phys. Fluids **22**, 2140–2146 (1979). doi:10.1063/1.862507
M.A. Raadu, The physics of double layers and their role in astrophysics. Phys. Rep. **178**, 25–97 (1989). doi:10.1016/0370-1573(89)90109-9
M.A. Raadu, J.J. Rasmussen, Dynamical aspects of electrostatic double layers. Astrophys. Space Sci. **144**, 43–71 (1988). doi:10.1007/BF00793172
G.D. Reeves, D.N. Baker, T.A. Fritz, Numerical tracing of energetic particle drifts in a model magnetosphere. J. Geophys. Res. **96**, 13997 (1991)
A. Retinò, R. Nakamura, A. Vaivads, Y. Khotyaintsev, T. Hayakawa, K. Tanaka, S. Kasahara, M. Fujimoto, I. Shinohara, J.P. Eastwood, M. André, W. Baumjohann, P.W. Daly, E.A. Kronberg, N. Cornilleau-Wehrlin, Cluster observations of energetic electrons and electromagnetic fields within a reconnecting thin current sheet in the Earth's magnetotail. J. Geophys. Res. **113**, A12215 (2008). doi:10.1029/2008JA013511
K. Rönnmark, Electron acceleration in the auroral current circuit. Geophys. Res. Lett. **26**, 983–986 (1999). doi:10.1029/1999GL900133
M. Roth, D. Evans, J. Lemaire, Theoretical structure of a magnetospheric plasma boundary: application to the formation of discrete auroral arcs. J. Geophys. Res. **98**, 11411–11423 (1993)
M. Roth, J. de Keyser, M.M. Kuznetsova, Vlasov theory of the equilibrium structure of tangential discontinuities in space plasmas. Space Sci. Rev. **76**, 251–317 (1996). doi:10.1007/BF00197842
A. Runov, V.A. Sergeev, R. Nakamura, W. Baumjohann, S. Apatenkov, Y. Asano, T. Takada, M. Volwerk, Z. Vörös, T.L. Zhang, J. Sauvaud, H. Rème, A. Balogh, Local structure of the magnetotail current sheet: 2001 Cluster observations. Ann. Geophys. **24**, 247–262 (2006)

A. Runov, V. Angelopoulos, M.I. Sitnov, V.A. Sergeev, J. Bonnell, J.P. McFadden, D. Larson, K. Glassmeier, U. Auster, THEMIS observations of an earthward-propagating dipolarization front. Geophys. Res. Lett. **36**, L14106 (2009). doi:10.1029/2009GL038980

R.Z. Sagdeev, V.D. Shapiro, Influence of transverse magnetic field on Landau damping. JETP Lett. **17**, 279 (1973)

E.T. Sarris, S.M. Krimigis, T.P. Armstrong, Observations of magnetospheric bursts of high-energy protons and electrons at approximately 35 Earth radii with Imp 7. J. Geophys. Res. **81**, 2341–2355 (1976). doi:10.1029/JA081i013p02341

J.A. Sauvaud, R.A. Kovrazhkin, Two types of energy-dispersed ion structures at the plasma sheet boundary. J. Geophys. Res. **109**(A18), A12213 (2004). doi:10.1029/2003JA010333

H. Schamel, S. Bujarbarua, Analytical double layers. Phys. Fluids **26**, 190–193 (1983). doi:10.1063/1.864006

K. Schindler, *Physics of Space Plasma Activity* (Cambridge University Press, Cambridge, 2006). doi:10.2277/0521858976

K. Schindler, M. Hesse, J. Birn, General magnetic reconnection, parallel electric fields, and helicity. J. Geophys. Res. **93**, 5547–5557 (1988)

V.A. Sergeev, R.J. Pellinen, T.I. Pulkkinen, Steady magnetospheric convection: a review of recent results. Space Sci. Rev. **75**, 551–604 (1996a)

V.A. Sergeev, T.I. Pulkkinen, R.J. Pellinen, Coupled-mode scenario for the magnetospheric dynamics. J. Geophys. Res. **101**, 13047–13065 (1996b)

V.A. Sergeev, D.A. Sormakov, S.V. Apatenkov, W. Baumjohann, R. Nakamura, A.V. Runov, T. Mukai, T. Nagai, Survey of large-amplitude flapping motions in the midtail current sheet. Ann. Geophys. **24**, 2015–2024 (2006)

V.A. Sergeev, V. Angelopoulos, S. Apatenkov, J. Bonnell, R. Ergun, R. Nakamura, J. McFadden, D. Larson, A. Runov, Kinetic structure of the sharp injection/dipolarization front in the flow-braking region. Geophys. Res. Lett. **36**, L21105 (2009). doi:10.1029/2009GL040658

C.E. Seyler, K. Liu, Particle energization by oblique inertial Alfvén waves in the auroral region. J. Geophys. Res. **112**(A11), A09302 (2007). doi:10.1029/2007JA012412

C.E. Seyler, K. Wu, Instability at the electron inertial scale. J. Geophys. Res. **106**, 21623–21644 (2001). doi:10.1029/2000JA000410

A.S. Sharma, R. Nakamura, A. Runov, E.E. Grigorenko, H. Hasegawa, M. Hoshino, P. Louarn, C.J. Owen, A. Petrukovich, J. Sauvaud, V.S. Semenov, V.A. Sergeev, J.A. Slavin, B.U.Ö. Sonnerup, L.M. Zelenyi, G. Fruit, S. Haaland, H. Malova, K. Snekvik, Transient and localized processes in the magnetotail: a review. Ann. Geophys. **26**, 955–1006 (2008)

M.A. Shay, J.F. Drake, B.N. Rogers, R.E. Denton, Alfvénic collisionless magnetic reconnection and the Hall term. J. Geophys. Res. **106**, 3759–3772 (2001). doi:10.1029/1999JA001007

N. Singh, I. Khazanov, Planar double layers in magnetized plasmas: Fine structures and their consequences. J. Geophys. Res. **110**, A04209 (2005). doi:10.1029/2004JA010620

N. Singh, H. Thiemann, R.W. Schunk, Electric fields and double layers in plasmas. Laser Part. Beams **5**, 233–255 (1987). doi:10.1017/S0263034600002743

N. Singh, G. Khazanov, A. Mukhter, Electrostatic wave generation and transverse ion acceleration by Alfvénic wave components of broadband extremely low frequency turbulence. J. Geophys. Res. **112**(A11), A06210 (2007). doi:10.1029/2006JA011933

B.U.Ö. Sonnerup, Adiabatic particle orbits in a magnetic null sheet. J. Geophys. Res. **76**, 8211–8222 (1971). doi:10.1029/JA076i034p08211

T.W. Speiser, Particle trajectories in model current sheets, 1. Analytical solutions. J. Geophys. Res. **70**, 4219–4226 (1965)

T.W. Speiser, Particle trajectories in model current sheets, 2. Applications to auroras using a geomagnetic tail model. J. Geophys. Res. **72**, 3919–3932 (1967)

T. Stallard, S. Miller, M. Lystrup, N. Achilleos, E.J. Bunce, C.S. Arridge, M.K. Dougherty, S.W.H. Cowley, S.V. Badman, D.L. Talboys, R.H. Brown, K.H. Baines, B.J. Buratti, R.N. Clark, C. Sotin, P.D. Nicholson, P. Drossart, Complex structure within Saturns infrared aurora. Nature **456**, 214–217 (2008). doi:10.1038/nature07440

C.R. Stark, A.P. Cran-McGreehin, A.N. Wright, Contributions to the magnetospheric parallel electric field. J. Geophys. Res. **116**(A15), A07216 (2011). doi:10.1029/2010JA016270

K. Stasiewicz, P. Bellan, C. Chaston, C. Kletzing, R. Lysak, J. Maggs, O. Pokhotelov, C. Seyler, P. Shukla, L. Stenflo, A. Streltsov, J.E. Wahlund, Small scale Alfvénic structure in the aurora. Space Sci. Rev. **92**, 423–533 (2000)

R.J. Stéfant, Alfvén wave damping from finite gyroradius coupling to the ion acoustic mode. Phys. Fluids **13**, 440–450 (1970). doi:10.1063/1.1692938

G.S. Stiles, E.W. Hones Jr., S.J. Bamen, J.R. Asbridge, Plasma sheet pressure anisotropy. J. Geophys. Res. **83**, 3166 (1978)
A.V. Streltsov, W. Lotko, Multiscale electrodynamics of the ionosphere-magnetosphere system. J. Geophys. Res. **109**(A18), A09214 (2004). doi:10.1029/2004JA010457
R.L. Swanson, Electron intensity and magnetic field changes at synchronous orbit for the auroral electrojet. MS thesis, Univ. of Minn., Minneapolis (1978)
S.W.Y. Tam, T. Chang, Double rank-ordering technique of ROMA (Rank-Ordered Multifractal Analysis) for multifractal fluctuations featuring multiple regimes of scales. Nonlinear Process. Geophys. **18**, 405–414 (2011). doi:10.5194/npg-18-405-2011
S.W.Y. Tam, T. Chang, P.M. Kintner, E.M. Klatt, Rank-ordered multifractal analysis for intermittent fluctuations with global crossover behavior. Phys. Rev. E **81**(3), 036414 (2010). doi:10.1103/PhysRevE.81.036414
T. Terasawa, A. Nishida, Simultaneous observations of relativistic electron bursts and neutral-line signatures in the magnetotail. Planet. Space Sci. **24**, 855–866 (1976). doi:10.1016/0032-0633(76)90076-3
B.J. Thompson, R.L. Lysak, Electron acceleration by inertial Alfvén waves. J. Geophys. Res. **101**, 5359–5370 (1996). doi:10.1029/95JA03622
M.F. Thomsen, J.E. Borovsky, D.J. McComas, M.B. Moldwin, Observations of Earth's plasma sheet at geosynchronous orbit, in *Workshop on the Earth's Trapped Particle Environment*, ed. by G.D. Reeves (Am. Inst. Physics, Woodbury, 1996), p. 25
B.A. Tverskoy, Main mechanisms in the formation of the Earth's radiation belts. Rev. Geophys. Space Phys. **7**, 219–231 (1969). doi:10.1029/RG007i001p00219
V.M. Uritsky, A.J. Klimas, D. Vassiliadis, D. Chua, G. Parks, Scale-free statistics of spatiotemporal auroral emissions as depicted by POLAR UVI images: Dynamic magnetosphere is an avalanching system. J. Geophys. Res. **107**, 1426 (2002). doi:10.1029/2001JA000281
D.L. Vainshtein, J. Büchner, A.I. Neishtadt, L.M. Zelenyi, Quasi-adiabatic description of nonlinear particle dynamics in typical magnetotail configurations. Nonlinear Process. Geophys. **12**, 101–115 (2005)
A. Vaivads, M. André, S. Buchert, A.I. Eriksson, A. Olsson, J.E. Wahlund, P. Janhunen, G. Marklund, L.M. Kistler, C. Mouikis, D. Winningham, A. Fazakerley, P. Newell, What high altitude observations tell us about the auroral acceleration: A Cluster/DMSP conjunction. Geophys. Res. Lett. **30**(3), 030000 (2003)
G.E. Vekstein, E.R. Priest, Nonlinear magnetic reconnection with collisionless dissipation. Phys. Plasmas **2**, 3169–3178 (1995). doi:10.1063/1.871149
P. Veltri, G. Zimbardo, A.L. Taktakishvili, L.M. Zelenyi, Effect of magnetic turbulence on the ion dynamics in the distant magnetotail. J. Geophys. Res. **103**, 14897–14916 (1998). doi:10.1029/98JA00211
M.F. Vogt, M.G. Kivelson, K.K. Khurana, R.J. Walker, B. Bonfond, D. Grodent, A. Radioti, Improved mapping of Jupiter's auroral features to magnetospheric sources. J. Geophys. Res. **116**, A03220 (2011). doi:10.1029/2010JA016148
J.E. Wahlund, H.J. Opgenoorth, I. Haggstrom, K.J. Winser, G.O.L. Jones, EISCAT observations of topside ionospheric ion outflows during auroral activity—Revisited. J. Geophys. Res. **97**, 3019–3037 (1992). doi:10.1029/91JA02438
D.R. Weimer, Maps of ionospheric field-aligned currents as a function of the interplanetary magnetic field derived from Dynamics Explorer 2 data. J. Geophys. Res. **106**, 12889–12902 (2001). doi:10.1029/2000JA000295
J.R. Wygant, A. Keiling, C.A. Cattell, M. Johnson, R.L. Lysak, M. Temerin, F.S. Mozer, C.A. Kletzing, J.D. Scudder, W. Peterson, C.T. Russell, G. Parks, M. Brittnacher, G. Germany, J. Spann, Polar spacecraft based comparisons of intense electric fields and Poynting flux near and within the plasma sheet-tail lobe boundary to UVI images: An energy source for the aurora. J. Geophys. Res. **105**, 18675–18692 (2000). doi:10.1029/1999JA900500
S. Zaharia, C.Z. Cheng, J.R. Johnson, Particle transport and energization associated with substorms. J. Geophys. Res. **105**, 18741 (2000)
L.M. Zelenyi, A.V. Milovanov, REVIEWS OF TOPICAL PROBLEMS: Fractal topology and strange kinetics: from percolation theory to problems in cosmic electrodynamics. Phys. Usp. **47**, 749–788 (2004). doi:10.1070/PU2004v047n08ABEH001705
L.M. Zelenyi, A.S. Lipatov, D.G. Lominadze, A.L. Taktakishvili, The dynamics of the energetic proton bursts in the course of the magnetic field topology reconstruction in the earth's magnetotail. Planet. Space Sci. **32**, 313–324 (1984). doi:10.1016/0032-0633(84)90167-3
L.M. Zelenyi, J.G. Lominadze, A.L. Taktakishvili, Generation of the energetic proton and electron bursts in planetary magnetotails. J. Geophys. Res. **95**, 3883–3891 (1990). doi:10.1029/JA095iA04p03883
L.M. Zelenyi, D.V. Zogin, J. Büchner, Quasi-adiabatic dynamics of charged particles in the tail of the magnetosphere. Cosm. Res. **28**, 369–380 (1990)
L.M. Zelenyi, M.I. Sitnov, H.V. Malova, A.S. Sharma, Thin and superthin ion current sheets. Quasi-adiabatic and nonadiabatic models. Nonlinear Process. Geophys. **7**, 127–139 (2000)

L.M. Zelenyi, M.S. Dolgonosov, E.E. Grigorenko, J. Sauvaud, Universal properties of the nonadiabatic acceleration of ions in current sheets. JETP Lett. **85**, 187–193 (2007) doi:10.1134/S0021364007040017

L.M. Zelenyi, A. Artemyev, H. Malova, A.V. Milovanov, G. Zimbardo, Particle transport and acceleration in a time-varying electromagnetic field with a multi-scale structure. Phys. Lett. A **372**, 6284–6287 (2008a). doi:10.1016/j.physleta.2008.08.035

L.M. Zelenyi, A.V. Artemyev, H.V. Malova, V.Y. Popov, Marginal stability of thin current sheets in the Earth's magnetotail. J. Atmos. Sol.-Terr. Phys. **70**, 325–333 (2008b). doi:10.1016/j.jastp.2007.08.019

L.M. Zelenyi, A.V. Artemyev, A.A. Petrukovich, R. Nakamura, H.V. Malova, V.Y. Popov, Low frequency eigenmodes of thin anisotropic current sheets and Cluster observations. Ann. Geophys. **27**, 861–868 (2009)

G. Zimbardo, A. Greco, L. Sorriso-Valvo, S. Perri, Z. Vörös, G. Aburjania, K. Chargazia, O. Alexandrova, Magnetic turbulence in the geospace environment. Space Sci. Rev. **156**, 89–134 (2010). doi:10.1007/s11214-010-9692-5

Q.G. Zong, T.A. Fritz, Z.Y. Pu, S.Y. Fu, D.N. Baker, H. Zhang, A.T. Lui, I. Vogiatzis, K.H. Glassmeier, A. Korth, P.W. Daly, A. Balogh, H. Rème, Cluster observations of earthward flowing plasmoid in the tail. Geophys. Res. Lett. **31**, L18803 (2004). doi:10.1029/2004GL020692